Green-Function Study of Electrified Solids

by

Ryan Alexander English

A thesis
presented to the University of Waterloo
in fulfillment of the
thesis requirement for the degree of
Doctor of Philosophy
in
Applied Mathematics

Waterloo, Ontario, Canada, 1997

The University of Waterloo requires the signatures of all persons using or photocopying this thesis. Please sign below, and give address and date.

Abstract

When a tight-binding chain of atoms is subjected to an electric field, its electronic energy spectrum takes on the form of the Wannier-Stark ladder. For such a system, successive use of the Dyson equation enables the recursive Green function to be derived analytically as a continued fraction, which can be expressed as a ratio of Bessel functions. The site representation of the Green function provides access to the local density of states. The versatility of this technique is illustrated via its application to infinite, semi-infinite and finite chains, as well as systems constructed piecewise from these components. In particular, the Wannier-Stark effect on surface states, hydrogen chemisorption on electrified substrates and electron transmission of molecular switches are investigated.

Acknowledgements

The direction of this work has been primarily driven by the invaluable collaboration I have had with the research group led by Dr. Sydney Davison. In his role as my supervisor, he has provided the inspiration and structure necessary for me to produce this thesis. The support I have received from Drs. Zoran Mišković and Frank Goodman have kept me on track and out of too much trouble researchwise. Communications with Drs. Terry Amos and Brian Burrows have also shaped the outcome of this project.

Financial support for this work has been provided, in part, by the Natural Sciences and Engineering Research Council of Canada, and the University of Waterloo.

Contents

Chapter 1 Introduction **1**

1.1 Motivation 1

1.2 Thesis Outline 2

1.3 Literature Review 3

Chapter 2 Wannier-Stark Effect **9**

2.1 Historical Development 9

2.2 Finite-Chain Ladders 14

2.3 Green-Function Approach 18

Chapter 3 Green-Function Method **21**

3.1 Basic Theory 21

3.2 Density of States 23

3.3 Causal-Surface Green-Function Technique 25

3.4 Recursive Green-Function Approach 29

Chapter 4 Continued Fractions 37

4.1 Basic Concepts 37

4.2 Pincherle's Theorem 39

4.3 Monatomic Semi-Infinite Chain 43

4.4 Infinite Chain Density of States 46

Chapter 5 Electrified Solids 48

5.1 Methodology 48

5.2 Finite Chain 52

5.3 Semi-infinite Chain 55

5.3.1 Infinite Chain 57

Chapter 6 Surface States 61

6.1 Zero-Field Theory 61

6.2 Surface-Field Effects 65

Chapter 7 Chemisorption 72

7.1 Methodology 72

7.2 Field-Enhanced Situation 80

7.3 H–Ti System 84

7.4 H–Cr 88

Chapter 8 Molecular Electronics 91

8.1 Zero-Field Model 91

8.2 Embedding Field-Enhanced Regions 98

8.3 Field Effect on Molecular Switching 107

Chapter 9 Conclusion 111

9.1 Results and Discussion 111

9.2 Future Directions 112

Appendix A Rydberg Atomic Units 114

Appendix B Creation and Annihilation Operators 116

Appendix C Summing Series of Matrices 120

Appendix D Matrix-Determinant Approach 123

Appendix E Crystal Orbital Surface States 125

Appendix F Lippmann-Schwinger Equation 132

Appendix G Maple Source Code 136

G.1 Surface States 136

G.2 Chemisorption 138

G.3 Molecular Electronics 141

Bibliography 144

List of Tables

7.1 Experimental data for chemisorbed H on Ti. 85

7.2 Magnetic and non-magnetic solutions of H–Ti system. 85

7.3 Experimental data for chemisorbed H on Cr. 88

7.4 Magnetic and non-magnetic solutions of H–Cr system. 88

List of Figures

2.1 One-dimensional periodic crystal lattice. 12

2.2 Tilted-band picture of WSL energy spectrum. 13

2.3 Lommel polynomial $R_{100,1-\nu}(10)$. 18

3.1 Building a linear chain by adding a bond at each iteration. 30

3.2 Sequence of linear chains extending to the left. 34

4.1 Density of states for linear semi-infinite chain. 45

4.2 One-dimensional LDOS for infinite linear chain. 47

5.1 Site energy shift due to applied field. 49

5.2 LDOS at $n = 0$ site of 100 atom chain. 53

5.3 Logarithmic plot of $I_k^0(X_k)$. 54

5.4 Transition from surface to bulk LDOS of semi-infinite chain. 56

5.5 Occupation number of states for infinite chain. 58

5.6 Bound-state existence regions. 59

6.1 Zero-field SDOS and surface intensities. 65

6.2 Graph of $J_{-X/F^{-1}}(-F^{-1})/J_{-X/F}(-F^{-1})$ for $F = 0.2$. 67

6.3 Surface intensity-energy distributions for $z = 1$. 69

6.4 Surface intensity-energy distributions for $F = 0.2$ 70

7.1 Energy diagram for adatom. 73

7.2 Quasi-band region of electrified chain of m atoms. 81

7.3 Self-consistency curves for $\eta = 1$ and F-values indicated. 84

7.4 Self-consistency plots for H–Ti. 86

7.5 Variation of H–Ti chemisorption energy and charge transfer. 87

7.6 Self-consistency plots for H–Cr. 89

7.7 Variation of H–Cr chemisorption energy and charge transfer. 90

8.1 Scattering amplitudes. 94

8.2 Model of molecular switch embedded in a linear monatomic chain. . 95

8.3 Band overlap regions. 105

8.4 Transmission probability of embedded field-states. 106

8.5 Field effects on switching parameters. 109

E.1 Cyclic representation of 1-dimensional infinite chain. 126

E.2 Solutions to $z = \sin(N+1)\theta/\sin N\theta$. 129

Acronyms

AO	atomic orbital
BF	Bessel function
CF	continued-fraction
DOS	density of states
EMA	effective mass approximation
FL	Fermi level
GF	Green function
GL	Gaussian-like
IF	iterating function
KP	Kronig-Penney
LDOS	local density of states
LS	Lippmann-Schwinger
ME	molecular electronic
NN	nearest-neighbour
PT	Pincherle's Theorem
QCSE	quantum confined Stark effect
QW	quantum well
SDOS	surface density of states
TB	tight-binding

TCNQ	tetracyanoquinodimethane
WFs	Wannier functions
WSL	Wannier-Stark ladder

Chapter 1

Introduction

1.1 Motivation

The main objective of this thesis is the development of a mathematical model for the description of charge transport along a polymer chain, i.e., a *molecular wire*, under the influence of an *applied electric field*. Previous work [1, 2, 3] on electron *transmission* through an impurity embedded in a polymer, *without* an applied field, has begun to catalogue desirable properties for potential molecular components from which *molecular electronic* (ME) devices might be constructed.

Over the past 20 years, the transdisciplinary field of MEs has emerged as an important area of research [4, 5, 6, 7]. The future miniaturization of electronic devices will begin to be dominated by quantum size effects, which will have serious consequences for the microtechnology industry. Biotechnology requires organic components, whose presence will not be rejected by living tissues, and which can interact with nature's multitude of charge-transfer mechanisms. Computer architects are seeking to increase memory capacity by storing information in the geometries of

multistable molecules. The discovery of *synthetic conducting polymers* in the late 1970's inspired researchers [8] to investigate possible solutions to these and other ME problems.

The application of applied constant-field theory to ME models is not a straightforward procedure. Though the description of a free electron in a linear potential has been well-established, the application to electrons bound in an electrified solid has met with less success. First, the analytical work is limited on even the simplest system, i.e., the infinite one-dimensional crystal in the *tight-binding* (TB) approximation, with even these results subject to questions of applicability. Secondly, the mathematics developed have been fairly cumbersome to apply, leading investigations to often rely heavily on numerical results to establish their conclusions. Thus, to achieve the desired results for ME, it has become necessary to develop new techniques in the theory of electrified solids.

Since the previous mathematical details in the theory of electrified solids do not readily admit applications to many of the problems studied in solid-state physics, the achievement of an elegant solution with which to analyze electrified solids will provide access to a broad range of investigations in the solid-state field.

1.2 Thesis Outline

Electrified solids have received much attention over the past 60 years, because some basic questions have taken a considerable amount of work to be satisfactorily answered. In particular, Wannier's 1960 prediction [9] that the energy spectrum of an infinite crystal would be *discretized* with the application of a constant field initially failed to receive conclusive experimental verification, which led to considerable debate and a wide assortment of different approaches to rigorously show either the

existence of either a *Wannier-Stark ladder* (WSL) or a *continuum* energy spectrum. The rest of this chapter is devoted to reviewing the extensive literature on the study of electrified solids.

In chapter 2, we re-derive the discretization of the energy spectrum into the WSL for both infinite and finite linear crystals, under the influence of a constant field.

Chapter 3 develops the required background in *Green function* (GF) theory and derives the components in terms of *continued-fraction* (CF) notation for which we shall need to obtain solutions in order to describe the electronic structure of an electrified solid. The mathematics for solving these CFs, *Pincherle's theorem*, is presented in chapter 4, and the results applied to obtain a new analysis of electrified solids in chapter 5.

In chapters 6 and 7, we explore the broad application of this new method by deriving results for *surface states* and *chemisorption*, respectively, on electrified solids.

One application of the theory to ME is presented in chapter 8, which leads into a description of possible future work using this method.

1.3 Literature Review

Investigations into the quantum description of electrified solids began in earnest following Zener's [10] work in 1934 on dielectric breakdown. Houston [11] and Slater [12] began the investigation of aperiodic perturbations to Bloch wavefunctions. Building on these results, James [13] examined the influence of a linear potential on an infinite crystal using the *effective mass approximation* (EMA) and,

in 1949, predicted quantization of the energy spectrum into *equally* spaced levels. Independently, Katsura *et al.* [14] came to the same conclusion using a one-band TB approximation by noting that the wavefunction solutions for the infinite crystal had Bessel function coefficients, whose energy-dependent order must be integer to satisfy normalizability conditions. This first proof of the existence of the WSL came a decade before Wannier's prediction [9] and two decades before Hacker and Obermair [15] rigorously established Wannier's result. In addition, they predicted a symmetric deviation from the *exact* WSL for finite crystals. Feuer [16] extended the theory to a two-band TB model, finding that the uncoupled bands generated a WSL with the spacing perturbed by the interband coupling.

Working in the crystal-momentum representation, derived by Adams [17, 18], Wannier [19, 20] and Adams and Argyles [21] began developing the wavefunctions as modified from Bloch functions by the presence of the electric field. Adams [22] delved into the "physical" interpretation of energy bands and showed that the EMA solutions were valid only for electric fields *sufficiently weak* as to satisfy an adiabatic condition.

In his discussion on Zener tunneling in semiconductors, Kane [23] was able to derive the WSL condition by solving the equation of motion in momentum space. In 1960, Wannier was able to combine the WSL result together with his field-modified wavefunctions, using translational properties of Bloch functions, to give an extensive description of the effects on a crystal electron due to the application of a linear potential [9, 24]. This basic derivation has been improved upon and extended by several authors, including Rees [25], Enderlein *et al.* [26], Henneberger and Röseler [27] and Fiddicke and Enderlein [28].

Modifications to Wannier's theory were employed by Callaway [29, 30], Wannier and Fredkin [31] and Rauh and Wannier [32] to provide a description of optical

absorption, whereby the phenomenon could be tested experimentally. The initial failure to obtain conclusive experimental verification [33, 34, 35] of a discrete WSL energy spectrum fostered strong criticism of Wannier's conclusions, led primarily by Zak [36, 37, 38, 39] and Rabinovitch [40, 41], who predicted instead a continuous energy spectrum under the influence of a constant applied field [42, 43]. They argued that Wannier's derivation (see § 2.1) applied only to the infinite crystal, as his translational operator technique must fail in the presence of end effects for a finite chain, and that the arbitrariness of the initial eigenenergy selection allowed for an entire interval of energies to be chosen, which would generate the continuous $(-\infty, \infty)$ energy spectrum.

Hacker and Obermair [15] addressed this last issue and rigorously obtained the WSL result for an infinite crystal by translating Katsura *et al.*'s [14] derivations into the language of creation and annihilation operators (see § 2.1) and concluded that discreteness was a valid prediction for single-band models. Davison and his co-workers [44, 45] modified this approach to include bond perturbations, due to the presence of the applied field, and overlap integrals to the TB model and still retained a discrete energy spectrum.

Shockley [46] argued that, away from the ends of a finite crystal, the energy spectrum must approximate to the infinite case and hence form a *quasi*-WSL. Heinrichs and Jones [47] examined the finite crystal using perturbation theory and developed a self-consistent CF equation (see § 2.2), which admitted the *exact* WSL only for the infinite case, but were numerically able to show that, well away from end effects, the discrete spectrum was well approximated by the WSL spacing. Stey and Gusman [48] were able to solve for the finite-chain energy spectrum analytically, by introducing Lommel polynomials, and showed that the quasi-WSL for the finite crystal asymptotically approached the exact WSL. Saitoh [49] and Fukuyama *et*

al. [50] extended this work to provide bounds on when discreteness was ensured and when the Rabinovitch-Zak continuum approximation would hold.

In light of these more rigorous derivations, Rabinovitch [51] analyzed the methods used in the literature and contended that:

(i) The crystal-momentum representation, while valid for finite crystals, was inapplicable to the infinite regime.

(ii) That discrete levels were due to the finiteness of the crystal and not the applied field.

(iii) The infinite crystal had a continuous energy spectrum.

Avron *et al.* [52] furthered this view by claiming that the energy uncertainty is never smaller than the WSL spacing predicted by the one-band approximation, and then obtained an absolutely continuous spectrum [53] based on an N-band analysis, which produced an N interspaced one-band WSL, becoming continuous for $N \to \infty$.

In parallel to the perturbative and TB approaches, Lukes and his co-workers [54, 55, 56] developed a time-dependent method of calculating the single-particle GF, in terms of the corresponding Feynman propagator [57], for a δ-potential in a uniform electric field, which enabled exact expressions to be derived formally for the *density of states* (DOS) and energy levels of an electrified *Dirac-delta comb* potential. Moyer [58, 59], in his GF treatment, invoked first-order perturbation theory to describe the motion of an electron in an infinite, electrified *Kronig-Penney* (KP) lattice. Unlike previous work, the GF approach did not need to assume any approximations in order to derive the WSL condition, as was shown by Lukes and Ringwood [60] (see § 2.3).

In the light of the general applicability of the GF solution, and new experimental evidence of the WSL effect by Maekawa [61], Koss and Lambert [62] and May and

Vecht [63], Rabinovitch [64], Avron [65], and Zak [66], all conceded that a quasi-WSL did result, even in the multi-band derivation of the energy spectrum for finite crystals. Exact numerical solutions to the Schrödinger equation for the applied field were conducted by Sessa and Sitte [67], again verifying the WSL result.

With the WSL existence controversy resolved, another decade passed before there was renewed interest in the topic. Emin and Hart [68, 69] decomposed the linear potential into its periodic effect and (non-periodic) constant site shift, showing that it was only the latter that generated the WSL.

Leo and MacKinnon [70] applied the TB model to a semiconductor superlattice in support of the experimental evidence obtained by Mendez *et al.* [71] and Voisin *et al.* [72] on such systems. Leavitt *et al.* [73, 74] and Ritze *et al.* [75] expanded on both the experimental and theoretical model for $GaAs/Al_xGa_{1-x}As$ superlattices.

A perturbative investigation of WSLs in infinite diatomic crystals was undertaken by Zhao [76, 77], who found that, in the 2-band energy spectrum, the WSLs were interspaced. For finite crystals, he also found that the interband matrix elements were non-zero[78].

Optical absorption in electrified δ-doped semiconductors was examined by Ahn [79]. Solving the Schrödinger equation for a V-shaped *quantum well* (QW) in an electric field, he predicted wide-range tuning of intersubband absorption by controlling planar doping, and also the presence of red- rather than blue-shifts associated with electro-adsorption in ordinary QWs. In a comparative study, Anwar and Jahan [80] performed a self-consistent calculation of the DOS of double-barrier QW structures in magnetic and electric fields, and described the energy redistribution and a phase-breaking mechanism. An electrified multi-band QW, in the form of a finite KP structure, was used by Vrubel and Borzdov [81] in their treatment of

the gradual transition from the *quantum confined Stark effect* (QCSE) to the WSL quantization. Stark localization and mixing phenomena between different WSLs in coupled QWs was reported by Sari *et al.* [82], who found that at intermediate WSL values a certain degree of carrier wave-function delocalization exists, while at large values the WSL states become localized inside individual QWs and a combined band structure occurs.

Experimentally, Cohen *et al.* [83] continued the investigation of the optical properties of a narrow-band GaAs/Al_x $Ga_{1-x}As$ superlattice and observed a modified WSL with both positive and negative orders appearing above the zero-order transition. QCSE in InGaAs/GaAs QWs under high electric fields was studied by Kovalianskas *et al.* [84] using photocurrent and electroreflectance spectroscopies. Evidence of exciton quenching and carrier tunneling out of the QWs was obtained, while coupling between quasi-bound and continuum states resulted in an absorption increase below the barrier band gap.

During the derivations of the present work, Dolcher *et al.* [85] reported a real-space GF analysis of WSLs based on a modified *Lanczos iterative procedure*, which was applied to 1-dimensional, one- and two-band TB systems, while the GF technique in the site representation was employed by Gvozdikov [86] to discuss the analogy between the *Landau spectrum* of a Bloch electron in a 2-dimensional anisotropic lattice and the WSL. Meanwhile, Zekri *et al.* [87] introduced disorder into an electrified KP model and investigated the short-range localization properties and effects on the transmission coefficient.

Chapter 2

Wannier-Stark Effect

2.1 Historical Development

The existence of a WSL energy spectrum was central to the results of Wannier, who employed the translational symmetry [9] of the solutions of the Hamiltonian, $\mathbb{H}$, describing a particle in a periodic potential that were modified by an applied field of strength (gradient) γ.

The periodic potential problem has been studied in great detail, e.g., see [88]. Let a be the lattice period in the direction of the applied field, so that the potential energy function satisfies

$$V(x + na) = V(x), \qquad n \in \mathbb{Z}. \tag{2.1}$$

Using *Rydberg atomic units* (Appendix A), the one-dimensional time-independent Schrödinger equation for an electron of energy E in the potential $V(x)$ may be written as

$$\psi''(x) + [E - V(x)]\psi(x) = 0. \tag{2.2}$$

Equation (2.2), subject to (2.1), is a *Floquet-type* differential equation whose quantal solutions are *Bloch* functions, which may be written as

$$\psi(x) = u_k(x)e^{ikx}, \tag{2.3}$$

with $k(E)$, the *wavenumber*, determined by the boundary conditions, and $u_k(x)$ a periodic function $u_k(x+na) = u_k(x)$, $n \in \mathbb{Z}$. Thus, we have

$$\psi(x+a) = u_k(x+a)e^{ik(x+a)} = u_k(x)e^{ik(x+a)}. \tag{2.4}$$

Along the direction of the applied field, the modified Schrödinger equation is, therefore,

$$\mathbb{H}\psi(x) = \left[p^2 + V(x) + \gamma x\right]\psi(x) = E\psi(x). \tag{2.5}$$

where $p = -i\partial/\partial x$. Consider now the translation operator $\mathbb{T}(a) = \exp(ipa)$, which has the commutator

$$\mathbb{T}(a)\mathbb{F}(x,p) = \mathbb{F}(x+a,p)\mathbb{T}(a). \tag{2.6}$$

Applying $\mathbb{T}$ to (2.5), we have

$$\mathbb{T}(a)\mathbb{H}\psi(x) = \left[p^2 + V(x+a) + \gamma(x+a)\right]\psi(x+a) = E\psi(x+a), \tag{2.7}$$

to which we apply the periodicity of V, and rewrite to recover the Hamiltonian in (2.5), namely,

$$\mathbb{H}\psi(x+a) = \left[p^2 + V(x) + \gamma x\right]\psi(x+a) = (E - a\gamma)\psi(x+a), \tag{2.8}$$

which implies that $\psi(x+a)$ is also an eigenfunction of $\mathbb{H}$ with eigenvalue of $E - a\gamma$. Iteration of this procedure, plus application of the inverse translational operator, $\mathbb{T}^{-1}(a) = \mathbb{T}(-a)$, leads to the WSL energy spectrum

$$E + na\gamma, \qquad n \in \mathbb{Z}. \tag{2.9}$$

The preceding argument does not take boundary conditions into account, which left it open to the criticism, primarily from Zak and Rabinovitch [37, 38, 39, 40, 42], that there is nothing in this derivation to restrict the initial choice of E. In the absence of the field, the energy spectrum is a *continuum*, so starting from $E' = E + \delta E$, another WSL could also be generated. Choosing all δE, the continuum would be recovered, even in the presence of an applied field.

Moreover, the derivation is highly dependent on the translational periodicity of the crystal. In particular, the *Born-von-Karman* boundary condition, viz.,

$$\psi(x) = \psi(x + L), \tag{2.10}$$

where $L = aN$ is the crystal length, is necessary for the properties of the infinite case to be valid in the finite situation. Rabinovitch [40] showed that this boundary condition is incompatible with (2.5). Born-von-Karman gives

$$\psi''(0) = \psi''(L), \tag{2.11}$$

while (2.5) can be rewritten to yield

$$\psi''(0) = -[E - V(0)]\psi(0) \tag{2.12}$$

and

$$\psi''(L) = -[E - V(L) - L\gamma]\psi(L) = -[E - V(0) - L\gamma]\psi(0), \tag{2.13}$$

which leads to a contradiction.

Hacker and Obermair [15] addressed the continuum issue by providing a more rigorous derivation, showing that the spectrum was indeed a *discrete* WSL. Consider the TB approximation for a linear chain of atoms with Coulomb integrals (site energies) at the atomic sites,

$$\alpha = \langle n | \, \mathbb{H}^0 \, | n \rangle \,, \tag{2.14}$$

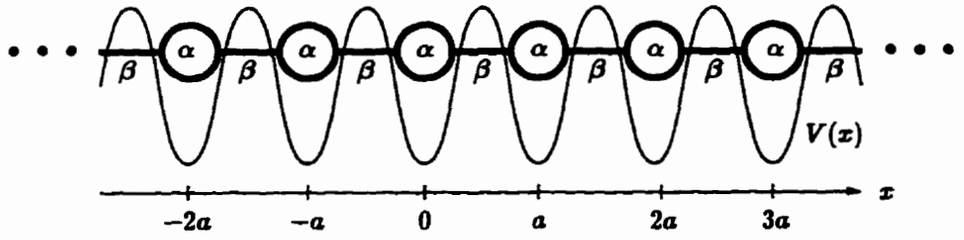

Fig. 2.1: One-dimensional periodic crystal lattice showing potential $V(x)$, Coulomb integral α and resonance integral β.

and resonance integrals (bond energies) between adjacent sites,

$$\beta = \langle n | \, \mathbb{H}^0 \, | n+1 \rangle \,, \tag{2.15}$$

where $|n\rangle$ is the atomic wavefunction at site $x = na$ (Fig. 2.1). The Hamiltonian is

$$\mathbb{H}^0 = \sum \left[\alpha \mathbb{C}_n^\dagger \mathbb{C}_n + \beta (\mathbb{C}_n^\dagger \mathbb{C}_{n+1} + \mathbb{C}_{n+1}^\dagger \mathbb{C}_n) \right], \tag{2.16}$$

where $\mathbb{C}_n^\dagger$ ($\mathbb{C}_n$) is the creation (annihilation) operator for an electron occupying the *Wannier state* localized at lattice-site na, $w_n(x) = w(x - na)$ (Fig. 2.2).

For the field-induced potential

$$\mathbb{V}(x) = \gamma x, \tag{2.17}$$

the component with respect to the *Wannier functions* (WFs) is given by

$$\langle n | \, \mathbb{V} \, | n' \rangle = na\gamma \delta_{nn'}. \tag{2.18}$$

Thus, the Hamiltonian subject to the applied field can be written, using $\Gamma = a\gamma$, as

$$\mathbb{H} = \sum_n \left[(\alpha + n\Gamma) \mathbb{C}_n^\dagger \mathbb{C}_n + \beta (\mathbb{C}_n^\dagger \mathbb{C}_{n+1} + \mathbb{C}_{n+1}^\dagger \mathbb{C}_n) \right]. \tag{2.19}$$

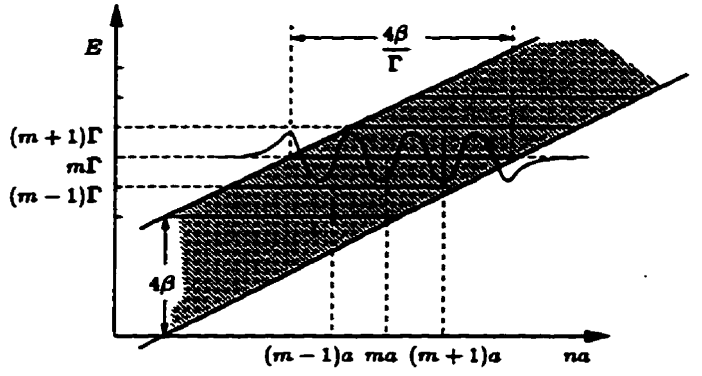

Fig. 2.2: Tilted-band picture of WSL energy spectrum showing Wannier functions, and localization length $L = 4\beta/\Gamma$ [15]

The anticommutation rules for creation and annihilation operators are:

$$\left\{\mathbb{C}_n^\dagger, \mathbb{C}_m\right\} = \delta_{nm}, \qquad \left\{\mathbb{C}_n^\dagger, \mathbb{C}_m^\dagger\right\} = 0, \tag{2.20}$$

see Appendix B, which allow us to determine commutators of the form

$$\left[\mathbb{C}_i^\dagger \mathbb{C}_j, \mathbb{C}_m^\dagger\right] = \mathbb{C}_i^\dagger \left\{\mathbb{C}_j, \mathbb{C}_m^\dagger\right\} - \left\{\mathbb{C}_i^\dagger, \mathbb{C}_m^\dagger\right\} \mathbb{C}_j = \mathbb{C}_i^\dagger \delta_{jm}. \tag{2.21}$$

Since the creation operators for the eigenfunctions of $\mathbb{H}$ diagonalize the Hamiltonian, we must have

$$\begin{aligned} E\mathbb{C}^\dagger(E) &= [H, \mathbb{C}^\dagger(E)] = [H, \sum_m a_m(E)\mathbb{C}_m^\dagger] \\ &= \left[\sum_n \left\{(\alpha + n\Gamma)\mathbb{C}_n^\dagger \mathbb{C}_n + \beta\left(\mathbb{C}_n^\dagger \mathbb{C}_{n+1} + \mathbb{C}_{n+1}^\dagger \mathbb{C}_n\right)\right\}, \sum_m a_m(E)\mathbb{C}_m^\dagger\right] \\ &= \sum_{n,m} a_m(E)\left\{(\alpha + n\Gamma\left[\mathbb{C}_n^\dagger \mathbb{C}_n, \mathbb{C}_m^\dagger\right] + \beta\left[\mathbb{C}_n^\dagger \mathbb{C}_{n+1}, \mathbb{C}_m^\dagger\right] + \beta\left[\mathbb{C}_{n+1}^\dagger \mathbb{C}_n, \mathbb{C}_m^\dagger\right]\right\} \\ &= \sum_{n,m} a_m(E)\left[(\alpha + n\Gamma)\mathbb{C}_n^\dagger \delta_{mn} + \beta\mathbb{C}_n^\dagger \delta_{m,n+1} + \beta\mathbb{C}_{n+1}^\dagger \delta_{mn}\right]. \end{aligned} \tag{2.22}$$

The coefficient of each $\mathbb{C}_n^\dagger$ must be independently zero, so reindexing the final

term of (2.21) and summing over m, we obtain

$$a_{n+1} + \frac{\alpha + n\Gamma - E}{\beta} a_n + a_{n-1} = 0, \tag{2.23}$$

which is the *Bessel function* (BF) recursion relation for

$$a_n(E) = P_{n-(E-\alpha)/\Gamma}\left(-\frac{2\beta}{\Gamma}\right), \tag{2.24}$$

where $P_\mu(z) = AJ_\mu(z) + BY_\mu(z)$ is any linear combination of BFs of the first and second kind.

As the a_n are the coefficients of the WFs, the normalizability condition requires that

$$\sum_n |a_n(E)|^2 < \infty. \tag{2.25}$$

The properties of BFs [89] show that $B = 0$ and $\mu = n - (E - \alpha)/\Gamma$ must be an integer for (2.25) to hold. Hence, the continuum energy spectrum is *not* available, but only those levels in the WSL, viz.,

$$E \equiv E_m = \alpha + m\Gamma, \qquad m \text{ integer}, \tag{2.26}$$

which produce BF coefficients to the WFs, i.e.,

$$a_n(E_m) = A(-1)^{n-m} J_{n-m}\left(\frac{2\beta}{\Gamma}\right). \tag{2.27}$$

2.2 Finite-Chain Ladders

The correspondence between the *infinite* and *finite* crystal ladders was addressed by several authors. Heinrichs and Jones [47] provided a TB analysis based on the

difference equations of a finite chain,

$$(\alpha + n\Gamma - E)c_n + \beta(c_{n+1} + c_{n-1}) = 0, \tag{2.28a}$$

$$(\alpha' - E)c_0 + \beta c_1 = 0, \tag{2.28b}$$

$$(\alpha' + (N-1)\Gamma - E)c_{N-1} + \beta c_{N-2} = 0, \tag{2.28c}$$

where α' is the perturbed Coulomb integral due to the termination of the crystal. For purposes of this analysis, we take $\alpha' = \alpha$.

We immediately see that a necessary condition for an approximate WSL, $E = \alpha + n\Gamma$, to be the solution is for $n\Gamma \gg \beta$, i.e., when the second term of (2.28a) can be neglected, which locates the level well away from the end effects at $n = 0$.

The TB approach is also particularly suited for applying *Brillouin-Wigner perturbation theory* [90], namely, the eigenvalue of a non-degenerate state, $|n\rangle$, can be calculated via

$$E_n = H_{nn} + \sum_{m \neq n} \frac{H_{nm}H_{mn}}{E_n - \epsilon_{nm}} + \sum_{\substack{m,k \neq n \\ m \neq k}} \frac{H_{nm}H_{mk}H_{kn}}{(E_n - \epsilon_{nm})(E_n - \epsilon_{nmk})} + \cdots \tag{2.29a}$$

$$\epsilon_{nm\cdots pq} = H_{qq} + \sum_{r \neq n,m,\ldots,p,q} \frac{H_{qr}H_{rq}}{E_n - \epsilon_{nm\cdots pqr}} + \sum_{\substack{r \neq n,m,\ldots,p,q \\ s \neq n,m,\ldots,p,q,r}} \frac{H_{qr}H_{rs}H_{sq}}{(E_n - \epsilon_{nm\cdots pqr})(E_n - \epsilon_{nm\cdots pqrs})} + \cdots, \tag{2.29b}$$

since terms beyond the interaction range are identically zero. Taking the *nearest-neighbour* (NN) approximation, only the first two terms of (2.29a) and (2.29b) survive. The NN Hamiltonian has only *tri-diagonal* matrix elements,

$$H_{nn} = \alpha + n\Gamma, \qquad n = 0, 1, \ldots, N-1, \tag{2.30a}$$

$$H_{nr} = H_{rn} = \beta(\delta_{r,n+1} + \delta_{r,n-1}), \qquad n = 1, 2, \ldots, N-2, \tag{2.30b}$$

$$H_{0r} = \beta\delta_{r1}, \tag{2.30c}$$

$$H_{N-1,r} = \beta\delta_{r,N-2}. \tag{2.30d}$$

We define the difference between the *modified* and *exact* WSL energies as

$$\Delta E_n = E_n - \alpha - n\Gamma, \tag{2.31}$$

whence,

$$\begin{aligned}
\Delta E_n &= E_n - H_{nn} = \sum_{m\neq n} \frac{H_{nm}H_{mn}}{E_n - \epsilon_{nm}} \\
&= \frac{\beta^2}{E_n - \epsilon_{n,n+1}} + \frac{\beta^2}{E_n - \epsilon_{n,n-1}} \\
&= \frac{\beta^2}{\Delta E_n - \Gamma - \dfrac{\beta^2}{E_n - \epsilon_{n,n+1,n+2}}} + \frac{\beta^2}{\Delta E_n + \Gamma - \dfrac{\beta^2}{E_n - \epsilon_{n,n-1,n-2}}} \\
&= \cfrac{\beta^2}{\Delta E_n - \Gamma - \cfrac{}{\ddots \; - \cfrac{\beta^2}{\Delta E_n - (N-2-n)\Gamma - \cfrac{\beta^2}{\Delta E_n - (N-1-n)\Gamma}}}} \\
&\quad + \cfrac{\beta^2}{\Delta E_n + \Gamma - \cfrac{}{\ddots \; - \cfrac{\beta^2}{\Delta E_n + (n-1)\Gamma - \cfrac{\beta^2}{\Delta E_n + n\Gamma}}}}.
\end{aligned} \tag{2.32}$$

This sum of CFs is a self-consistency equation. The exact WSL occurs only when (2.32) is zero, which is only the case when there are an equal number of terms in each CF. Hence, for a finite chain, only the center state lies on the *true* WSL energy, while for the infinite chain, *every* allowed energy is a WSL energy.

The self-consistent form of (2.32) makes it useful, primarily for obtaining numerical results, and leads only to approximate bounds on the location of the energy spectrum in the finite chain.

Saitoh [49], following the work of Stey and Gusman [48], obtained analytic formulae for the eigenenergies of the finite chain by applying the boundary conditions to the solutions in (2.24).

The *rigid-wall* boundary conditions, $a_0 = a_{N+1} = 0$, yield the requirement that

$$\begin{vmatrix} J_{-\nu} & Y_{-\nu} \\ J_{N+1-\nu} & Y_{N+1-\nu} \end{vmatrix} = 0, \qquad \nu = -(E-\alpha)/\Gamma, \tag{2.33}$$

for non-trivial coefficients, A and B, to exist. By using the *Lommel polynomials*, defined by

$$R_{N,\mu}(x) = \frac{1}{2}\pi x \left[Y_{N+\mu}(x)J_{\mu-1}(x) - J_{N+\mu}(x)Y_{\mu-1}(x)\right], \tag{2.34}$$

with $x = -2\beta/\Gamma$, if we multiply (2.33) by $\pi x/2$, we obtain

$$R_{N,1-\nu}(x) = 0, \tag{2.35}$$

whose solutions $\nu = \nu_n$ for fixed N and x define the *existence condition* for the energy eigenstates in the spectrum (Fig. 2.3).

The property of Lommel polynomials that

$$R_{N,\mu}(x) = (-1)^N R_{N,1-N-\mu}(x) \tag{2.36}$$

means that the energy spectrum is symmetrically dispersed about the center located at

$$E = \alpha + \frac{N+1}{2}\Gamma, \tag{2.37}$$

with the result that

$$E_n + E_{N+1-n} = 2\alpha + (N+1)\Gamma, \tag{2.38}$$

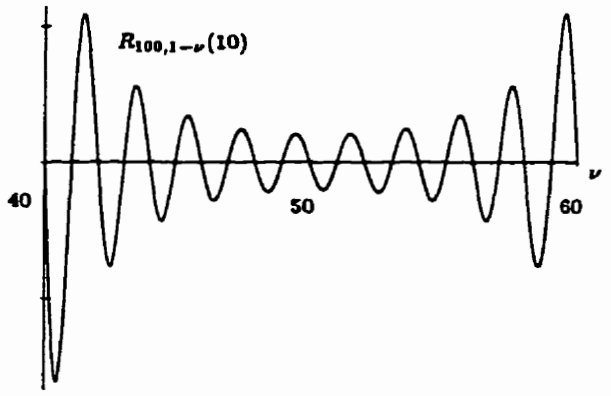

Fig. 2.3: Lommel polynomial $R_{100,1-\nu}(10)$ near center of quasi-WSL $\nu \in (40, 60)$ for chain of $N = 100$ atoms and field of $\Gamma = -\beta/5$.

for all states.

For the *periodic* boundary conditions, $a_0 = a_n$ and $a_1 = a_{N+1}$, we have the condition

$$\begin{vmatrix} J_{-\nu} - J_{N-\nu} & Y_{-\nu} - Y_{N-\nu} \\ J_{1-\nu} - J_{N+1-\nu} & Y_{1-\nu} - Y_{N+1-\nu} \end{vmatrix} = 0 \tag{2.39}$$

or, multiplying through by $-\pi x/2$ and using $J_{\mu+1}(x)Y_{\mu}(x) - J_{\mu}(x)Y_{\mu+1}(x) = 2/\pi x$, we find

$$R_{N,1-\nu}(x) - R_{N-2,2-\nu}(x) - 2 = 0, \tag{2.40}$$

via (2.34). In this case, we again do not recover the exact WSL, but one that *asymptotically* approaches it.

2.3 Green-Function Approach

Using a GF approach, Lukes and Ringwood [60] avoided much of the controversy surrounding the validity of perturbation methods to derive the WSL result. Be-

ginning with the 3-dimensional Feynman propagator [54, 57] for a particle in an electric field, $\boldsymbol{\gamma}$,

$$\langle \mathbf{r}| e^{-i\mathbf{H}t} |\mathbf{r}'\rangle = (4\pi i t)^{-3/2} \exp\left\{ i \left[\frac{1}{4t}(\mathbf{r}-\mathbf{r}')^2 + \frac{t}{2}\boldsymbol{\gamma}\cdot(\mathbf{r}+\mathbf{r}') - \frac{\gamma^2 t^3}{12} \right] \right\}. \quad (2.41)$$

The GF is obtained from the propagator via a Laplace transform, i.e.,

$$G^0(\mathbf{r},\mathbf{r}',E) = -i\int_0^\infty e^{iEt} \langle \mathbf{r}| e^{-i\mathbf{H}t} |\mathbf{r}'\rangle \, dt. \quad (2.42)$$

If we apply a spatial translation $\mathbf{R}$ to the coordinates, we obtain

$$\begin{aligned} G^0(\mathbf{r}+\mathbf{R},\mathbf{r}'+\mathbf{R},E) &= -i\int_0^\infty e^{iEt} \langle \mathbf{r}+\mathbf{R}| e^{-i\mathbf{H}t} |\mathbf{r}'+\mathbf{R}\rangle \, dt \\ &= -i\int_0^\infty e^{iEt} \langle \mathbf{r}| e^{-i\mathbf{H}t} |\mathbf{r}'\rangle \, e^{it\boldsymbol{\gamma}\cdot\mathbf{R}} \, dt \\ &= -i\int_0^\infty e^{i(E+\boldsymbol{\gamma}\cdot\mathbf{R})t} \langle \mathbf{r}| e^{-i\mathbf{H}t} |\mathbf{r}'\rangle \, dt \\ &= G^0(\mathbf{r},\mathbf{r}',E+\boldsymbol{\gamma}\cdot\mathbf{R}), \end{aligned} \quad (2.43)$$

which is true for any vector $\mathbf{R}$.

The addition of a periodic lattice potential, $V(\mathbf{r}) = \sum_i v(\mathbf{r}-\mathbf{R}_i)$, where $\mathbf{R}_i$ is a lattice vector means that the potential is translational invariant only for lattice vectors, $\mathbf{R} = \mathbf{R}_j$. The application of the Dyson equation (see § 3.1) leads to an infinite series in terms of the unperturbed GF and the potential. The translational properties of the modified GF are

$$\begin{aligned} &G(\mathbf{r}+\mathbf{R}_i,\mathbf{r}'+\mathbf{R}_i,E) \\ &\quad = G^0(\mathbf{r}+\mathbf{R}_i,\mathbf{r}'+\mathbf{R}_i,E) \\ &\qquad + \sum_j \int G^0(\mathbf{r}+\mathbf{R}_i,\mathbf{r}'',E) v(\mathbf{r}''-\mathbf{R}_j) G^0(\mathbf{r}'',\mathbf{r}'+\mathbf{R}_i,E)\, d\mathbf{r}'' + \cdots \\ &\quad = G^0(\mathbf{r},\mathbf{r}',E+\boldsymbol{\gamma}\cdot\mathbf{R}_i) \\ &\qquad + \sum_j \int G^0(\mathbf{r}+\mathbf{R}_i,\mathbf{r}'''+\mathbf{R}_i,E) v(\mathbf{r}'''+\mathbf{R}_i-\mathbf{R}_j) G^0(\mathbf{r}'''+\mathbf{R}_i,\mathbf{r}'+\mathbf{R}_i,E)\, d\mathbf{r}''' \end{aligned}$$

$$
\begin{aligned}
&+ \cdots \\
&= G^0(\mathbf{r}, \mathbf{r}', E + \boldsymbol{\gamma} \cdot \mathbf{R}_i) \\
&\quad + \sum_k \int G^0(\mathbf{r}, \mathbf{r}''', E + \boldsymbol{\gamma} \cdot \mathbf{R}_i) v(\mathbf{r}''' - \mathbf{R}_k) G^0(\mathbf{r}''', \mathbf{r}', E + \boldsymbol{\gamma} \cdot \mathbf{R}_i)\, d\mathbf{r}''' + \cdots \\
&= G(\mathbf{r}, \mathbf{r}', E + \boldsymbol{\gamma} \cdot \mathbf{R}_i), \qquad (2.44)
\end{aligned}
$$

where we have introduced $\mathbf{r}''' = \mathbf{r}'' - \mathbf{R}_i$ and reindexed the lattice sum with $\mathbf{R}_k = \mathbf{R}_j - \mathbf{R}_i$ for all orders of the series. This is an exact result, without making any assumption other than the lattice periodicity.

The DOS is obtained from the imaginary part of the GF (see § 3.1) via

$$
n(E) = -\pi^{-1} \mathrm{Im} \int G(\mathbf{r}, \mathbf{r}', E)\, dE = n(E + \boldsymbol{\gamma} \cdot \mathbf{R}_i), \qquad (2.45)
$$

whence, if G is singular at E (see § 3.1), then it is at $E + \boldsymbol{\gamma} \cdot \mathbf{R}_i$ as well, and not for $\mathbf{R} \neq \mathbf{R}_i$, which is a generalized version of the exact WSL condition.

Chapter 3

Green-Function Method

3.1 Basic Theory

It is often found, when dealing with large systems, that direct application of the Schrödinger equation becomes cumbersome, requiring perturbation techniques in order to proceed, which produce only approximate results.

As an alternative, we introduce the GF of the system, which is the *inverse* to the Schrödinger equation, and so the solutions contain equivalent information. We define the *Greenian* operator to be

$$\mathbb{G} = (E - \mathbb{H})^{-1}. \tag{3.1}$$

The element of (3.1) between two states

$$G(m, n; E) = \langle m | (E - \mathbb{H})^{-1} | n \rangle \tag{3.2}$$

yields the GF describing the propagation of the system in state $|n\rangle$ to state $|m\rangle$ at

energy E. By introducing the eigenstates of $\mathbb{H}$, $|\phi_k\rangle$, we can write

$$\begin{aligned} G(m,n;E) &= \langle m| \left[(E-\mathbb{H})^{-1} \sum_k |\phi_k\rangle \langle\phi_k| \right] |n\rangle \\ &= \langle m| \left[\sum_k |\phi_k\rangle (E-E_k)^{-1} \langle\phi_k| \right] |n\rangle , \end{aligned} \tag{3.3}$$

which shows, in particular, that the energy spectrum can be extracted from the *poles* of $G(m,n;E)$. At a particular E_k, the residue of the GF is simply the product of the projections of the k^{th} eigenstate onto the two states connected by the GF, viz., $\langle m \mid \phi_k\rangle \langle\phi_k \mid n\rangle$.

If we have the solution for a given system, i.e.,

$$\mathbb{G}^0 = \left(E - \mathbb{H}^0\right)^{-1}, \tag{3.4}$$

then adding a perturbing potential V to the Hamiltonian gives $H = H^0 + V$, which yields

$$\mathbb{G} = \left(E - \mathbb{H}^0 - V\right)^{-1}, \tag{3.5}$$

whence, via (3.4),

$$\mathbb{G} = \left((\mathbb{G}^0)^{-1} - V\right)^{-1}. \tag{3.6}$$

Operating on the left of (3.6) by $(\mathbb{G}^0)^{-1} - V$, we have

$$(\mathbb{G}^0)^{-1}\mathbb{G} - V\mathbb{G} = 1, \tag{3.7}$$

which, through an application of $\mathbb{G}^0$ on the left, can be rearranged into the *Dyson equation*,

$$\mathbb{G} = \mathbb{G}^0 + \mathbb{G}^0 V \mathbb{G}. \tag{3.8}$$

Since (3.8) is a *recursive* definition, it can be expanded in an infinite series,

$$\mathbb{G} = \mathbb{G}^0 + \mathbb{G}^0 V \mathbb{G}^0 + \mathbb{G}^0 V \mathbb{G}^0 V \mathbb{G}^0 + \cdots, \tag{3.9}$$

or, by considering elements of the Greenian via (3.2), we may obtain a system of coupled GF equations to solve.

3.2 Density of States

There is much useful information about a given system that can be derived from its *electronic density of states*, which is accessible from the GF description of the system. Following [88], consider the trace of $\mathbb{G}(E)$ with respect to the eigenfunctions of $\mathbb{H}$. Using (3.5), we have

$$\begin{aligned} \mathrm{Tr}\left(\mathbb{G}(E)\right) &= \sum_k \langle\phi_k|\,\mathbb{G}(E)\,|\phi_k\rangle = \sum_k \langle\phi_k|\,(E-H)^{-1}\,|\phi_k\rangle \\ &= \sum_k (E-E_k)^{-1}, \end{aligned} \tag{3.10}$$

There are singularities at $E = E_k$ along the path of integration, which can be avoided by using *complex energy*:

$$E \longrightarrow E + is \tag{3.11}$$

where we take the limit $s \to 0^+$. Applying this concept to (3.10), we obtain

$$\mathrm{Tr}\left(\mathbb{G}(E)\right) = \lim_{s\to 0^+} \sum_k (E+is-E_k)^{-1} = \lim_{s\to 0^+} \sum_k \frac{E-E_k-is}{(E-E_k)^2+s^2}. \tag{3.12}$$

At the poles of (3.12), the real part of the GF is *singular*, while an evaluation of the imaginary part gives

$$\mathrm{Im}\left(\mathrm{Tr}\left(\mathbb{G}(E)\right)\right) = \lim_{s\to 0^+} \sum_k \frac{-s}{(E-E_k)^2+s^2}. \tag{3.13}$$

We wish to relate the right-hand side of (3.13) to better known functions. First, we consider the discrete summation. For $k = N$, we have

$$\lim_{s\to 0^+} \frac{-s}{(E-E_N)^2+s^2} = \begin{cases} -\infty, & E = E_N, \\ 0, & E \neq E_N. \end{cases} \tag{3.14}$$

For the continuous band, centered at $E = E_N$ and of width $2c$, we have

$$\lim_{s\to 0^+} \int_{E_N-c}^{E_N+c} \frac{-s\,dE}{(E-E_N)^2+s^2} = \lim_{s\to 0^+} \left[\tan^{-1}\left(\frac{-c}{s}\right) - \tan^{-1}\left(\frac{c}{s}\right)\right] = -\pi. \quad (3.15)$$

If we contrast (3.14) and (3.15) with the Dirac δ-function,

$$\delta(E-E_N) = \begin{cases} +\infty, & E = E_N, \\ 0, & E \neq E_N \end{cases} \quad (3.16)$$

and

$$\int_{-\infty}^{\infty} \delta(E-E_N)\,dE = 1, \quad (3.17)$$

we see that

$$\lim_{s\to 0^+} \frac{-s}{(E-E_N)^2+s^2} = -\pi\delta(E-E_N). \quad (3.18)$$

Substituting (3.18) into (3.13), we find

$$-\frac{1}{\pi}\,\mathrm{Im}\,(\mathrm{Tr}\,(\mathbb{G}(E))) = \sum_k \delta(E-E_k), \quad (3.19)$$

for which the right-hand side defines the *total density of states*, $\rho(E)$, via[1]

$$\rho(E)\,dE = -\frac{1}{\pi}\,\mathrm{Im}\,(\mathrm{Tr}\,[\mathbb{G}(E)])\,dE. \quad (3.20)$$

Since the trace of an operator is independent of the basis, (3.20) will hold with respect to the *atomic orbital* (AO) states. In particular, we define the *local density of states* (LDOS) at site n by

$$\rho_n(E) = -\frac{1}{\pi}\,\mathrm{Im}\,(\langle n|\,\mathbb{G}(E)\,|n\rangle) = -\frac{1}{\pi}\,\mathrm{Im}\,[G(n,n;E)]. \quad (3.21)$$

When (3.21) applies to a site located at an endpoint, it is called a *surface density of states* (SDOS).

[1]The DOS is defined only over the allowed energy spectrum. When this spectrum is discrete, the measure of the spectrum is weighted by a δ-function distribution, which is often included in the DOS, even when the measure is otherwise suppressed on both sides, to indicate the discreteness of the eigenenergies.

3.3 Causal-Surface Green-Function Technique

Recently, Pendry *et al.* [91] have developed a powerful *numerical* technique for approximating the surface GF of multi-dimensional systems by recursively adding mesh sites to the system from an initial internal seed site. We shall be interested in following some parts of this methodology to develop the one-dimensional surface GF into a form from which we can extract *analytic* results.

The system is defined in terms of regular mesh sites, which are initially considered isolated from each other. The mesh is chosen, so that the on-site Hamiltonian elements are known for each isolated site, while the interaction terms are zero. The seed site (labeled 1) is composed of a single isolated site,

$$G_1(1,1) = (E - H_{11})^{-1}, \tag{3.22}$$

where $H_{mn} = \langle m|\,\mathbb{H}\,|n\rangle$. Here, and henceforth, we shall suppress the E dependence of the GF for brevity, except where needed.

The next step is to modify the system by adding in a single bond to an adjoining mesh site (labeled 2), by setting $V_{12} = H_{12}$ and $V_{21} = H_{21}$. The result is a two-site *cluster* embedded in the mesh of isolated sites.

Applying the Dyson equation, (3.8), we obtain

$$G_2(1,1) = G_1(1,1) + G_1(1,1)H_{12}G_2(2,1), \tag{3.23}$$

since $G_1(1,2) = 0$. Equation (3.23) is still in terms of an element of the two-site GF, which can be written as

$$G_2(2,1) = G_1(2,2)H_{21}G_2(1,1). \tag{3.24}$$

Inserting (3.24) into (3.23) yields

$$G_2(1,1) = G_1(1,1) + G_1(1,1)H_{12}G_1(2,2)H_{21}G_2(1,1), \tag{3.25}$$

which we iteratively expand into a geometric series and, by *assuming* convergence occurs, we solve for the series,

$$\begin{aligned} G_2(1,1) &= G_1(1,1) + G_1(1,1)\left[H_{12}G_1(2,2)H_{21}G_1(1,1)\right] \\ &\quad + G_1(1,1)\left[H_{12}G_1(2,2)H_{21}G_1(1,1)\right]\left[H_{12}G_1(2,2)H_{21}G_1(1,1)\right] \\ &\quad + \cdots \\ &= \frac{G_1(1,1)}{1 - H_{12}G_1(2,2)H_{21}G_1(1,1)}. \end{aligned} \tag{3.26}$$

Using this solution in (3.24), we have

$$G_2(2,1) = \frac{G_1(2,2)H_{21}G_1(1,1)}{1 - H_{12}G_1(2,2)H_{21}G_1(1,1)}. \tag{3.27}$$

Hence, we have obtained two of the non-zero elements for the points in the two-site cluster in terms of the isolated site GFs. The remaining two elements are found using the same algorithm, namely,

$$G_2(2,2) = G_1(2,2) + G_1(2,2)H_{21}G_2(1,2), \tag{3.28}$$

and

$$G_2(1,2) = G_1(1,1)H_{12}G_2(2,2), \tag{3.29}$$

are obtained by application of (3.8), which we combine into an implicitly defined equation,

$$G_2(2,2) = G_1(2,2) + G_1(2,2)H_{21}G_1(1,1)H_{12}G_2(2,2), \tag{3.30}$$

which we iterate into a geometric series and solve,

$$\begin{aligned} G_2(2,2) &= G_1(2,2) + G_1(2,2)\left[H_{21}G_1(2,2)H_{21}G_1(1,1)\right] \\ &\quad + G_1(1,1)\left[H_{12}G_1(2,2)H_{21}G_1(1,1)\right]\left[H_{12}G_1(2,2)H_{21}G_1(1,1)\right] \\ &\quad + \cdots \\ &= \frac{G_1(2,2)}{1 - H_{12}G_1(2,2)H_{21}G_1(1,1)}. \end{aligned} \tag{3.31}$$

With the aid of (3.29), this solution yields the fourth GF element of our two-site cluster,

$$G_2(1,2) = \frac{G_1(2,2)H_{12}G_1(1,1)}{1 - H_{12}G_1(2,2)H_{21}G_1(1,1)}. \tag{3.32}$$

This algorithm now generalizes for obtaining elements of $\mathbb{G}_{N+1}$ in terms of the previously known $\mathbb{G}_N$ Greenian elements, where the system is being modified by adding a direct connection between sites l and m. Once we have at least a four-site cluster, however, it becomes possible in higher dimensions that the mesh connection we are adding is between two sites already in the cluster. In such a case, there may already be non-zero elements $G_N(l,m)$ and $G_N(m,l)$. To keep track of these potential interaction, we introduce the matrices

$$h = \begin{bmatrix} 0 & H_{lm} \\ H_{ml} & 0 \end{bmatrix}, \qquad g = \begin{bmatrix} G_N(l,l) & G_N(l,m) \\ G_N(m,l) & G_N(m,m) \end{bmatrix}, \tag{3.33}$$

whose components are considered to occupy the l and m rows and columns, i.e., $g_{ab} = G_N(a,b)$ when $a,b \in \{l,m\}$. Keeping this notation for matrix products of h and g, we can develop the generalized series for the GF, i.e.,

$$\begin{aligned} G_{N+1}(i,j) &= G_N(i,j) + \sum_{a\in\{l,m\}} \sum_{b\in\{l,m\}} [G_N(i,a)h_{ab}G_N(b,j) \\ &\quad + G_N(i,a)[ghg]_{ab}G_N(b,j) + G_N(i,a)[ghghg]_{ab}G_N(b,j) \\ &\quad + \cdots] \\ &= G_N(i,j) + \sum_{a\in\{l,m\}} \sum_{b\in\{l,m\}} G_N(i,a)[h^{-1} - g]^{-1}_{ab}G_N(b,j), \end{aligned} \tag{3.34}$$

where the summation of the series is shown in Appendix C.

The inverted matrix can be obtained from the components of h and g. We begin

by inverting h,

$$h^{-1} = \frac{\mathrm{adj}(h)}{\det(h)} = \frac{1}{-H_{lm}H_{ml}} \begin{bmatrix} 0 & -H_{lm} \\ -H_{ml} & 0 \end{bmatrix} = \begin{bmatrix} 0 & \frac{1}{H_{ml}} \\ \frac{1}{H_{lm}} & 0 \end{bmatrix}. \tag{3.35}$$

Subtracting g from this yields,

$$h^{-1} - g = \begin{bmatrix} -G_N(l,l) & \frac{1}{H_{ml}} - G_N(l,m) \\ \frac{1}{H_{lm}} - G_N(m,l) & -G_N(m,m) \end{bmatrix}, \tag{3.36}$$

which we invert to obtain

$$\left[h^{-1} - g\right]^{-1} = \frac{1}{\Delta} \begin{bmatrix} -G_N(m,m) & G_N(l,m) - \frac{1}{H_{ml}} \\ G_N(m,l) - \frac{1}{H_{lm}} & -G_N(l,l) \end{bmatrix}, \tag{3.37}$$

where

$$\begin{aligned} \Delta &= G_N(l,l)G_N(m,m) \\ &\quad - \left(G_N(l,m) - \frac{1}{H_{ml}}\right)\left(G_N(m,l) - \frac{1}{H_{lm}}\right). \end{aligned} \tag{3.38}$$

Since this method relies heavily on the convergence of products of GFs, it is necessary to keep $G_N(l,l)H_{lm}G_N(m,m)H_{ml}$ from exceeding unity. However, since $\mathbb{G}_N$ is singular at it's eigenenergies, every non-zero interaction will produce regions in the energy spectrum where the algorithm will be unstable. In particular, Pendry's method cannot access the DOS for a given system, as that is precisely where it breaks down.

3.4 Recursive Green-Function Approach

Let us begin with the Greenian for a series of isolated atoms beginning at site M and continuing to the right up to site N. Let $H_{nn} = \alpha_n$ be the site energy for the atom at site n. In the TB approximation, each site contributes a single AO state, $|n\rangle$, which form an orthonormal set. Thus, projecting the Greenian onto these states gives a spatially-based, i.e., at the atomic sites, description of the system. We label the Greenian by the first and last atom *connected* in the chain. Since the initial chain contains only isolated atoms, we have

$$\mathbb{G}_{M,M} = \sum_{n=M}^{N} \frac{|n\rangle \langle n|}{E - \alpha_n}. \tag{3.39}$$

Of note, this initial Greenian has the following relevant elements

$$\begin{aligned} G_{M,M}(M,M) &= \langle M| \mathbb{G}_{M,M} |M\rangle = (E - \alpha_M)^{-1}, \\ G_{M,M}(M+1,M+1) &= \langle M+1| \mathbb{G}_{M,M} |M+1\rangle = (E - \alpha_{M+1})^{-1}, \\ G_{M,M}(M+1,M) &= G_{M,M}(M,M+1) = 0. \end{aligned} \tag{3.40}$$

To generate the full arbitrary chain, we take the current system and increase the connected chain portion by one site by adding a bond between the chain and the next isolated atom (Fig. 3.1). Iterating this process allows us to generate a chain of any finite length, and the convergence of this iterated function system will yield results for the semi-infinite chain.

The first step is to introduce a bond between the M and $M+1$ sites, viz.,

$$V_{M+1} = \beta_{M,M+1} \left[|M\rangle \langle M+1| + |M+1\rangle \langle M| \right]. \tag{3.41}$$

To obtain the new GF, we apply (3.8),

$$\mathbb{G}_{M,n+1} = \mathbb{G}_{M,n} + \mathbb{G}_{M,n} V_{n+1} \mathbb{G}_{M,n+1}, \tag{3.42}$$

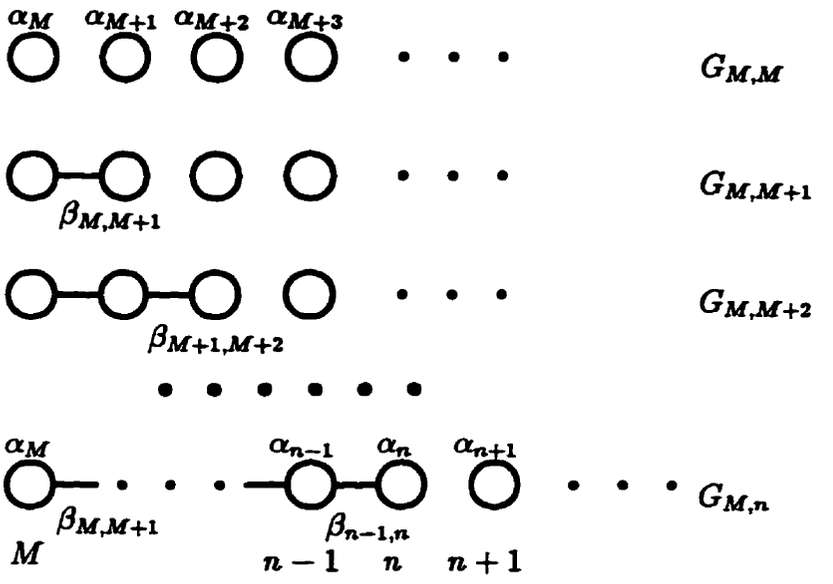

Fig. 3.1: Building a linear chain by adding a bond at each iteration.

to (3.39) with (3.41) and $n = M$.

At this point, we note that there are *two* surface atoms, one will be fixed at M and the other at the site we have just bonded to the chain. We shall concentrate on the surface site being added at each iteration. Hence, the surface element of the GF is calculated via

$$\begin{aligned} & G_{M,M+1}(M+1,M+1) \\ & \quad = G_{M,M}(M+1,M+1) \\ & \qquad + G_{M,M}(M+1,M)\beta_{M,M+1}G_{M,M+1}(M+1,M+1) \\ & \qquad + G_{M,M}(M+1,M+1)\beta_{M,M+1}G_{M,M+1}(M,M+1) \\ & \quad = G_{M,M}(M+1,M+1) \\ & \qquad + G_{M,M}(M+1,M+1)\beta_{M,M+1}G_{M,M+1}(M,M+1), \end{aligned} \tag{3.43}$$

which is equivalent to (3.23). To solve (3.43), we follow the Pendry algorithm, and

so require

$$\begin{aligned} & G_{M,M+1}(M, M+1) \\ & \quad = G_{M,M}(M, M+1) \\ & \qquad + G_{M,M}(M, M)\beta_{M,M+1}G_{M,M+1}(M+1, M+1) \\ & \qquad + G_{M,M}(M, M+1)\beta_{M,M+1}G_{M,M+1}(M, M+1) \\ & \quad = G_{M,M}(M, M)\beta_{M,M+1}G_{M,M+1}(M+1, M+1). \end{aligned} \tag{3.44}$$

Whence, inserting(3.44) in (3.43) yields

$$\begin{aligned} & G_{M,M+1}(M+1, M+1) \\ & \quad = G_{M,M}(M+1, M+1) \\ & \qquad + G_{M,M}(M+1, M+1)\beta_{M,M+1}^2 G_{M,M}(M, M)G_{M,M+1}(M+1, M+1), \end{aligned} \tag{3.45}$$

which implicitly defines the GF at the new surface. Here, we depart from the Pendry algorithm. Instead of expanding into a geometric series, we solve directly for the modified GF, and so do not introduce any convergence requirements at this stage. Solving (3.45), we obtain

$$\begin{aligned} G_{M,M+1}(M+1, M+1) &= \frac{G_{M,M}(M+1, M+1)}{1 - \beta_{M,M+1}^2 G_{M,M}(M+1, M+1)G_{M,M}(M, M)} \\ &= \frac{1}{G_{M,M}(M+1, M+1)^{-1} - \beta_{M,M+1}^2 G_{M,M}(M, M)} \\ &= \frac{1}{(E - \alpha_{M+1}) - \dfrac{\beta_{M,M+1}^2}{E - \alpha_M}}. \end{aligned} \tag{3.46}$$

Following the above procedure, the n^{th} iteration is applied to the $M, n-1$ chain

to give the required elements of $\mathbb{G}_{M,n}$, namely,

$$\begin{aligned} G_{M,n}(n,n) &= G_{M,n-1}(n,n) + G_{M,n-1}(n,n-1)\beta_{n-1,n}G_{M,n}(n,n) \\ &\quad + G_{M,n-1}(n,n)\beta_{n-1,n}G_{M,n}(n-1,n) \\ &= G_{M,n-1}(n,n) + G_{M,n-1}(n,n)\beta_{n-1,n}G_{M,n}(n-1,n), \end{aligned} \tag{3.47}$$

and

$$\begin{aligned} G_{M,n}(n-1,n) &= G_{M,n-1}(n-1,n) + G_{M,n-1}(n-1,n-1)\beta_{n-1,n}G_{M,n}(n,n) \\ &\quad + G_{M,n-1}(n-1,n)\beta_{n-1,n}G_{M,n}(n-1,n) \\ &= G_{M,n-1}(n-1,n-1)\beta_{n-1,n}G_{M,n}(n,n). \end{aligned} \tag{3.48}$$

The one-dimensional TB chain has the property that, unless a direct bond exists, a site will be isolated from the rest of the chain, which means that there can be no indirect interaction term in the $\mathbb{G}_{M,n-1}$ Greenian. This allows us to proceed exactly as we did for the two-site GFs, so that

$$\begin{aligned} G_{M,n}(n,n) &= G_{M,n-1}(n,n) \\ &\quad + G_{M,n-1}(n,n)\beta_{n-1,n}G_{M,n-1}(n-1,n-1)\beta_{n-1,n}G_{M,n}(n,n), \end{aligned} \tag{3.49}$$

which, since the $G_{M,n-1}(n,n)$ GF is for an isolated atom, yields a solution dependent only on the surface GF of the previous iteration, whereby,

$$\begin{aligned} G_{M,n}(n,n) &= \frac{G_{M,n-1}(n,n)}{1-\beta_{n-1,n}^2 G_{M,n-1}(n,n)G_{M,n-1}(n-1,n-1)} \\ &= \frac{1}{G_{M,n-1}(n,n)^{-1} - \beta_{n-1,n}^2 G_{M,n-1}(n-1,n-1)} \\ &= \frac{1}{(E-\alpha_n) - \beta_{n-1,n}^2 G_{M,n-1}(n-1,n-1)}. \end{aligned} \tag{3.50}$$

Thus, the process of constructing the surface GF can be considered as an *iterating function* (IF). Again, solutions to (3.50) do not require the convergence conditions

which appear in the Pendry algorithm, so we have complete access to the entire energy spectrum. An alternate approach to derive this result is given in Appendix D.

The form of the IF in (3.50) generates, in fact, a CF

$$\begin{aligned} G_{M,n}(n,n) &= \cfrac{1}{(E-\alpha_n) - \cfrac{\beta^2_{n-1,n}}{(E-\alpha_{n-1}) - \beta^2_{n-2,n-1} G_{M,n-2}(n-2,n-2)}} \\ &= \cfrac{1}{(E-\alpha_n) - \cfrac{\beta^2_{n-1,n}}{(E-\alpha_{n-1}) - \ddots - \cfrac{\beta^2_{M+1,M+2}}{(E-\alpha_{M+1}) - \cfrac{\beta^2_{M,M+1}}{(E-\alpha_M)}}}}, \end{aligned} \tag{3.51}$$

which can be represented in standard CF notation [92]

$$\frac{1}{a_1} \mathop{\mathcal{K}}_{i=1}^{n-M+1} (a_i; b_i) = \cfrac{a_1}{b_1 + \cfrac{a_2}{b_2 + \ddots + \cfrac{a_{n-M}}{b_{n-M} + \cfrac{a_{n-M+1}}{b_{n-M+1}}}}}, \tag{3.52}$$

where the components for the TB system are

$$a_i = -\beta^2_{n+1-i,n+2-i}, \qquad b_i = E - \alpha_{n+1-i}. \tag{3.53}$$

Note that $a_1 = -\beta^2_{n,n+1}$, which is zero for $G_{M,n}(n,n)$, appears in the definition of the CF, but is formally divided out. Equivalently, we can use the non-zero value of $\beta_{n,n+1}$, which is introduced at the $(n+1)^{\text{st}}$ iteration. Again, division by a_1 ensures that this term does not actually appear in the $G_{M,n}(n,n)$ equation.

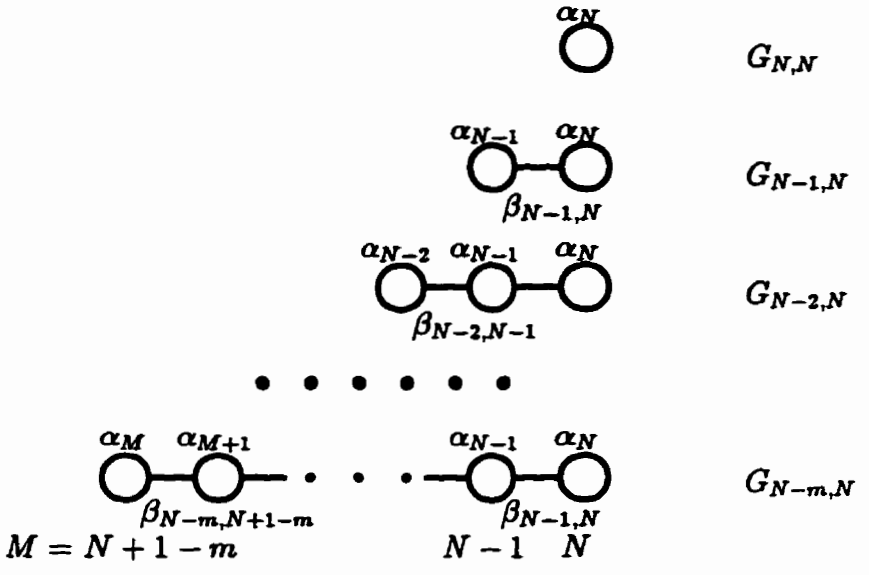

Fig. 3.2: Sequence of linear chains extending to the left from a surface at site N.

So far, we have been developing the surface GF at the *dynamic* end of our recursion process. We now turn to the surface located at the beginning of the chain and consider it's influence on the GF. Taking $n = N$ fixed, and $M = N + 1 - m$ for $m \geq 1$, we have a chain of atomic sites of m atoms starting at N and moving to the left.

Treating $m = N + 1 - M$ as the variable, we can define the IF for the surface GF as

$$G_{N+1-m,N}(N,N) = -\beta_{N,N+1}^{-2} \overset{m}{\underset{i=1}{\mathcal{K}}} \left(-\beta_{N+1-i,N+2-i}^2; E - \alpha_{N+1-i}\right), \tag{3.54}$$

which forms the sequence of chain GFs shown in Fig. 3.2. Letting $m \to \infty$, we obtain the semi-infinite chain extending to the left with surface at N, i.e.,

$$\begin{aligned} G_{N^-}(N,N) &= \lim_{m\to\infty} G_{N+1-m,N}(N,N) \\ &= -\beta_{N,N+1}^{-2} \overset{\infty}{\underset{i=1}{\mathcal{K}}} \left(-\beta_{N+1-i,N+2-i}^2; E - \alpha_{N+1-i}\right), \end{aligned} \tag{3.55}$$

so long as the GFs in (3.54) converge as $m \to \infty$. Thus, we are interested in the conditions for which the sequence

$$\{G_{N+1-m,N}(N,N)\}_{m=0}^{\infty} \tag{3.56}$$

of CFs converges.

Equations (3.54) and (3.55) give the surface GF for chains extending to the *left* of site N. To obtain the GF at a surface with the crystal to the *right*, we repeat the process for $m < N$, whence (3.50) becomes

$$G_{m,N}(m,m) = \frac{1}{E - \alpha_m - \beta_{m,m+1}^2 G_{m+1,N}(m+1,m+1)}, \tag{3.57}$$

yielding the CF

$$\begin{aligned} G_{m,N}(m,m) &= \cfrac{1}{(E-\alpha_m) - \cfrac{\beta_{m,m+1}^2}{(E-\alpha_{m+1}) - \ddots \; - \cfrac{\beta_{N-2,N-1}^2}{(E-\alpha_{N-1}) - \cfrac{\beta_{N-1,N}^2}{(E-\alpha_N)}}}}, \\ &= \frac{1}{a_1} \mathop{\mathcal{K}}_{i=1}^{N-m+1} (a_i; b_i) \end{aligned} \tag{3.58}$$

with

$$a_i = -\beta_{m-2+i,m-1+i}^2, \qquad b_i = E - \alpha_{m-1+i}. \tag{3.59}$$

Fixing $m = M$ and defining $n = N + 1 - M$ as the variable, (3.58) becomes

$$G_{M,N-1+n}(M,M) = -\beta_{M-1,M}^{-2} \mathop{\mathcal{K}}_{i=1}^{n} \left(-\beta_{M-2+i,M-1+i}^2; E - \alpha_{M-1+i}\right), \tag{3.60}$$

for a finite chain, while letting $n \to \infty$ gives

$$\begin{aligned} G_{M+}(M,M) &= \lim_{n\to\infty} G_{M,N-1+n}(M,M) \\ &= -\beta_{M-1,M}^{-2} \mathop{\mathcal{K}}_{i=1}^{\infty} \left(-\beta_{M-2+i,M-1+i}^2; E - \alpha_{M-1+i}\right), \end{aligned} \tag{3.61}$$

for the semi-infinite chain to the right.

We are also able to calculate the GF through the chain, i.e.,

$$G_{M,n}(M,n) = \beta_{M-1,M}^{-1} \prod_{m=M}^{n} \beta_{m-1,m} G_{M,m}(m,m). \tag{3.62}$$

We show this by induction. The $n = M+1$ case is given in (3.44). If we now assume (3.62) holds up to $n-1$, then

$$\begin{aligned} G_{M,n}(M,n) &= G_{M,n-1}(M,n) + G_{M,n-1}(M,n-1)\beta_{n-1,n}G_{M,n}(n,n) \\ &\quad + G_{M,n-1}(M,n)\beta_{n-1,n}G_{M,n}(n-1,n) \\ &= G_{M,n-1}(M,n-1)\beta_{n-1,n}G_{M,n}(n,n) \\ &= \left[\beta_{M-1,M}^{-1} \prod_{m=M}^{n-1} \beta_{m-1,m} G_{M,m}(m,m)\right] \beta_{n-1,n}G_{M,n}(n,n) \\ &= \beta_{M-1,M}^{-1} \prod_{m=M}^{n} \beta_{m-1,m} G_{M,m}(m,m), \end{aligned} \tag{3.63}$$

as required.

Chapter 4

Continued Fractions

4.1 Basic Concepts

CF concepts have been in existence at least since Euclid's report from c. 290 B.C. of the method of determining the *greatest common divisor* of two integers [93].

We develop the mathematical concepts for CFs as a generalization of those used for *series* following [92]. Recall that, for a sequence of complex numbers $\{a_n\}$, the series is defined as

$$\sum_{n=1}^{\infty} a_n = a_1 + a_2 + \cdots + a_n + \cdots, \tag{4.1}$$

with the *partial sums* of (4.1) defined by

$$P_m = \sum_{n=1}^{m} a_n = a_1 + a_2 + \cdots + a_m. \tag{4.2}$$

Convergence of the series (4.1) is defined as the convergence of the sequence of partial sums $\{P_m\}$ to a complex number P, i.e.,

$$P = \lim_{m \to \infty} P_m = \sum_{n=1}^{\infty} a_n. \tag{4.3}$$

We define similar concepts for CFs. First, consider the sequence $\{a_n\}$, with all $a_n \neq 0$, and define the CF by

$$\mathop{\mathcal{K}}_{n=1}^{\infty}(a_n;1) = \cfrac{a_1}{1+\cfrac{a_2}{1+\cfrac{a_3}{1+\ddots}}}. \tag{4.4}$$

We also can define another type of CF for *any* sequence $\{b_n\}$ as

$$\mathop{\mathcal{K}}_{n=1}^{\infty}(1;b_n) = \cfrac{1}{b_1+\cfrac{1}{b_2+\cfrac{1}{b_3+\ddots}}}. \tag{4.5}$$

These two types of CFs can be considered elements of two one-dimensional subspaces of a broader two-dimensional solution space for the general CF. Given two sequences, $\{a_n\}$ with $a_n \neq 0$ and $\{b_n\}$, we define

$$\mathop{\mathcal{K}}_{n=1}^{\infty}(a_n;b_n) = \cfrac{a_1}{b_1+\cfrac{a_2}{b_2+\cfrac{a_3}{b_3+\ddots}}}. \tag{4.6}$$

The *approximants* to (4.6)are defined by

$$K_m = \mathop{\mathcal{K}}_{n=1}^{m}(a_n;b_n), \tag{4.7}$$

and *convergence* of (4.6) is defined via the convergence of the sequence $\{K_m\}$ to a complex number,

$$K = \lim_{m\to\infty} K_m, \tag{4.8}$$

which leads to the formal definition of a CF [92]

Definition 1 *A continued fraction is an ordered pair*

$$[(\{a_n\},\{b_n\}),\{K_n\}], \tag{4.9}$$

where $\{a_n\}$ *and* $\{b_n\}$ *are given sequences of complex numbers* $a_n \neq 0$, *and* $\{K_n\}$ *is the sequence of extended complex numbers, given by*

$$K_n = S_n(0), \qquad n = 1, 2, \ldots, \tag{4.10}$$

where $S_0(w) = w$ *and*

$$S_n(w) = S_{n-1}\left(\frac{a_n}{b_n + w}\right), \qquad n = 1, 2, \ldots. \tag{4.11}$$

The *continued fraction algorithm* is the function $\mathcal{K}$ mapping a pair of sequences $(\{a_n\}, \{b_n\})$ onto the sequence $\{K_n\}$ defined by (4.10) and (4.11). If this sequence converges to K, we write

$$K = \mathop{\mathcal{K}}_{n=1}^{\infty}(a_n; b_n), \tag{4.12}$$

if it does not converge, the right-hand side of (4.12) still provides the appropriate notation for discussing CFs.

The relation between three-term recursion relations and CFs has also been known for a considerable length of time, first appearing around 1150 in Bhascara II's *Līlāvatī*, but was not in widespread use until it was rediscovered by Wallis in 1655.

4.2 Pincherle's Theorem

In letting the chain become infinite to the left, convergence of the IF in (3.50) corresponds to the convergence of the CF in (3.55). We are interested in a certain class of systems for which convergence occurs. These systems satisfy a three-term recurrence relation, which allows us to use the results of *Pincherle's Theorem* (PT) [92].

Theorem 4.1 *Given a continued fraction*

$$\mathop{\mathcal{K}}_{n=1}^{\infty}(a_n;b_n) = \cfrac{a_1}{b_1+\cfrac{a_2}{b_2+\ddots}}, \tag{4.13}$$

whose terms satisfy the three-term recurrence relation

$$C_n = b_nC_{n-1} + a_nC_{n-2}, \qquad \forall n, \tag{4.14}$$

and if $\{Y_n\}$ *and* $\{Z_n\}$ *are linearly independent solutions to (4.14) such that*

$$\lim_{n\to\infty}\frac{Y_n}{Z_n} = 0, \tag{4.15}$$

then

$$\mathop{\mathcal{K}}_{n=1}^{\infty}(a_n;b_n) = -\frac{Y_0}{Y_{-1}}. \tag{4.16}$$

Proof:

Let us define

$$S_n(w) = \cfrac{a_1}{b_1+\cfrac{a_2}{b_2+\ddots+\cfrac{a_{n-1}}{b_{n-1}+\cfrac{a_n}{b_n+w}}}}. \tag{4.17}$$

In particular, note that

$$S_1(w) = \frac{a_1}{b_1+w} \tag{4.18}$$

and

$$S_n(w) = S_{n-1}\left(\frac{a_n}{b_n+w}\right). \tag{4.19}$$

Let us also define

$$\begin{aligned} A_{-1} &= 1, \qquad A_0 = 0, \\ B_{-1} &= 0, \qquad B_0 = 1, \end{aligned} \tag{4.20}$$

and generate the sequences $\{A_n\}$ and $\{B_n\}$ for $n \geq 1$ via (4.14) and (4.20). Hence,

$$\begin{aligned} A_1 &= b_1 A_0 + a_1 A_{-1} = a_1, \\ B_1 &= b_1 B_0 + a_1 B_{-1} = b_1, \end{aligned} \tag{4.21}$$

so that

$$\frac{A_1 + A_0 w}{B_1 + B_0 w} = \frac{a_1}{b_1 + w} = S_1(w), \tag{4.22}$$

via (4.18), (4.20), and (4.21). In general,

$$\begin{aligned} A_n &= b_n A_{n-1} + a_n A_{n-2}, \\ B_n &= b_n B_{n-1} + a_n B_{n-2}. \end{aligned} \tag{4.23}$$

Using induction, we suppose we have

$$\frac{A_{n-1} + A_{n-2} w}{B_{n-1} + B_{n-2} w} = S_{n-1}(w), \tag{4.24}$$

so, for $n \geq 1$,

$$\begin{aligned} \frac{A_n + A_{n-1} w}{B_n + B_{n-1} w} &= \frac{(b_n A_{n-1} + a_n A_{n-2}) + A_{n-1} w}{(b_n B_{n-1} + a_n B_{n-1}) + B_{n-1} w} \\ &= \frac{(b_n + w) A_{n-1} + A_{n-2} a_n}{(b_n + w) B_{n-1} + B_{n-2} a_n} \\ &= \frac{A_{n-1} + A_{n-1} \dfrac{a_n}{b_n + w}}{B_{n-1} + B_{n-2} \dfrac{a_n}{b_n + w}} \\ &= S_{n-1}\left(\frac{a_n}{b_n + w}\right) \\ &= S_n(w), \end{aligned} \tag{4.25}$$

by using (4.19), (4.23), and (4.24). From (4.22) and (4.25), we conclude that

$$S_n(w) = \frac{A_n + A_{n-1} w}{B_n + B_{n-1} w}, \qquad \forall n \geq 1. \tag{4.26}$$

The choice $w = 0$ allows us to obtain the approximants to (4.13), i.e.,

$$S_m(0) = \frac{A_m}{B_m} = \mathop{\mathcal{K}}_{n=1}^{m} (a_n; b_n)\,. \tag{4.27}$$

Since $\{A_n\}$ and $\{B_n\}$ satisfy (4.14), each can be written as a linear combinations of $\{Y_n\}$ and $\{Z_n\}$, viz.,

$$\begin{aligned} A_n &= \alpha_1 Y_n + \alpha_2 Z_n, \\ B_n &= \beta_1 Y_n + \beta_2 Z_n. \end{aligned} \tag{4.28}$$

Applying (4.28) to (4.20), we find

$$\begin{aligned} 0 = A_0 = \alpha_1 Y_0 + \alpha_2 Z_0 \quad &\Rightarrow \quad \alpha_2 = -\alpha_1 \frac{Y_0}{Z_0}, \\ 1 = A_{-1} = \alpha_1 Y_{-1} + \alpha_2 Z_{-1} \quad &\Rightarrow \quad Z_0 = \alpha_1 Y_{-1} Z_0 - \alpha_1 Y_0 Z_{-1}. \end{aligned} \tag{4.29}$$

Since $\{Y_n\}$ and $\{Z_n\}$ are linearly independent, we must have the Wronskian

$$Y_{-1} Z_0 - Y_0 Z_{-1} \neq 0. \tag{4.30}$$

Consequently,

$$\alpha_1 = \frac{Z_0}{Y_{-1} Z_0 - Y_0 Z_{-1}}, \qquad \alpha_2 = -\frac{Y_0}{Y_{-1} Z_0 - Y_0 Z_{-1}}. \tag{4.31}$$

Similarly,

$$\begin{aligned} 0 = B_{-1} = \beta_1 Y_{-1} + \beta_2 Z_{-1} \quad &\Rightarrow \quad \beta_2 = -\beta_1 \frac{Y_{-1}}{Z_{-1}}, \\ 1 = B_0 = \beta_1 Y_0 + \beta_2 Z_0 \quad &\Rightarrow \quad Z_{-1} = \beta_1 Y_0 Z_{-1} - \beta_1 Y_0 Z_{-1}, \end{aligned} \tag{4.32}$$

which gives

$$\beta_1 = -\frac{Z_{-1}}{Y_{-1} Z_0 - Y_0 Z_{-1}}, \qquad \beta_2 = \frac{Y_{-1}}{Y_{-1} Z_0 - Y_0 Z_{-1}}. \tag{4.33}$$

Thus, substituting (4.31) and (4.33) into (4.28), and the result into (4.27), yields

$$S_m(0) = \frac{Z_0 Y_m - Y_0 Z_m}{-Z_{-1} Y_m + Y_{-1} Z_m}. \tag{4.34}$$

Dividing numerator and denominator by Z_m and recalling (4.15), we have

$$\lim_{m\to\infty} S_m(0) = \lim_{m\to\infty} \frac{Z_0\dfrac{Y_m}{Z_m} - Y_0}{-Z_{-1}\dfrac{Y_m}{Z_m} + Y_{-1}} = -\frac{Y_0}{Y_{-1}}. \tag{4.35}$$

Finally, using (4.27), we obtain (4.16). □

Corollary 4.1 *The finite continued fraction*

$$\mathop{\mathcal{K}}_{n=1}^{m}(a_n; b_n) = \frac{Z_0 Y_m - Y_0 Z_m}{-Z_{-1}Y_m + Y_{-1}Z_m}, \tag{4.36}$$

when a_n, b_n, Y_n, and Z_n satisfy Pincherle's theorem for the infinite continued fraction.

Proof:

Applying (4.27) to (4.34), yields (4.36). □

4.3 Monatomic Semi-Infinite Chain

To apply the preceding results to the linear monatomic semi-infinite chain to the left, we consider $\alpha_n = \alpha$ and $\beta_{n-1,n} = \beta$ for all $n \leq M$. Inserting these into (3.53), we find that the three-term recurrence relation, (4.14) becomes

$$C_n = (E - \alpha)C_{n-1} - \beta^2 C_{n-2}, \tag{4.37}$$

or

$$\beta^{-1}C_n + \beta C_{n-2} = 2XC_{n-1}, \tag{4.38}$$

where $X = (E - \alpha)/2\beta$.

Two linearly independent solutions are

$$C_n^{\pm} = \beta^n \left(X \pm \sqrt{X^2-1}\right)^n. \tag{4.39}$$

Using (4.39), we have

$$\begin{aligned}
&\beta^{-1}C_n + \beta C_{n-2} \\
&\quad = \beta^{n-1}\left(X \pm \sqrt{X^2-1}\right)^n + \beta^{n-1}\left(X \pm \sqrt{X^2-1}\right)^{n-2} \\
&\quad = \beta^{n-1}\left(X \pm \sqrt{X^2-1}\right)^{n-1}\left[\left(X \pm \sqrt{X^2-1}\right) + \left(X \mp \sqrt{X^2-1}\right)\right] \\
&\quad = \beta^{n-1}\left(X \pm \sqrt{X^2-1}\right)^{n-1} 2X \\
&\quad = 2XC_{n-1},
\end{aligned} \tag{4.40}$$

where we have used the property that

$$\frac{1}{X \pm \sqrt{X^2-1}} = X \mp \sqrt{X^2-1}. \tag{4.41}$$

To satisfy PT, we must choose *minimal* and *dominant* combinations of $C_n^{\pm}$, so that (4.15) is satisfied. We note that

$$\frac{C_n^{\pm}}{C_n^{\mp}} = \left(\frac{X \pm \sqrt{X^2-1}}{X \mp \sqrt{X^2-1}}\right)^n = \left(X \pm \sqrt{X^2-1}\right)^{2n}. \tag{4.42}$$

Therefore, in order to converge to zero, we must choose the minimal solution with the sign opposite to that of X. Hence,

$$Y_n = \begin{cases} \beta^n(X - \sqrt{X^2-1})^n, & X > 0 \\ \beta^n(X + \sqrt{X^2-1})^n, & X < 0 \end{cases} \tag{4.43}$$

$$= \beta^n(X - \mathrm{sgn}(X)\sqrt{X^2-1})^n, \tag{4.44}$$

and

$$Z_n = \beta^n(X + \mathrm{sgn}(X)\sqrt{X^2-1})^n. \tag{4.45}$$

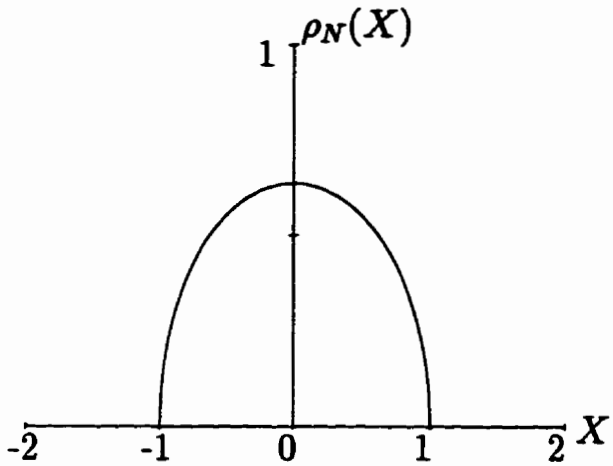

Fig. 4.1: Density of states for linear semi-infinite chain.

Applying PT to (3.55), along with our choice of α_n and $\beta_{n-1,n}$, we have

$$\begin{aligned} G_{M-}(M,M) &= -\beta^{-2}\left(-\frac{Y_0}{Y_{-1}}\right) \\ &= \beta^{-2}\frac{1}{\beta^{-1}\left(X-\mathrm{sgn}(X)\sqrt{X^2-1}\right)^{-1}} \\ &= \beta^{-1}\left[X-\mathrm{sgn}(X)\sqrt{X^2-1}\right]. \end{aligned} \tag{4.46}$$

The LDOS is given by the imaginary part of the GF divided by π via (3.21). Since $G_{M-}(M,M)$ is real for all $|X| \geq 1$, the LDOS at the surface is nonzero only in the band $-1 \leq X \leq 1$, with

$$\rho_{M-}(X) = \frac{1}{\pi}\mathrm{Im}\left[G_{M-}(M,M)\right] = \frac{1}{\pi\beta}\sqrt{1-X^2}, \tag{4.47}$$

which is indeed the correct SDOS for the linear *semi-infinite* chain [94] which is shown in Fig. 4.1.

4.4 Infinite Chain Density of States

Since the GF for the left semi-infinite chain given by (4.46) is independent of M, (3.61) also yields

$$G_{M^+}(M,M) = \beta^{-1}\left[X - \mathrm{sgn}(X)\sqrt{X^2-1}\right], \qquad \forall M. \tag{4.48}$$

We define the Greenian operator, $\mathbb{G}^0$, by the superposition of the Greenians of two noninteracting semi-infinite chains, i.e., $\mathbb{G}_{M^-}$ ($\mathbb{G}_{(M+1)^+}$) for the left- (right-) hand chain, gives

$$\mathbb{G}^0 = \mathbb{G}_{M^-} + \mathbb{G}_{(M+1)^+}. \tag{4.49}$$

Note that, the GFs

$$G^0(n,m) = G_{M^-}(n,m), \qquad \forall n,m \leq M, \tag{4.50}$$

$$G^0(n,m) = G_{(M+1)^+}(n,m), \qquad \forall n,m \geq M+1, \tag{4.51}$$

$$G^0(n,m) = G^0(m,n) = 0, \qquad \forall n \leq M \leq m. \tag{4.52}$$

Using the Dyson equation, (3.8), we attach the two semi-infinite chains via the *bond-projection operator*

$$V = \beta\left[|M\rangle\langle M+1| + |M+1\rangle\langle M|\right]. \tag{4.53}$$

Thus, using (4.52), we have

$$G_\infty(M,M) = G^0(M,M) + \beta G^0(M,M) G_\infty(M+1,M), \tag{4.54}$$

and

$$G_\infty(M+1,M) = \beta G^0(M+1,M+1) G_\infty(M,M), \tag{4.55}$$

so that

$$G_\infty(M,M) = G^0(M,M) + \beta G^0(M,M)\beta G^0(M+1,M+1) G_\infty(M,M). \tag{4.56}$$

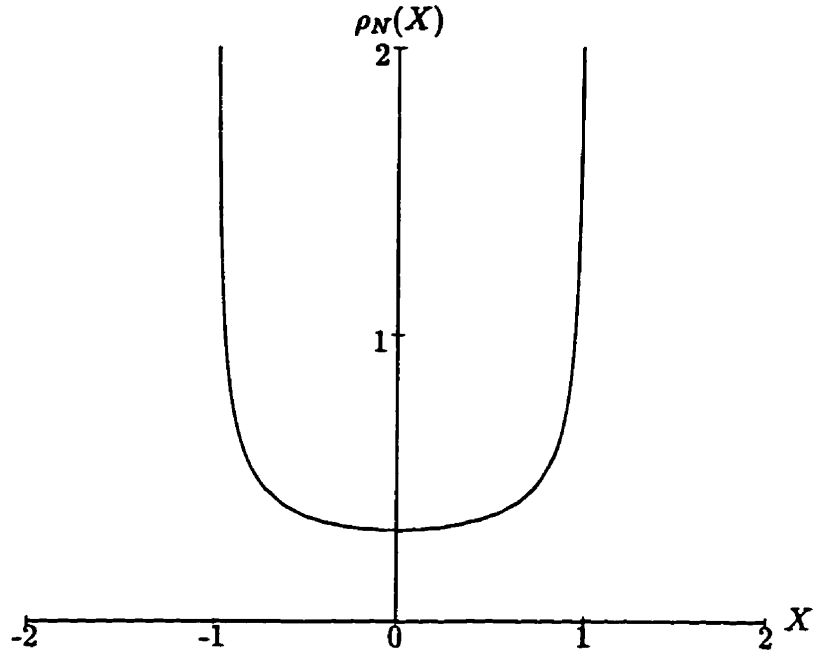

Fig. 4.2: One-dimensional LDOS for infinite linear chain.

Solving (4.56), we obtain

$$\begin{aligned} G_\infty(M,M) &= \frac{G^0(M,M)}{1-\beta^2 G^0(M,M)G^0(M+1,M+1)} \\ &= \beta^{-1}\frac{1}{\beta^{-1}G^0(M,M)^{-1}-\beta G^0(M+1,M+1)} \\ &= \beta^{-1}\frac{1}{\left(X+\mathrm{sgn}(X)\sqrt{X^2-1}\right)-\left(X-\mathrm{sgn}(X)\sqrt{X^2-1}\right)} \\ &= \beta^{-1}\frac{1}{2\mathrm{sgn}(X)\sqrt{X^2-1}}. \end{aligned} \tag{4.57}$$

Again, we find that (4.57) has an imaginary part only in the band $-1 \leq X \leq 1$, so that

$$\rho_M(X) = \frac{1}{\pi}\mathrm{Im}\,[G_\infty(M,M)] = \frac{1}{2\pi\beta\sqrt{1-X^2}}, \tag{4.58}$$

which gives the well-known one-dimensional LDOS for the *infinite* crystal (Fig. 4.2).

Chapter 5

Electrified Solids

5.1 Methodology

Consider a monatomic chain of $N+1$ atoms, whose site energies are $\alpha_n = \alpha$, with the first atom located at site M. When a field of gradient γ is applied to the chain, its site energies are altered to $\alpha_n = \alpha + (n + M - 1)\Gamma$, see Fig. 5.1, where $\Gamma = \gamma a$, a being the lattice spacing. The bond energies are considered to be unaffected, so that $\beta_{n-1,n} = \beta$. We define the *reduced field energy* to be $F = \Gamma/2\beta$.

Since $n = 1$ is the surface atom, where $\alpha_1 = \alpha + M\Gamma$, the application of these α_n and $\beta_{n-1,n}$ in (3.53) to (4.14) yields the three-term recurrence relation for this system, namely,

$$C_n = [E - \alpha - (n + M - 1)\Gamma]\, C_{n-1} - \beta^2 C_{n-2}, \tag{5.1}$$

which we can write as

$$\beta^{-1} C_n + \beta C_{n-2} = 2\,[X - (n + M - 1)F]\, C_{n-1}. \tag{5.2}$$

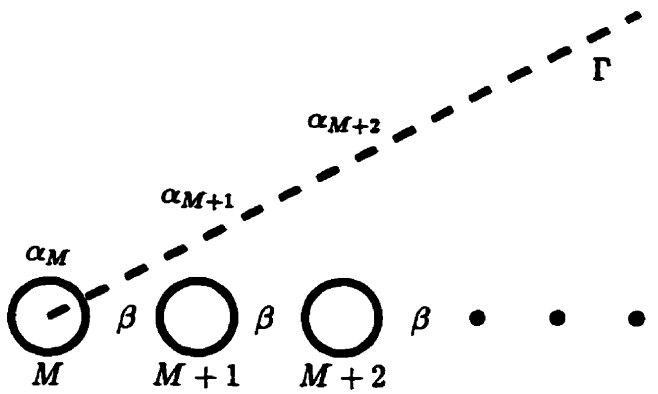

Fig. 5.1: Site energy shift due to applied field.

The solutions to (5.2) are of the form

$$C_n = \beta^n P_{\nu+n+M}(x) \tag{5.3}$$

where

$$x = -F^{-1} \tag{5.4}$$

and

$$\nu = xX, \tag{5.5}$$

$P_\mu(x)$ being any linear combination of the BFs $J_\mu(x)$ and $Y_\mu(x)$.

The large-order asymptotics for $J_\mu(x)$ and $Y_\mu(x)$ [89] are

$$J_\mu(x) \to \frac{1}{\sqrt{2\pi\mu}}\left(\frac{ex}{2\mu}\right)^\mu, \tag{5.6}$$

$$Y_\mu(x) \to \sqrt{2\pi\mu}\left(\frac{ex}{2\mu}\right)^{-\mu}, \tag{5.7}$$

and so, as $n \to \infty$, we see that

$$\lim_{n\to\infty} \frac{J_{\nu+n+M}(x)}{Y_{\nu+n+M}(x)} = 0. \tag{5.8}$$

Thus, by (4.36) and (3.60), we have

$$G_{M,M+N}(M,M) = -\beta^{-1}\frac{J_{\nu+M+N}(x)Y_{\nu+M}(x) - J_{\nu+M}(x)Y_{\nu+M+N}(x)}{J_{\nu+M-1}(x)Y_{\nu+M+N}(x) - J_{\nu+M+N}(x)Y_{\nu+M-1}(x)}, \quad (5.9)$$

for the *finite* chain. Similarly, (4.16) and (3.55) lead to

$$\begin{aligned} G_{M-}(M,M) &= \beta^{-1}\frac{J_{-\nu-M}(-x)}{J_{-\nu-M-1}(-x)} \\ &= \beta^{-1}\frac{e^{i\pi(-\nu-M)}J_{-\nu-M}(x)}{e^{i\pi(-\nu-M-1)}J_{-\nu-M-1}(x)} \\ &= -\beta^{-1}\frac{J_{\nu-M}(-x)}{J_{-\nu-M-1}(x)}, \end{aligned} \quad (5.10)$$

for the *semi-infinite* chain to the left, while (4.16) and (3.61) yield

$$G_{M+}(M,M) = \beta^{-1}\frac{J_{\nu+M}(x)}{J_{\nu+M-1}(x)}, \quad (5.11)$$

for the *semi-infinite* chain to the right.

Following (4.49) through (4.56), we solve for G_∞ using the field-modified results in (5.10) and (5.11),

$$G_\infty(M,M) = -\beta^{-1}\frac{J_{\nu+M}(x)J_{-\nu-M}(x)}{J_{\nu+1+M}(x)J_{-\nu-M}(x) + J_{\nu+M}(x)J_{-\nu-M-1}(x)}. \quad (5.12)$$

However, the denominator in (5.12) is the *Wronskian* [89]

$$W[J_\mu(x), J_{-\mu}(x)] = -\frac{2}{\pi x}\sin\mu\pi, \quad (5.13)$$

so (5.12) reads

$$G_\infty(M,M) = \beta^{-1}\frac{\pi x J_{\nu+M}(x)J_{-\nu-M}(x)}{2\sin(\nu+M)\pi}. \quad (5.14)$$

Having found the GFs for the three cases in question, we can now obtain their LDOS at the site n via (3.21). In all three cases, wherever it is defined, $G(M,M;X)$ is *real valued*, i.e., the imaginary part is zero except, perhaps, at the eigenenergies, X_k, provided by the *poles*, ν_k, of the GF via (5.5).

Since all the poles are *simple*, we invoke the following result from the theory of residues [95] to obtain the imaginary part of the GF at its poles.

Theorem 5.1 *If $f(z) = h(z)/k(z)$, where h and k are holomorphic in a disk about a point $z = a$, with $h(a) \neq 0$, $k(a) = 0$, and $k'(a) \neq 0$, then*

$$\mathrm{Res}\,(f(z); z = a) = \frac{h(a)}{k'(a)}. \tag{5.15}$$

Proof:

Since the residue is defined as the coefficient to the $(z-a)^{-1}$ term in the Laurent expansion of $f(z)$ about a, we have

$$\begin{aligned}\mathrm{Res}\,(f(z); z = a) &= \lim_{z\to a}(z-a)f(z) = \lim_{z\to a}(z-a)\frac{h(z)}{k(z)} \\ &= \lim_{z\to a} h(z)\frac{(z-a)}{k(z)-k(a)} = \frac{h(a)}{k'(a)}.\end{aligned} \tag{5.16}$$

Consider an interval $[X_-, X_+]$ which contains exactly one solution, X_k. If we enclose the pole with a clockwise oriented curve that passes through X_- and X_+, the contour will be equivalent to integrating along the interval twice. Hence, we can write

$$\mathrm{Im}\,G(M, M; X_k) = \pi\mathrm{Res}\,(G(M, M; X); X = X_k)\,. \tag{5.17}$$

□

Using (5.17), we can express the LDOS, at site n, in reduced energy as

$$\rho_n(X) = \sum_k I_k^n(X_k)\delta(X - X_k)/(2\beta), \tag{5.18}$$

where

$$I_k^n(X_k) = 2\beta\mathrm{Res}\,(G(n, n; X); X = X_k)\,. \tag{5.19}$$

is the *intensity energy distribution* at the atom n, which can also be interpreted as the electron *occupation number* of the state k. Since we have one electron associated with each atomic site, (5.19) satisfies the *charge conservation condition*,

$$\sum_k I_k(X_k) = 1. \tag{5.20}$$

We are now in the position to address the LDOS for the above cases separately.

5.2 Finite Chain

The plots of the LDOS at the $n = M = 0$ site of a 100-atom chain are presented in Fig. 5.2 for the various fields indicated. The intensities, $I_k^0(X_k)$, in (5.19) were obtained by using the exact rational polynomial form of (5.9), which can be derived from the Wronskian equations for both numerator and denominator, where the reduced energies, X_k, are provided by the poles of (5.9), i.e., the solutions of

$$J_{\nu_k-1}(x)Y_{\nu_k+99}(x) - J_{\nu_k+99}(x)Y_{\nu_k-1}(x) = 0. \tag{5.21}$$

Figure 5.2a depicts the *discretized* form of the familiar semi-elliptic LDOS for the zero-field case [88]. On applying the small field $F = 0.005$, the band picture of Fig. 5.2b arises, in which the most striking feature is the appearance of the *linear-ramp* region of negative slope covering the lower quarter of the quasi-band. In addition, the quasi-band is rigidly shifted slightly to higher energies, the intensities decaying exponentially beyond the upper-band edge at $X = 1$. Note also, the redistribution of the X_k-values, compared with those in Fig. 5.2a. Increasing the field to $F = 0.01$, the linear-region in Fig. 5.2c now extends over *all* the lower half of the band, and about half its intensities exceed the maximum of those in the semi-elliptic portion. Doubling the field to $F = 0.02$, the linear-region *completely*

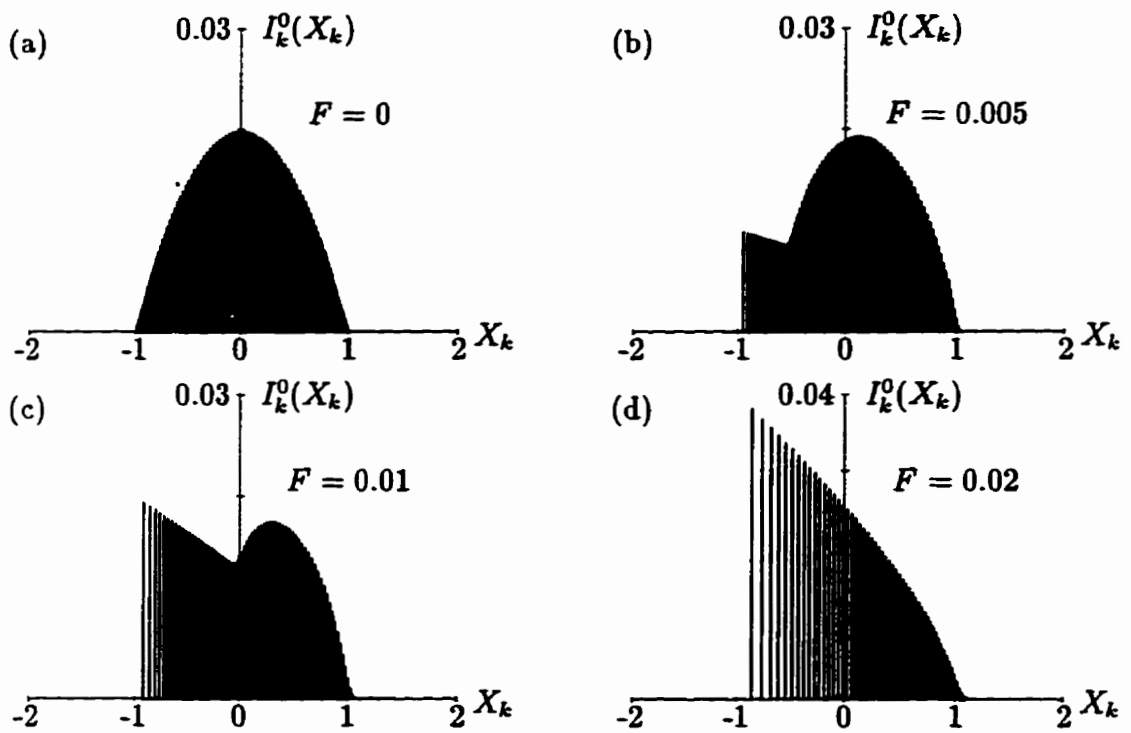

Fig. 5.2: LDOS at $n = 0$ site of 100 atom chain. As field increases, semi-elliptical shape is dominated by linear potential. Field strengths are as indicated.

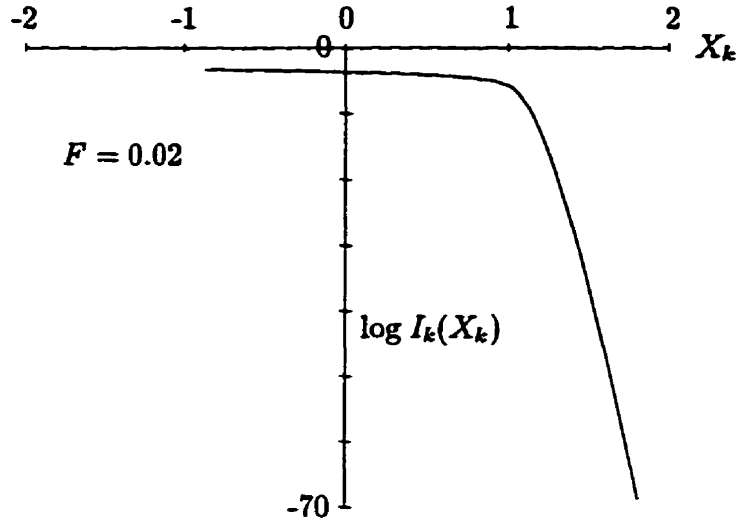

Fig. 5.3: Logarithmic plot of $I_k^0(X_k)$ in Fig. 5.2d showing quasi-band region.

supersedes the semi-elliptic one, as in Fig. 5.2d, and is again accompanied by the rigid shift to higher X_k-values and the exponential tailing above $X = 1$. Moreover, the $I_k^0(X_k)$ values are markedly enhanced to those in the $F = 0$ situation in Fig. 5.2a, particularly in the lower half of the quasi-band. In the case of F *negative*, the corresponding LDOS plots are those of Fig. 5.2, reflected in the $X = 0$ vertical axis.

Although the energy spectrum is discrete, we can identify a *quasi-band* by looking at the logarithm of (5.19). In the region $|X_k - NF| \approx 1$, $\log I_k(X_k)$ undergoes a transition from an exponential-like decay *inside* the quasi-band to a dramatically stronger decay *outside* the quasi-band (Fig. 5.3).

5.3 Semi-infinite Chain

Here, we use (5.11) in (5.19) and (5.16), with $n = M = 0$, to obtain

$$\begin{aligned} I_k^0(X_k) &= 2\beta \mathrm{Res}\left(G_{0+}(0,0;X); X = X_k\right) \\ &= 2\frac{J_{xX_k}(x)}{\left.\frac{\partial}{\partial X} J_{xX-1}(x)\right|_{X=X_k}} \\ &= \frac{2}{x}\frac{J_{\nu_k}(x)}{\left.\frac{\partial}{\partial \mu} J_\mu(x)\right|_{\mu=\nu_k-1}}. \end{aligned} \tag{5.22}$$

the X_k-values being the solutions of

$$J_{\nu_k-1}(x) = 0, \tag{5.23}$$

i.e., the poles of (5.11). This set of solutions, $\{X_k\}_{k=0}^{\infty}$, exhibits a minimum separation of F between solutions and asymptotically approaches the Stark ladder, $X_k \to kF$ as $k \to \infty$, by the properties of BFs [96].

Contrary to the finite and infinite chains' LDOS plots at the $n = 0$ site, here we are concerned with the LDOS at a *number* of sites in the chain, when the field is *fixed* at $F = 0.02$. Starting at the end site, $n = 0$, we immediately see that Fig. 5.4a essentially replicates that of Fig. 5.2d, for this site of the finite chain under the same field. Moving to the next site at $n = 1$, Fig. 5.4b shows that a drastic change has occurred in the LDOS, at this first *subsurface* atom. The distinct features are the extremely high spike at the lower-band edge followed by a steep decline to $I_k^0(0) = 0$ over the bottom half of the quasi-band, while in the top half we witness the emergence of the first *bulk* contribution in the form of a *discretized hump*. Penetrating the chain further, to the $n = 5$ site, Fig. 5.4c displays a *series of spike clusters of Gaussian-like* (GL) *shape*, except at the lower-band edge, where

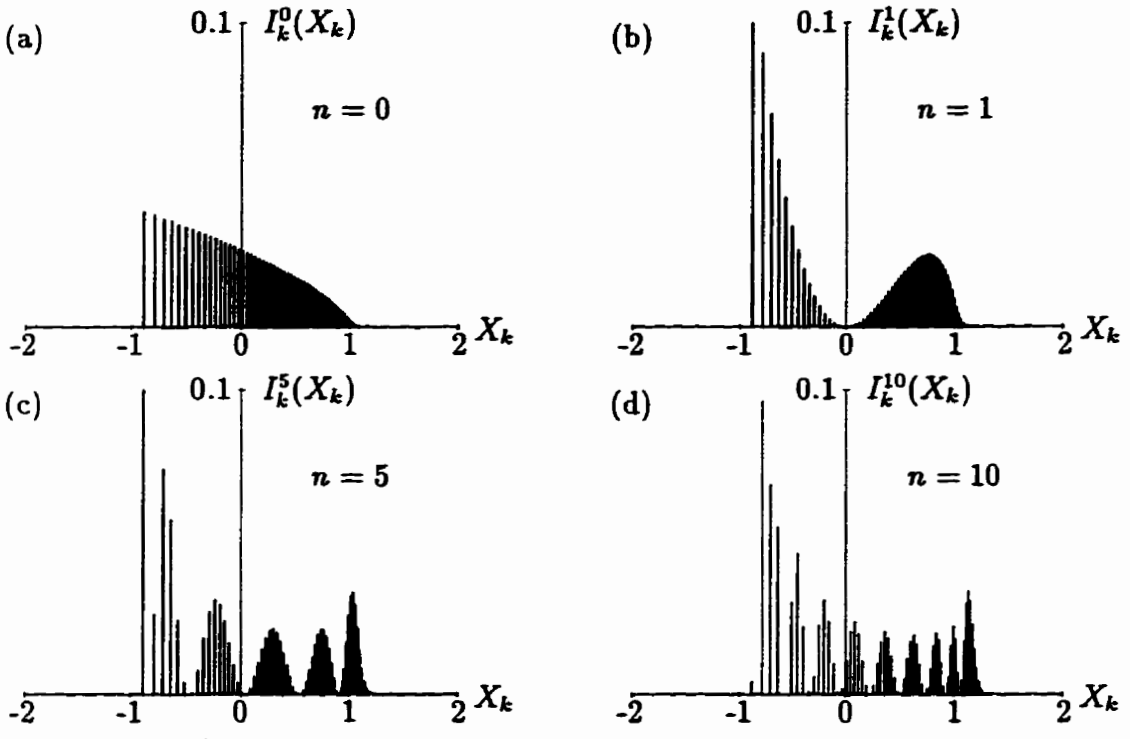

Fig. 5.4: Transition from surface ($n = 0$) to bulk ($n = 10$) LDOS of semi-infinite chain subject to a linear potential of $F = 0.02$. Site positions are as shown.

the dominant spike is again present. We also notice that the envelope through the GL peak maxima takes on the familiar U-shape of a bulk LDOS. The $I_k^{10}(X_k)$ plot of Fig. 5.4d is for the *bulk* site at $n = 10$. As in Fig. 5.4c, we find a series of GL peaks, each separated by a *node* (i.e., $I_k^{10}(X_k) = 0$). The number of nodes (and peaks) increases with n. Note that the bulk character of this LDOS is reflected in the disappearance of the dominant spike at the lower-band edge, which is connected with the *surface state* [88] associated with the end atom at $n = 0$. The U-shape envelope is, of course, still retained and the band tailing at the upper-band edge has become more pronounced, in conjunction with the rigid shift of the quasi-band, as n increases.

5.3.1 Infinite Chain

From (5.14) and (5.19), we find that at $M = 0$,

$$I_k^0(X_k) = 2\beta \left[\beta^{-1} \frac{\pi x J_{\nu_k}(x) J_{-\nu_k}(x)}{2\dfrac{\partial}{\partial X} \sin(xX\pi)\Big|_{X=X_k}} \right]$$

$$= \sec(\nu_k \pi) J_{\nu_k}(x) J_{-\nu_k}(x), \tag{5.24}$$

the poles of (5.14) providing the X_k-values, viz,

$$\sin \nu_k \pi = 0, \tag{5.25}$$

i.e.,

$$X_k = kF, \quad k = 0, \pm 1, \pm 2, \ldots, \tag{5.26}$$

by (5.5) and (5.4). Thus $\nu_k = -k$, and so

$$\sec(\nu_k \pi) = (-1)^k = (-1)^{\nu_k}. \tag{5.27}$$

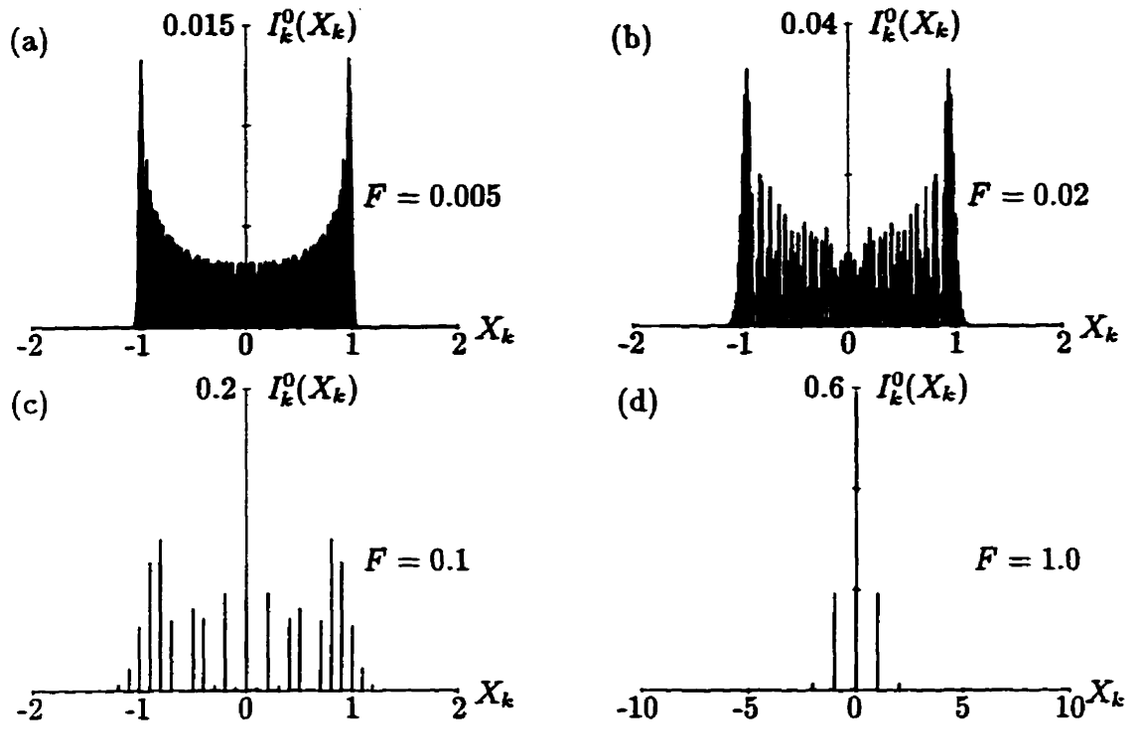

Fig. 5.5: Occupation number of states for infinite chain. Continuous field transition from discretized U-shape of zero-field to the localized peak for $F \geq 1$ occurs by combining both U and GL features into multiple Stark-Ladders. Field strengths are as indicated.

Since $J_{-\nu}(x) = (-1)^{\nu} J_{\nu}(x)$ [89], it follows from (5.3) that $I_k^0(X_k)$ in (5.24) varies as the probability, $|C_k^0|^2$, giving the link to the k-state occupation number at the zero atom. Note, (5.26) defines a *true* WSL, in contrast to the *quasi*-WSLs given by the BF conditions in (5.21) and (5.23).

The LDOS are shown in Fig. 5.5 for the F-values indicated. The low-field ($F = 0.005$) case of Fig. 5.5a has the U-shape appearance of the $F = 0$ situation [88], and the *discrete details* are reminiscent of the $\Gamma = 0.01$ plot of the *ground-*

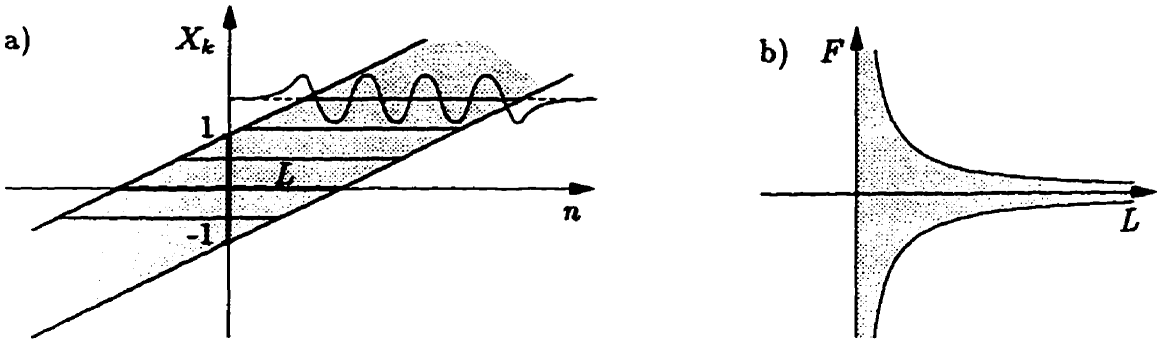

Fig. 5.6: (a) Quasi-band showing localization length L and wavefunction behaviour. (b) Rectangular hyperbolae $FL = \pm 2$ bounding shaded region in which (F, L) values give rise to band state.

state profile obtained numerically by Dolcher *et al.* [85], including the band tailing at *both* band edges. For $F = 0.02$, in Fig. 5.5b, the *fine structure* of the discrete details is resolved, showing the intensity spikes are again clustered into energy regions, which we identify as the break-up of the *single* quasi-band into the *multiple mini-bands* and were suggested by Moyer [58] as a means of approaching the zero-field limit in a proper manner. Further increase of the field to $F = 0.1$ results in Fig. 5.5c, where the heights of the intensity spikes are greatly diminished and their separation and band tailing markedly enhanced, making the characteristic U-shape barely discernible. Taking the field to $F = 1.0$, the quasi-band structure is reduced to that in Fig. 5.5d, whose few spikes form a *single* GL distribution about the central dominant spike at $X_k = 0$, the U-shape being completely destroyed. Conversely, the single GL peak can be regarded as the *basic unit* from which the other WSL spectra are generated.

Let us now address the question of the *number* of states in the quasi-band

at a given field strength. The *tilted band picture* of the WSL (5.26) is shown in Fig. 5.6a, where X_k vs. n is drawn. The *upper* (*lower*) band edge is the line $X_k = n + 1$ ($X_k = n - 1$). Between these lines, the vertical (horizontal) bandwidth is 2 (L), L being the so-called *localization length*, over (beyond) which the BF is oscillatory (damped exponentially). From the geometry of Fig. 5.6a, we see that the field gradient $F = \pm 2/L$, or $|FL| = 2$. Thus, for a state to be *in* the band, the *rectangular hyperbolic condition* (Fig. 5.6b)

$$|FL| \leq 2 \tag{5.28}$$

must be satisfied. Since, in the 1-electron approximation, each chain atom contributes one state, the actual number of states in the quasi-band corresponds to the number over which L ($= 2F^{-1}$) extends. Hence, when $F = 1$, $L = 2$, the number of states supported by the quasi-band at $n = 0$ is *three*, as in Fig. 5.5d, where the band-tailing states beyond the edges are *neglected*. Reducing F to 0.1 (Fig. 5.5c), we find *21 states* in the band, corresponding to $L = 20$. Whence, in general, the number of states in the quasi-band is

$$N = 2[\![L/2]\!] + 1 = 2[\![1/|F|]\!] + 1 = 2[\![|x|]\!] + 1, \tag{5.29}$$

where the square brackets indicate the integer part of the argument.

Chapter 6

Surface States

6.1 Zero-Field Theory

When dealing with a terminated (i.e., finite or semi-infinite) crystal, the sites located next to a termination site, or *surface*, can have significantly different electronic characteristics than those found at internal sites. Such an electronic difference may give rise to *surface states*, which were first considered by Tamm[88]. The basic theory of surface states has recently been described in detail by Davison and Stęślicka [88].

There are two standard ways to generate information about a surface termination from the known properties of the infinite chain. First, we can consider taking a cyclic chain of N atoms, breaking a bond and perturbing one, or both, of the resulting surface sites of the now *finite* chain (Appendix E). We shall, however, consider here the second method, namely, by cleaving an infinite chain into two *semi-infinite* chains and perturbing the surface site.

In the TB approximation, using the nearest-neighbor Hamiltonian, the recur-

rence relation for the infinite chain is

$$(E-\alpha)c_m = \beta(c_{m+1}+c_{m-1}), \tag{6.1}$$

where the coefficients, c_m, arise in the expansion of the crystal wavefunction in terms of the AO states, namely,

$$|\psi\rangle = \sum_n c_n |n\rangle . \tag{6.2}$$

To solve (6.1), we assume the power-law solution,

$$c_m = At^m, \tag{6.3}$$

A being the *normalization constant*, which allows us to rewrite (6.1) as

$$t^2 - 2Xt + 1 = 0. \tag{6.4}$$

By (4.57), the energy band is restricted to $-1 < X < 1$ for the infinite chain, so we introduce the parameter θ via

$$X = \cos\theta, \tag{6.5}$$

whence, the roots of (6.4) yield the solutions

$$t_\pm = e^{\pm i\theta}. \tag{6.6}$$

Combining (6.5) and (6.6), we find

$$t_+ = \begin{cases} X + i\sqrt{1-X^2}, & |X| < 1, \\ X - \mathrm{sgn}(X)\sqrt{X^2-1}, & |X| > 1, \end{cases} \tag{6.7}$$

and $t_- = t_+^{-1}$. The infinite crystal has the well-known GF [88],

$$G^0(n,m) = \frac{e^{i|n-m|\theta}}{-2\beta i \sin\theta}. \tag{6.8}$$

We obtain the semi-infinite chain by *cleaving* the crystal between sites -1 and 0. We ignore the portion for $n \leq -1$, setting all the GFs across the cleavage to zero. The atom at site 0 is now the *surface atom*, whose site energy we modify to account for having only one, not two, NN bonds. Thus, the potential is

$$\begin{aligned} \mathbf{V} &= (\alpha' - \alpha)\,|0\rangle\langle 0| - \beta\,(|0\rangle\langle -1| + |-1\rangle\langle 0|)\,, \\ &= \beta\,(z\,|0\rangle\langle 0| - |0\rangle\langle -1| - |-1\rangle\langle 0|) \end{aligned} \tag{6.9}$$

where

$$z = \frac{\alpha' - \alpha}{\beta} \tag{6.10}$$

is the *dimensionless surface perturbation parameter.*

Applying (6.9) to (3.8) for $m \geq 0$, and remembering to set cross-gap terms to zero, we obtain

$$G(m,m) = G^0(m,m) + z\beta G^0(m,0)G(0,m) - \beta G^0(m,-1)G(0,m). \tag{6.11}$$

Setting $m = 0$ yields

$$G(0,0) = G^0(0,0) + z\beta G^0(0,0)G(0,0) - \beta G^0(0,-1)G(0,0), \tag{6.12}$$

which, upon rearranging, gives

$$G(0,0) = \frac{G^0(0,0)}{1 - z\beta G^0(0,0) + \beta G^0(0,-1)}. \tag{6.13}$$

Thus, using (6.8) in (6.13), we have the surface GF equation

$$G(0,0) = \beta^{-1}\frac{1}{e^{-i\theta} - z}, \tag{6.14}$$

whose *poles* locate the surface state, i.e., the condition,

$$z = e^{-i\theta} = \cos\theta - i\sin\theta = X - i\sqrt{1 - X^2}. \tag{6.15}$$

Rearranging (6.15), and squaring, we find

$$X^2 - 1 = (X - z)^2 = X^2 - 2zX + z^2, \tag{6.16}$$

which yields the surface-state energy

$$X_s = \frac{z^2 + 1}{2z} = \frac{1}{2}\left(z + \frac{1}{z}\right). \tag{6.17}$$

So far, (6.5) indicates that we are restricted to the region $-1 \leq X \leq 1$ *in* the band. To access energies outside the band, we allow θ to become complex, viz.,

$$\theta = \zeta + i\mu, \qquad \mu \text{ real} > 0. \tag{6.18}$$

Inserting (6.18) into (6.6), we see that

$$t_{\pm} = e^{\pm i\theta} = e^{\pm i\zeta} e^{\mp\mu}, \tag{6.19}$$

which, along with (6.15), yields the *existence condition* for a *localized surface state* lying *outside* the energy band, namely,

$$|z| = |t_-| > 1. \tag{6.20}$$

Rationalizing (6.14), and using (6.17), we have for $|X| < 1$,

$$G(0,0) = \beta^{-1}\frac{X - z + i\sqrt{1 - X^2}}{(X - z)^2 + (1 - X^2)} = \beta^{-1}\frac{X - z + i\sqrt{1 - X^2}}{2z(X_s - X)}, \tag{6.21}$$

which, via (3.21), leads to the SDOS *inside* the band

$$\rho_0^b(X) = (2\pi\beta z)^{-1}\frac{\sqrt{1 - X^2}}{X_s - X}. \tag{6.22}$$

If $|X_s| < 1$, then the so-called *surface resonance* state lies embedded in the SDOS band and (6.22) gives the entire energy spectrum. When $|X_s| > 1$, we have a *discrete* localized surface state *outside* the band, which we describe via (5.18), viz.,

$$\rho_0^s(X) = (2\beta)^{-1} I_s^0(X_s)\delta(X - X_s), \tag{6.23}$$

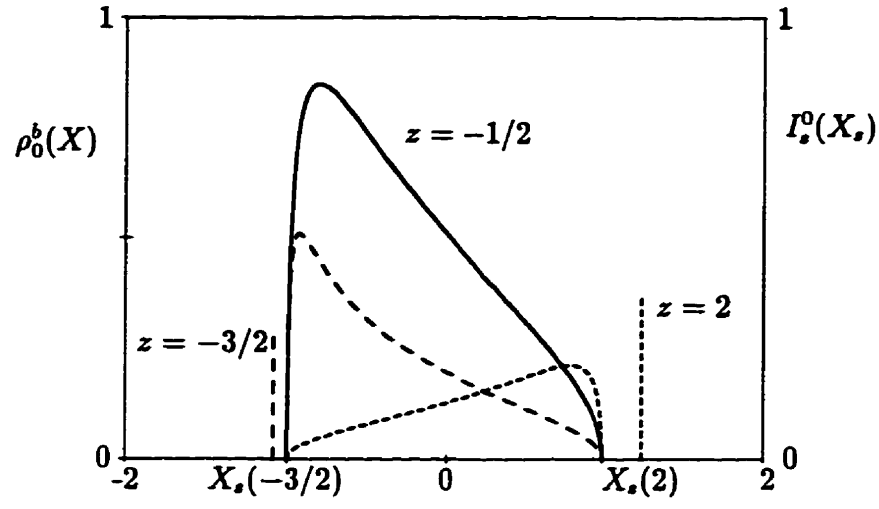

Fig. 6.1: Zero-field SDOS and surface intensities for indicated values of z.

where (5.16) and (5.19) with (6.14) give

$$I_s^0(X_s) = \frac{1}{2}\left(1 - \frac{1}{z^2}\right). \tag{6.24}$$

As z increases from a large negative value, the surface state approaches the band from below for $z < -1$, moves through it when $-1 < z < 1$, and appears above the band at $z > 1$ values (Fig. 6.1).

6.2 Surface-Field Effects

In order to study surface effects on an electrified solid [97], we investigate a semi-infinite chain to the right, beginning at $n = 1$, and subject to an applied field of gradient Γ, i.e., we have the GF

$$G_{1+}(1,1) = \beta^{-1}\frac{J_{\nu+1}(x)}{J_\nu(x)}, \tag{6.25}$$

by setting $n = 1$ in (5.10).

We now consider the addition of an isolated atom at the origin, whose site energy $\alpha_0 = \alpha'$. The GF for this isolated atom is

$$G_{00}(0,0) = \frac{1}{E-\alpha_0} = \beta^{-1}\frac{1}{2X-z}. \tag{6.26}$$

We define an unperturbed Greenian by the superposition of these two systems, so that

$$\mathbb{G}^0 = \mathbb{G}_{00} + \mathbb{G}_{1+}. \tag{6.27}$$

We now attach the isolated atom to the chain, by using the perturbation bond projection operator

$$V = \beta\left[|0\rangle\langle 1| + |1\rangle\langle 0|\right], \tag{6.28}$$

in the Dyson equation (3.8). We wish to obtain the on-site GF at $(0,0)$, viz.,

$$G^s_{0+}(0,0) = G^0(0,0) + \beta G^0(0,0)G^s_{0+}(1,0) + \beta G^0(0,1)G^s_{0+}(0,0), \tag{6.29}$$

where the last term is zero, due to the two systems being initially isolated, so that $G^0(0,1) = G^0(1,0) = 0$. To obtain the middle term, we need

$$\begin{aligned} G^s_{0+}(1,0) &= G^0(1,0) + \beta G^0(1,0)G^s_{0+}(0,0) + \beta G^0(1,1)G^s_{0+}(0,0) \\ &= \beta G^0(1,1)G^s_{0+}(0,0). \end{aligned} \tag{6.30}$$

Inserting (6.30) into (6.29) yields

$$G^s_{0+}(0,0) = G^0(0,0) + \beta^2 G^0(0,0)G^0(1,1)G^s_{0+}(0,0), \tag{6.31}$$

which defines $G^s_{0+}(0,0)$ implicitly in terms of the $\mathbb{G}^0$ elements. Solving (6.31), we find

$$G^s_{0+}(0,0) = \frac{G^0(0,0)}{1-\beta^2 G^0(0,0)G^0(1,1)} = \beta^{-1}\frac{1}{\beta^{-1}G^0(0,0)^{-1} - \beta G^0(1,1)}. \tag{6.32}$$

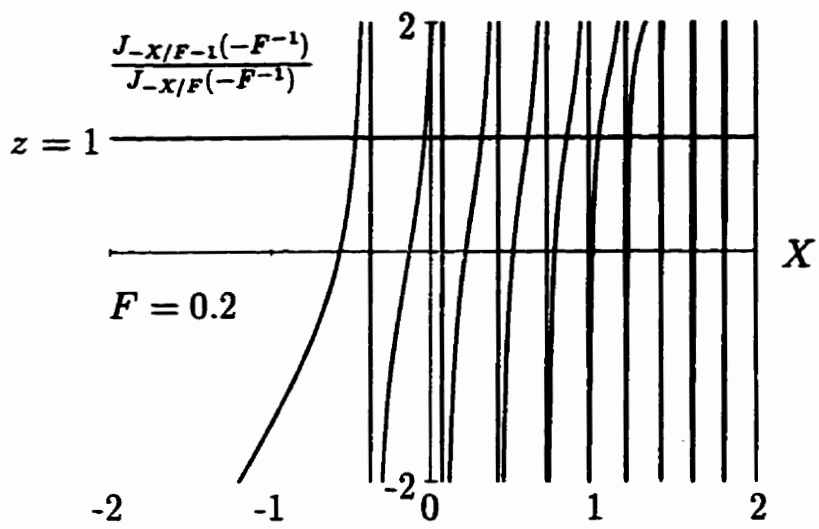

Fig. 6.2: Graph of $J_{-X/F-1}(-F^{-1})/J_{-X/F}(-F^{-1})$ for $F = 0.2$. Horizontal z-lines intersect curves at X_k^s corresponding to poles of (6.33).

Using (6.25) and (6.26) in (6.32), we arrive at

$$G_{0+}^s(0,0) = \beta^{-1}\frac{1}{(2X-z)-\dfrac{J_{\nu+1}(x)}{J_\nu(x)}} = \beta^{-1}\frac{J_\nu(x)}{(2X-z)J_\nu(x)-J_{\nu+1}(x)}.$$

$$= \beta^{-1}\frac{J_\nu(x)}{J_{\nu-1}(x)-zJ_\nu(x)}, \tag{6.33}$$

where we have used the recursion relation (5.2) to combine the BFs in the denominator.

The energy spectrum, displayed in Fig. 6.2, is given by the poles of (6.33), i.e.,

$$z = \frac{J_{\nu-1}(x)}{J_\nu(x)}. \tag{6.34}$$

Note the similarity with the zero-field case given by (E.17) and Fig. E.2. Unlike the

zero-field case, no solutions are lost as we vary z. Since there is no band restriction on the eigenenergies, there is *no condition* whereby we can *distinguish* a state as a surface-state. *All* states are discrete, and several states may be localized on the surface site.

We obtain the intensity for the field-modified states by following (5.19), thus,

$$\begin{aligned} I_k^s(X_k^s) &= \frac{2\beta}{\pi}\mathrm{Im}\, G_{0+}^s(0,0;X_k^s) \\ &= 2\mathrm{Res}\left(\frac{J_{zX}(x)}{J_{zX-1}(x)-zJ_{zX}(x)};X=X_k^s\right) \\ &= 2\frac{J_{zX_k^s}(x)}{\dfrac{\partial}{\partial X}\left(J_{zX-1}(x)-zJ_{zX}(x)\right)\Big|_{X=X_k^s}} \\ &= 2\frac{J_{\nu_k^s}(x)}{J'_{\nu_k^s-1}(x)-zJ'_{\nu_k^s}(x)}, \end{aligned} \tag{6.35}$$

where the prime indicates differentiation with respect to *order*. The *surface* DOS can therefore be written as

$$\rho_s(X) = (2\beta)^{-1}\sum_k I_k^s(X_k^s)\delta(X-X_k^s). \tag{6.36}$$

Plots of $I_k^s(X_k^s)$ are depicted in Fig. 6.3 for $z=1$, i.e., on the upper edge of the quasi-band, and for the F-values indicated. We see that, as F decreases from 0.2 to 0.01, the number of spikes increases markedly in the quasi-band, and coalesce about a *surface resonance* state at $X=z=1$ (cf. Fig. 6.1).

As z varies over the range $-2(1)3$, Fig. 6.4 represents the evolution of the intensity-energy distribution. Initially, a *surface state* spike exists *below* the quasi-band. At $z=-1$, the state becomes a *surface resonance*, coincident with the lower quasi-band edge. When $z=0$, there is no surface perturbation, so *no* surface state exists. For $z=1$, the surface state is *aligned* with the *upper* quasi-band edge,

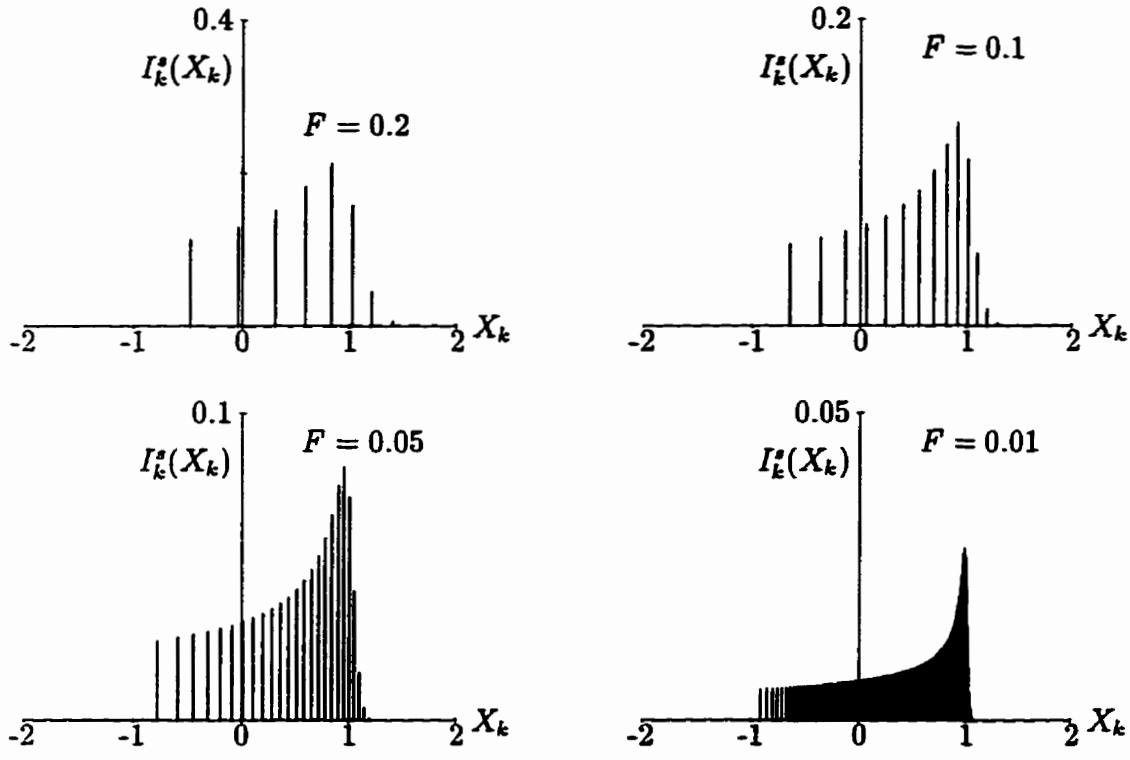

Fig. 6.3: Surface intensity-energy distributions for $z = 1$ and F-values indicated.

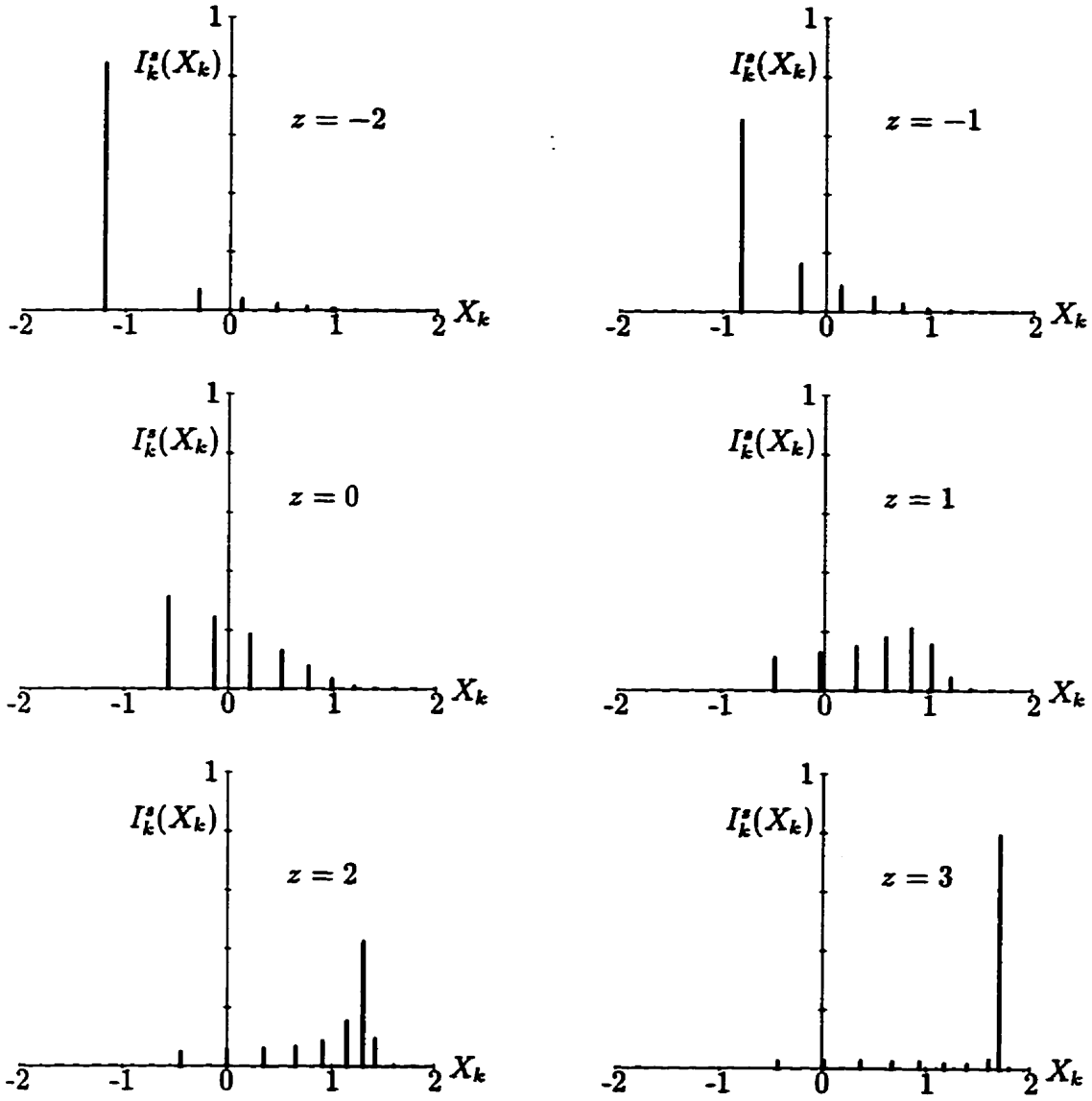

Fig. 6.4: Surface intensity-energy distributions for $F = 0.2$ and z-values indicated.

and *emerges* from the edge as the tallest spike in the $z = 2$ case, being further removed from it when $z = 3$. It is therefore apparent that the $I^s_k(X_k)$ distribution is very sensitive to the choice of the surface-perturbation parameter and is, in fact, reminiscent of the SDOS behaviour for the zero-field case [88].

Chapter 7

Chemisorption

7.1 Methodology

We now turn to a problem that is of great relevance to many fields of interest, including catalysis, epitaxy, and scanning tunneling microscopy. Instead of requiring the surface atom to be of the same material as the bulk of the crystal (§ 6.1), we consider *chemically attaching* a different atom to the end of the chain, by the so-called *chemisorption* process.

In particular, we wish to quantitatively describe the characteristic changes between the *pre-chemisorption system*, i.e., one isolated atom and the crystal substrate, and the combined *post-chemisorption* system, where the atom is *adsorbed* onto the crystal's surface and is called an *adatom*.

We assume that the adatom has initially a single electron in its valence state at an energy ε_a, and that the crystal has one valence electron associated with each of the N atomic sites that doubly occupy the delocalized crystal states, thus filling them up to the *Fermi level* (FL), i.e., we neglect temperature effects. When

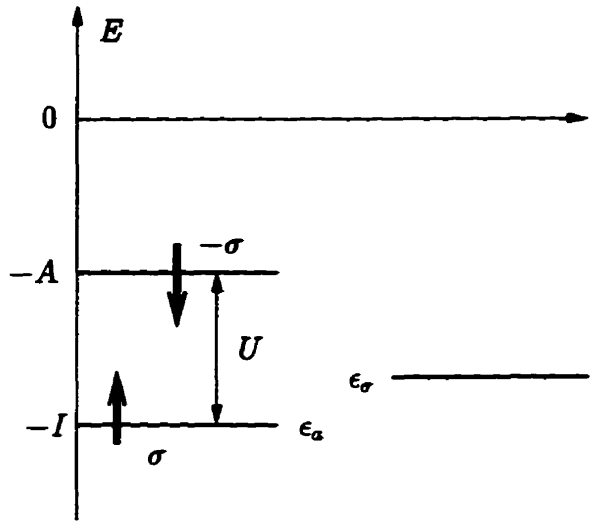

Fig. 7.1: Energy diagram for adatom, including Coulomb repulsion.

chemisorption occurs, the addition of the adatom electron introduces modifications to the crystal states of $O(1/N)$ and so, for sufficiently large substrates, we can ignore the chemisorption-induced changes to the crystal parameters, which is *not* the case for the adatom.

The adatom-substrate interaction means that the isolated adatom state becomes accessible to the crystal electrons, and vice-versa, so that a *charge transfer*, Δq, takes place between them. The resulting modifications to the adatom state are accounted for by adopting the *Anderson-Newns model* [94], and writing

$$\varepsilon_{a\sigma} = \varepsilon_a + U\langle \mathrm{N}_{a,-\sigma}\rangle, \tag{7.1}$$

where σ labels the *spin* of the adatom electron, U is the intra-atomic *Coulomb repulsion* between two electrons on the adatom, and $\langle \mathrm{N}_{a,-\sigma}\rangle$ is the adatom *occupation number* of the opposite-spin state.

The value of U is dependent on the properties of the adatom, being the difference

between its *ionization energy*, I, and *electron affinity*, A, (Fig. 7.1), i.e.,

$$U = I - A. \tag{7.2}$$

Since we are now dealing with electron-electron interactions, at least on the adatom, we can no longer describe the system by using a one-electron Hamiltonian. We do assume that the crystal-state wavefunctions, $|\psi_k\rangle$ with energies ε_k, have already been obtained via the TB Hamiltonian. Using these, plus the spin-dependent adatom states, as a basis set, we turn to the language of *second quantization* [98] to describe the chemisorbed system.

Let $\mathbb{C}_n^\dagger$ ($\mathbb{C}_n$) be the fermion *creation* (*annihilation*) operator for the state n, $n \in \{a, k\}$ ($k = 1, \ldots, N$), from which we define the *number operator*, $\mathbb{N}_n = \mathbb{C}_n^\dagger \mathbb{C}_n$ (cf. § 2.1 and Appendix B). The *Fock Hamiltonian* of the chemisorbed system can then be written as

$$\mathbb{H}_\sigma = \varepsilon_{a\sigma}\mathbb{N}_{a\sigma} + \sum_k \varepsilon_k \mathbb{N}_{k\sigma} + \sum_k \left(V_{ak}\mathbb{C}_{a\sigma}^\dagger \mathbb{C}_{k\sigma} + V_{ka}^*\mathbb{C}_{k\sigma}^\dagger \mathbb{C}_{a\sigma} \right), \tag{7.3}$$

where V_{nm} denotes the *hopping* term between states n and m. The *total* Hamiltonian is the sum over both spins, $\mathbb{H} = \sum_\sigma \mathbb{H}_\sigma$. We obtain Hartree-Fock solutions to (7.3) by generating N-particle antisymmetrized wavefunctions through the application of the creation operator to the vacuum state, $|0\rangle$. For the ground state, precisely those states below the FL are included, i.e.,

$$|\Phi_0\rangle = \prod_{\substack{n \\ \text{occ}}} \mathbb{C}_n^\dagger |0\rangle, \tag{7.4}$$

where E_n are the energy eigenvalues and E_f is the Fermi energy. The Schrödinger equation then becomes

$$\mathbb{H}_\sigma |\Phi_0\rangle = E |\Phi_0\rangle. \tag{7.5}$$

An application of the creation operator $\mathbb{C}^\dagger_{n\sigma}$ adds an electron of energy $E_{n\sigma}$ to the system, whence

$$\mathbb{H}_\sigma \mathbb{C}^\dagger_{n\sigma} |\Phi_0\rangle = (E + E_{n\sigma}) \mathbb{C}^\dagger_{n\sigma} |\Phi_0\rangle , \tag{7.6}$$

which, using (7.5), leads to

$$\left[\mathbb{H}_\sigma, \mathbb{C}^\dagger_{n\sigma}\right] |\Phi_0\rangle = E_{n\sigma} \mathbb{C}^\dagger_{n\sigma} |\Phi_0\rangle . \tag{7.7}$$

Inserting (7.3) into the commutator, we obtain

$$\begin{aligned} \left[\mathbb{H}_\sigma, \mathbb{C}^\dagger_{n\sigma}\right] &= \varepsilon_{a\sigma} \left[\mathbb{N}_{a\sigma}, \mathbb{C}^\dagger_{n\sigma}\right] + \sum_k \varepsilon_k \left[\mathbb{N}_{k\sigma}, \mathbb{C}^\dagger_{n\sigma}\right] \\ &\quad + \sum_k \left(V_{ak} \left[\mathbb{C}^\dagger_{a\sigma} \mathbb{C}_{k\sigma}, \mathbb{C}^\dagger_{n\sigma}\right] + V^*_{ka} \left[\mathbb{C}^\dagger_{k\sigma} \mathbb{C}_{a\sigma}, \mathbb{C}^\dagger_{n\sigma}\right] \right) \\ &= \varepsilon_{a\sigma} \mathbb{C}^\dagger_{a\sigma} \delta_{an} + \sum_k \varepsilon_k \mathbb{C}^\dagger_{k\sigma} \delta_{kn} + \sum_k \left(V_{ak} \mathbb{C}^\dagger_{a\sigma} \delta_{kn} + V^*_{ka} \mathbb{C}^\dagger_{k\sigma} \delta_{an} \right) , \end{aligned} \tag{7.8}$$

where we have used (2.21) and (B.5) to evaluate the commutators. Taking the adatom and substrate states separately, we find

$$\begin{aligned} \left[\mathbb{H}_\sigma, \mathbb{C}^\dagger_{a\sigma}\right] &= \varepsilon_{a\sigma} \mathbb{C}^\dagger_{a\sigma} + \sum_k V^*_{ka} \mathbb{C}^\dagger_{k\sigma}, \qquad n = a \\ \left[\mathbb{H}_\sigma, \mathbb{C}^\dagger_{k\sigma}\right] &= \varepsilon_k \mathbb{C}^\dagger_{k\sigma} + V_{ak} \mathbb{C}^\dagger_{a\sigma}, \qquad n = k. \end{aligned} \tag{7.9}$$

Since n may be either the adatom or a crystal state, we expand $\mathbb{C}^\dagger_{n\sigma}$ into all possible basis states and project back onto the chemisorption state n, i.e.,

$$\mathbb{C}^\dagger_{n\sigma} = \langle n \mid a \rangle_\sigma \mathbb{C}^\dagger_{a\sigma} + \sum_k \langle n \mid k \rangle_\sigma \mathbb{C}^\dagger_{k\sigma}, \tag{7.10}$$

where $|q\rangle_\sigma$ ($|m\rangle$) are the unperturbed (perturbed) eigenstates. Applying (7.10) to both sides of (7.7), we obtain the operator equation

$$\langle n \mid a \rangle_\sigma \left[H_\sigma, \mathbb{C}^\dagger_{a\sigma}\right] + \sum_k \langle n \mid k \rangle_\sigma \left[H_\sigma, \mathbb{C}^\dagger_{k\sigma}\right] = E_{n\sigma} \langle n \mid a \rangle_\sigma \mathbb{C}^\dagger_{a\sigma} + E_{n\sigma} \sum_k \langle n \mid k \rangle_\sigma \mathbb{C}^\dagger_{k\sigma}, \tag{7.11}$$

which, with the aid of (7.9), becomes

$$\left(\langle n \mid a\rangle_\sigma \varepsilon_{a\sigma} + \sum_k \langle n \mid k\rangle_\sigma V_{ak}\right) \mathbb{C}^\dagger_{a\sigma} + \sum_k \left(\langle n \mid a\rangle_\sigma V^*_{ka} + \langle n \mid k\rangle_\sigma \varepsilon_k\right) \mathbb{C}^\dagger_{k\sigma}$$
$$= E_{n\sigma} \langle n \mid a\rangle_\sigma \mathbb{C}^\dagger_{a\sigma} + E_{n\sigma} \sum_k \langle n \mid k\rangle_\sigma \mathbb{C}^\dagger_{k\sigma}. \tag{7.12}$$

Equating coefficients of $\mathbb{C}^\dagger_{a\sigma}$ and $\mathbb{C}^\dagger_{k\sigma}$ in (7.12), we obtain the so-called *equations of motion* for $\langle n \mid a\rangle_\sigma$ and $\langle n \mid k\rangle_\sigma$, viz.,

$$E_{n\sigma} \langle n \mid a\rangle_\sigma = \langle n \mid a\rangle_\sigma \varepsilon_{a\sigma} + \sum_k \langle n \mid k\rangle_\sigma V_{ak}, \tag{7.13}$$

$$E_{n\sigma} \langle n \mid k\rangle_\sigma = \langle n \mid k\rangle_\sigma \varepsilon_k + \langle n \mid a\rangle_\sigma V^*_{ka}. \tag{7.14}$$

Multiplying (7.13) by ${}_\sigma\langle a \mid n\rangle$ and (7.14) by ${}_\sigma\langle k \mid n\rangle$, we use the results to sum over the entire unperturbed basis, whereupon the completeness property

$$|\langle n \mid a\rangle_\sigma|^2 + \sum_k |\langle n \mid k\rangle_\sigma|^2 = 1, \tag{7.15}$$

leads to

$$\begin{aligned} E_{n\sigma} &= |\langle n \mid a\rangle_\sigma|^2 \varepsilon_{a\sigma} + \sum_k |\langle n \mid k\rangle_\sigma|^2 \varepsilon_k \\ &\quad + \sum_k \left({}_\sigma\langle a \mid n\rangle \langle n \mid k\rangle_\sigma V_{ak} + {}_\sigma\langle k \mid n\rangle \langle n \mid a\rangle_\sigma V^*_{ka}\right) \\ &= \sum_m |\langle n \mid m\rangle_\sigma|^2 \varepsilon_m + \sum_k \left({}_\sigma\langle a \mid n\rangle \langle n \mid k\rangle_\sigma V_{ak} + {}_\sigma\langle k \mid n\rangle \langle n \mid a\rangle_\sigma V^*_{ka}\right) \\ &\quad + U\langle \mathbb{N}_{a,-\sigma}\rangle |\langle n \mid a\rangle_\sigma|^2, \end{aligned} \tag{7.16}$$

where we have expanded $\varepsilon_{a\sigma}$ by (7.1) and m runs over all a and k values.

At this point, we wish to observe the following identity,

$$\langle \mathbb{C}^\dagger_{m\sigma} \mathbb{C}_{p\sigma} \rangle = \sum_{\substack{n \\ \text{occ}}} \langle n | \mathbb{C}^\dagger_{m\sigma} \mathbb{C}_{p\sigma} | n \rangle$$

$$= \sum_{\substack{n \\ \text{occ}}} \langle n| \left(|m\rangle_\sigma \langle 0|\right) \left(|0\rangle_\sigma \langle p|\right) |n\rangle$$
$$= \sum_{\substack{n \\ \text{occ}}} \langle n \mid m\rangle_\sigma \, {}_\sigma\langle p \mid n\rangle , \tag{7.17}$$

so, in particular, for $p = m = a$ we find

$$\langle \mathbb{N}_{a\sigma} \rangle = \sum_{\substack{n \\ \text{occ}}} |\langle n \mid a\rangle_\sigma|^2, \tag{7.18}$$

which inspires the summation of (7.16) over all n and both spins, so that

$$\begin{aligned}
\sum_{\substack{n\sigma \\ \text{occ}}} E_{n\sigma} &= \sum_{\substack{n\sigma \\ \text{occ}}} \Bigg[\sum_m |\langle n \mid m\rangle_\sigma|^2 \varepsilon_m \\
&\quad + \sum_k \left({}_\sigma\langle a \mid n\rangle \langle n \mid k\rangle_\sigma V_{ak} + {}_\sigma\langle k \mid n\rangle \langle n \mid a\rangle_\sigma V_{ka}^* \right) \Bigg] \\
&\quad + U \sum_\sigma \langle \mathbb{N}_{a,-\sigma} \rangle \sum_{\substack{n \\ \text{occ}}} |\langle n \mid a\rangle_\sigma|^2 \\
&= \sum_{\substack{n\sigma \\ \text{occ}}} \Bigg[\sum_m |\langle n \mid m\rangle_\sigma|^2 \varepsilon_m \\
&\quad + \sum_k \left({}_\sigma\langle a \mid n\rangle \langle n \mid k\rangle_\sigma V_{ak} + {}_\sigma\langle k \mid n\rangle \langle n \mid a\rangle_\sigma V_{ka}^* \right) \Bigg] \\
&\quad + 2U \langle \mathbb{N}_{a,-\sigma} \rangle \langle \mathbb{N}_{a\sigma} \rangle,
\end{aligned} \tag{7.19}$$

where the symmetry of the last term allows the summation over spin to double the term.

The energy can be directly calculated from the expectation value of the Fock Hamiltonian with (7.1) applied, namely,

$$\begin{aligned}
E = \langle \mathbb{H} \rangle &= \sum_{\substack{n\sigma \\ \text{occ}}} \Bigg[\sum_m |\langle n \mid m\rangle_\sigma|^2 \varepsilon_m \\
&\quad + \sum_k \left({}_\sigma\langle a \mid n\rangle \langle n \mid k\rangle_\sigma V_{ak} + {}_\sigma\langle k \mid n\rangle \langle n \mid a\rangle_\sigma V_{ka}^* \right) \Bigg] \\
&\quad + U \langle \mathbb{N}_{a,-\sigma} \rangle \langle \mathbb{N}_{a\sigma} \rangle .
\end{aligned} \tag{7.20}$$

Comparing (7.19) and (7.20) allows us to conclude that the energy of the chemisorbed system can be written as

$$E = \sum_{\substack{n\sigma \\ \text{occ}}} E_{n\sigma} - U\langle \mathbb{N}_{a\sigma}\rangle\langle \mathbb{N}_{a,-\sigma}\rangle \mathbb{N}_{a\sigma}\rangle. \tag{7.21}$$

Using the energy of the unperturbed system,

$$E_0 = \varepsilon_a + 2\sum_{\substack{k \\ \text{occ}}} \varepsilon_k, \tag{7.22}$$

we define the *chemisorption energy* via

$$\Delta E_c = E - E_0 = \sum_{\substack{n\sigma \\ \text{occ}}} E_{n\sigma} - 2\sum_{\substack{k \\ \text{occ}}} \varepsilon_k - \varepsilon_a - U\langle \mathbb{N}_{a\sigma}\rangle\langle \mathbb{N}_{a,-\sigma}\rangle. \tag{7.23}$$

We now turn to the problem of obtaining $\langle \mathbb{N}_{a\sigma}\rangle$. By (7.18), we see that it is dependent on the chemisorption wavefunctions $|n\rangle$. However, through (7.1), the Hamiltonian (7.3) which generates the $|n\rangle$ is itself dependent on $\langle \mathbb{N}_{a,-\sigma}\rangle$, i.e., we have the *self-consistency* equation

$$\langle \mathbb{N}_{a\sigma}\rangle = N\left(\langle \mathbb{N}_{a,-\sigma}\rangle\right) = N\left[N\left(\langle \mathbb{N}_{a\sigma}\rangle\right)\right]. \tag{7.24}$$

In general, there is no *analytical* procedure for solving (7.24), so we must obtain the solutions *numerically*. We do know, however, that we can always find a *non-magnetic* (~~M~~) solution, $\langle \mathbb{N}_{a\sigma}\rangle = \langle \mathbb{N}_{a,-\sigma}\rangle$, and may be several additional *magnetic* (M) solutions.

The solutions to (7.24) gives a measure of the charge occupying each spin-state on the adatom. Comparing with the charge of $q_e = -e$ from the single electron of the isolated adatom, we define

$$\Delta q = q_e\left(\sum_{\sigma}\langle \mathbb{N}_{a\sigma}\rangle - 1\right), \tag{7.25}$$

to be the *charge transfer* to the adatom.

The remaining terms in (7.23) may be obtained directly from the energy spectra of the unperturbed and chemisorbed systems, which we are able to extract from the poles of the appropriate GFs. Following the procedures of Chapter 6, we describe the unperturbed system by the Greenian $\mathbf{G}_{1+}$ and the modified-isolated atom GF, in this case,

$$G_{00}(0,0) = \frac{1}{E - \varepsilon_{a\sigma}} = \beta^{-1}\frac{1}{2X - z_{a\sigma}} \tag{7.26}$$

with

$$z_{a\sigma} = \frac{\varepsilon_{a\sigma} - \alpha}{\beta}. \tag{7.27}$$

Since the adatom does not have the same bonding properties as the crystal atoms, we attach the two via a *chemisorption bond* of energy β_a, so that (6.28) becomes

$$V = \beta_a \left[|0\rangle\langle 1| + |1\rangle\langle 0|\right], \tag{7.28}$$

whence, following (6.29) through (6.32), we obtain

$$\begin{aligned} G_a^s(0,0) &= \frac{G^0(0,0)}{1 - \beta_a^2 G^0(0,0)G^0(1,1)} \\ &= \beta^{-1}\frac{1}{\beta^{-1}G^0(0,0)^{-1} - \beta_a^2\beta^{-1}G^0(1,1)} \\ &= \beta^{-1}\frac{1}{\beta^{-1}G^0(0,0)^{-1} - \eta^2\beta G^0(1,1)}, \end{aligned} \tag{7.29}$$

where we have defined

$$\eta = \frac{\beta_a}{\beta}. \tag{7.30}$$

When $G^0(1,1)$ is *complex*, we introduce the *chemisorption functions* [94] defined as

$$\Lambda(X) = \eta^2\beta\ \mathrm{Re}\,G^0(1,1;X), \tag{7.31}$$

and

$$\Delta(X) = \eta^2\beta\ \mathrm{Im}\,G^0(1,1;X), \tag{7.32}$$

which allow us to write (7.29) as

$$G_a^s(0,0) = \beta^{-1}\frac{1}{2X - z_a - \Lambda(X) - i\Delta(X)} = \beta^{-1}\frac{2X - z_a - \Lambda(X) + i\Delta(X)}{[2X - z_a - \Lambda(X)]^2 + \Delta(X)^2}. \tag{7.33}$$

In particular, since the DOS is dependent only on the imaginary part of the GF, we find

$$\rho_a^s(X) = \frac{1}{\beta\pi}\frac{\Delta(X)}{[2X - z_a - \Lambda(X)]^2 + \Delta(X)^2}. \tag{7.34}$$

7.2 Field-Enhanced Situation

A semi-infinite chain under any linear potential is physically unrealizable, even as an approximation. Consider what happens on the surface atom when the field is switched on. The allowed energy band, corresponding to zero field, discretizes with a minimum separation of F between levels. For a semi-infinite chain, this generates states that have infinite energy. In particular, the FL rises to infinity, i.e., the atoms become *ionized* and the crystal *disintegrates*.

To maintain the integrity of the system, we require that the reduced-energy FL, X_f, remains within the *quasi-band* region of the surface atom, defined by the allowed energy band in zero field, i.e., $|MF| < 2$, as shown in Fig. 7.2. This condition ensures the existence of at least one delocalized state across the entire chain.

The surface GF of the m-atom crystal is calculated by applying $M = 1$ and $N = m - 1$ to (5.9), which yields

$$G_{1,m}(1,1) = \beta^{-1}\frac{Y_{\nu+1}(x)J_{\nu+m}(x) - J_{\nu+1}(x)Y_{\nu+m}(x)}{Y_\nu(x)J_{\nu+m}(x) - J_\nu(x)Y_{\nu+m}(x)}. \tag{7.35}$$

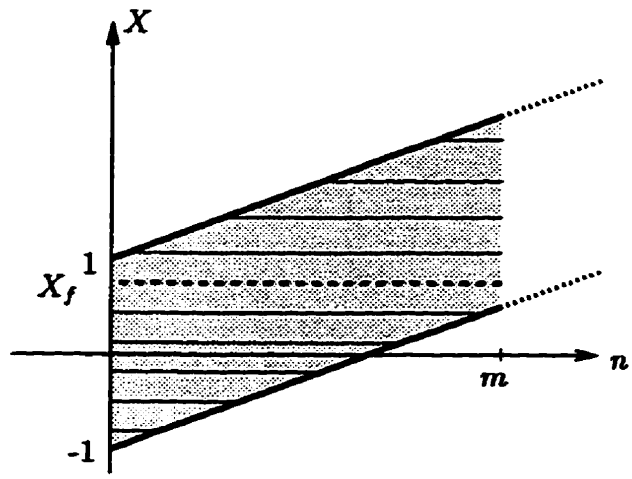

Fig. 7.2: Quasi-band region of electrified chain of m atoms from $n = 1$ to $n = m$.

The allowed-energy states form a discrete spectrum of m states, which are located at the poles of (7.35), viz.,

$$Y_\nu(x)J_{\nu+m}(x) - J_\nu(x)Y_{\nu+m}(x) = 0, \tag{7.36}$$

for which we order the solutions via energy to form the set $\{X_k^0\}_{k=1}^{m+1}$..

We now use the finite chain results to describe the chemisorption of an adatom, located at site $n = 0$ with modified-site energy $\alpha_0 = \varepsilon_{a\sigma} = \varepsilon_a + U\langle \mathbb{N}_{a-\sigma}\rangle$, to an electrified substrate, on the right from site $M = 1$ to m, by a bond $\beta_{0,1} = \beta_a$. Inserting these into (7.29), we have the adatom GF

$$\begin{aligned} G^a_{0,m}(0,0) &= \beta^{-1}\frac{1}{2X - z_\sigma - \eta^2\beta G_{1,m}(1,1)} \\ &= \beta^{-1}\frac{1}{2X - z_a - \hat{U}\langle \mathbb{N}_{a\sigma}\rangle - \eta^2\beta G_{1,m}(1,1)}, \end{aligned} \tag{7.37}$$

where

$$z_a = \frac{\varepsilon_a - \alpha}{2\beta}, \qquad \hat{U} = \frac{U}{2\beta}. \tag{7.38}$$

We note that (7.35) is *real-valued* everywhere it is defined, which complicates the extraction of the chemisorption functions. The application of (7.31) is straightforward, yielding

$$\Lambda(X) = \eta^2\beta \operatorname{Re} G_{1,m}(1,1) = \eta^2 \frac{J_{\nu+m}(x)Y_\nu(x) - J_\nu(x)Y_{\nu+m}(x)}{J_{\nu+m}(x)Y_{\nu-1}(x) - J_{\nu-1}(x)Y_{\nu+m}(x)}. \tag{7.39}$$

To obtain $\Delta(X)$, however, we must first look explicitly at the poles of (7.35), namely,

$$\begin{aligned}
\operatorname{Im} G_{1,m}(1,1;X_k^0) &= \lim_{X\to X_k^0} \operatorname{Im}\left(\frac{\Lambda(X)}{\eta^2\beta}\right) = \operatorname{Re}\left[-i\frac{1}{2}\oint_\gamma \frac{1}{\eta^2\beta}\Lambda(X)\delta(X-X_k^0)\,dX\right] \\
&= \frac{1}{2\eta^2\beta} 2\pi \operatorname{Res}\left(\Lambda(X)\delta(X-X_k^0); X = X_k^0\right) \\
&= i\frac{\pi}{\eta^2\beta} \operatorname{Res}\left(\frac{\delta(X-X_k^0)}{\Lambda(X)^{-1}}; X = X_k^0\right) \\
&= i\frac{\pi}{\eta^2\beta}\frac{1}{[\Lambda(X_k^0)^{-1}]'}
\end{aligned} \tag{7.40}$$

where the last equality holds by Theorem 5.1.

Since $\Lambda(X)$ is real everywhere it is defined, so is $\Lambda(X)^{-1}$. Thus, (7.40) is purely imaginary, and we obtain

$$\begin{aligned}
\Delta(X) &= \eta^2\beta \operatorname{Im} G_{1,m}(1,1;X) \\
&= \eta^2\beta \sum_{k=1}^{m} \operatorname{Im} G_{1,m}(1,1;X_k^m)\delta(X-X_k^0) \\
&= \eta^2\beta \sum_{k=1}^{m} \pi \frac{1}{\eta^2\beta[\Lambda(X_k^0)^{-1}]'}\delta(X-X_k^0) \\
&= \frac{1}{2}\eta^2\pi \sum_k I_k^s(X_k^0)\delta(X-X_k^0),
\end{aligned} \tag{7.41}$$

where we have defined the *surface-intensity energy distribution* of the crystal to be

$$I_k^s(X_k^0) = 2\left\{\eta^2[\Lambda(X_k^0)^{-1}]'\right\}^{-1} \tag{7.42}$$

which, by (7.39), is the same result we obtained in § 5.2.

Furthermore, the existence of $\Delta(X) \neq 0$ is limited to where $\Lambda(X)$ is *undefined*, which prohibits the use of (7.34) to determine the SDOS of the adatom. Instead, we must locate the poles of (7.33), X_m, and determine the intensity-energy distribution on the adatom, $I_k^a(X_m)$, which we use in (5.18) to obtain the adatom SDOS.

The inherent discreteness of the states under an applied field, allows the *chemisorption energy* to be directly calculated from (7.23) which, in reduced notation, becomes

$$\Delta X_c = \sum_{\sigma} \Delta X^{l\sigma} - z_a - \hat{U}\langle \mathbb{N}_{a\sigma}\rangle\langle \mathbb{N}_{a-\sigma}\rangle\,, \tag{7.43}$$

where

$$\Delta X^{l\sigma} = \sum_{\substack{n \\ \text{occ}}} X_{n\sigma} - \sum_{\substack{k \\ \text{occ}}} X^0_{k\sigma}, \tag{7.44}$$

($X^0_{k\sigma}$) $X_{n\sigma}$ being the (un)perturbed eigenenergies, and $X_f = X^0_{[\![(N+1)/2]\!]}$, the double square brackets indicating integer value.

The adatom occupancy is obtained from the intensities on the adatom of the occupied states of the chemisorbed system, i.e.,

$$\begin{aligned}\langle \mathbb{N}_{a\sigma}\rangle &= \sum_{\substack{m \\ \text{occ}}} \langle \mathbb{N}_{a\sigma}\rangle_m = \sum_{\substack{m \\ \text{occ}}} I_m^a(X_{m\sigma}) \\ &= \sum_{\substack{m \\ \text{occ}}} 2\beta\,[2\beta - \Lambda'(X_{m\sigma})]^{-1}\,,\end{aligned} \tag{7.45}$$

where, again, the imaginary component of the GF is obtained by differentiating the denominator of G, this time in (7.37).

The *self-consistent curves* of (7.24), for the model situation where $\eta = 1(\beta_a = \beta)$ in (7.37), are displayed in Fig. 7.3 for the F-values indicated. The $F = 0$ case, reproduces Newns' non-magnetic (~~M~~) and magnetic (M) solutions [94]. As the

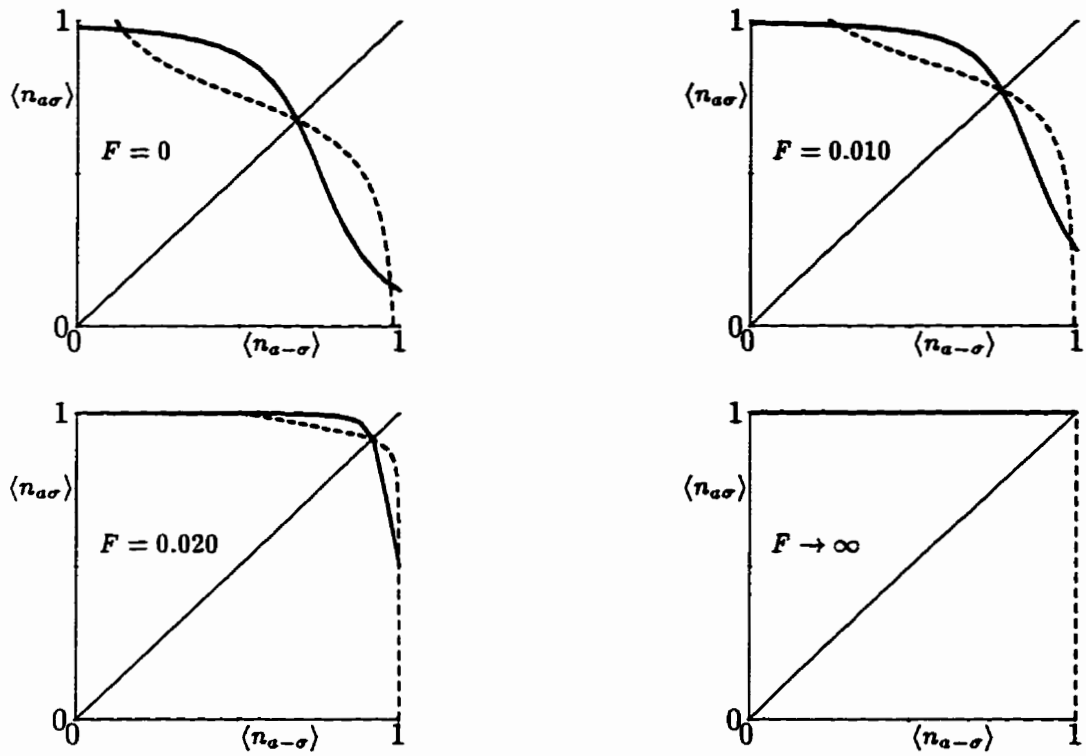

Fig. 7.3: Self-consistency curves for $\eta = 1$ and F-values indicated. (Non-)magnetic intersections occur for $\langle \mathbb{N}_{a\sigma}\rangle (=) \neq \langle \mathbb{N}_{a-\sigma}\rangle$.

field increases, the intersection points are driven towards the point $(1, 1)$, so that the M-points are eventually eliminated.

7.3 H–Ti System

We apply the results of § 7.2 to the system composed of a hydrogen adatom and a titanium substrate of 100 atoms in length, which will allow fields of up to $|F| = 0.02$, expanding on the results given by English *et al.* [99]. We convert the experimental

	4β	ε_a	U	ϕ	β_a
Expt.	8.60 eV	-13.60 eV	12.9 eV	3.86 eV	3.72 eV
	β	z_a	$\hat{U}$	α	η
Reduced	2.15 eV	-2.27	3.00	3.86 eV	1.73

Table 7.1: Experimental data [94] for chemisorbed H on Ti and corresponding reduced parameters.

F	-.020	-.015	-.010	-.005	.000	.005	.010	.015	.020
$\not{\mathbf{M}}$	0.546	0.567	0.584	0.607	0.632	0.658	0.687	0.720	0.762
M	0.872	0.794	0.759	0.720	N/A	0.737	0.819	0.909	0.991
	0.054	0.288	0.381	0.483	N/A	0.574	0.547	0.482	0.424

Table 7.2: $\not{\mathbf{M}}$ and M solutions $\langle \mathbb{N}_{a\sigma} \rangle$ and $\langle \mathbb{N}_{a-\sigma} \rangle$ of the H–Ti system.

data to reduced notation in Table 7.1.

Applying these parameters to (7.24), we obtain numerically the self-consistency curves for values of F by locating the poles of (7.37) and summing the intensities of the occupied states as $\langle \mathbb{N}_{a,-\sigma} \rangle$ is varied as an independent variable. Intersecting this result with its own inverse, see Fig. 7.4, locates the $\not{\mathbf{M}}$ and any M solutions. In fact, the zero field case has only a $\not{\mathbf{M}}$ solution, but the application of any field, positive or negative, creates M solutions, see Table 7.2.

Inserting these occupation values back into (7.37), enables the energy eigenvalues of the chemisorbed H–Ti system to be obtained. Delineated in Fig. 7.5a (Fig. 7.5b) is the behaviour of the *chemisorption energy* (7.43) (*adatom charge transfer* (7.25)) as the field strength varies. The $\not{\mathbf{M}}$ (M)variation is portrayed by the solid (broken) line in both figures. With no field, only the $\not{\mathbf{M}}$ solution exists,

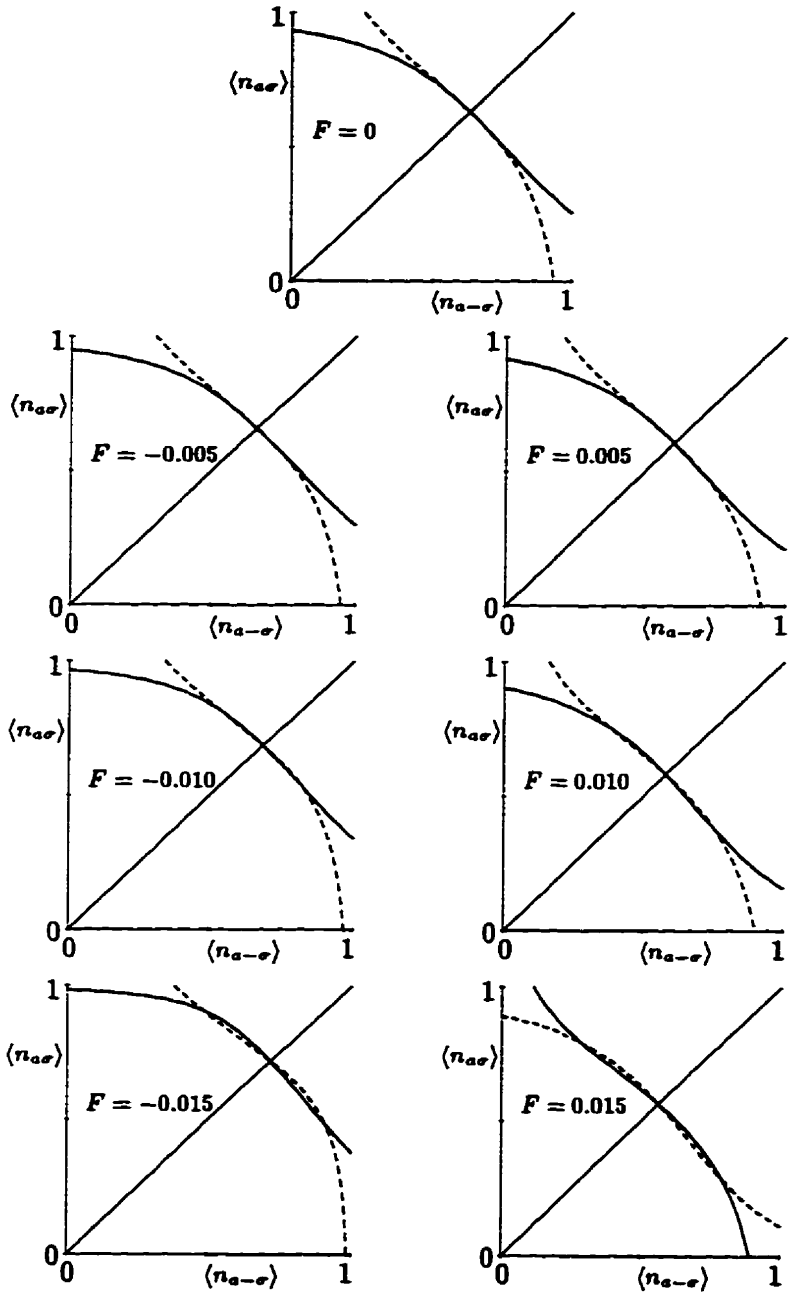

Fig. 7.4: Self-consistency (adatom occupation number) plots are shown for H–Ti system with parameter values $\eta = 1.73$, $z_a = -2.27$, and $\hat{U} = 3.00$.

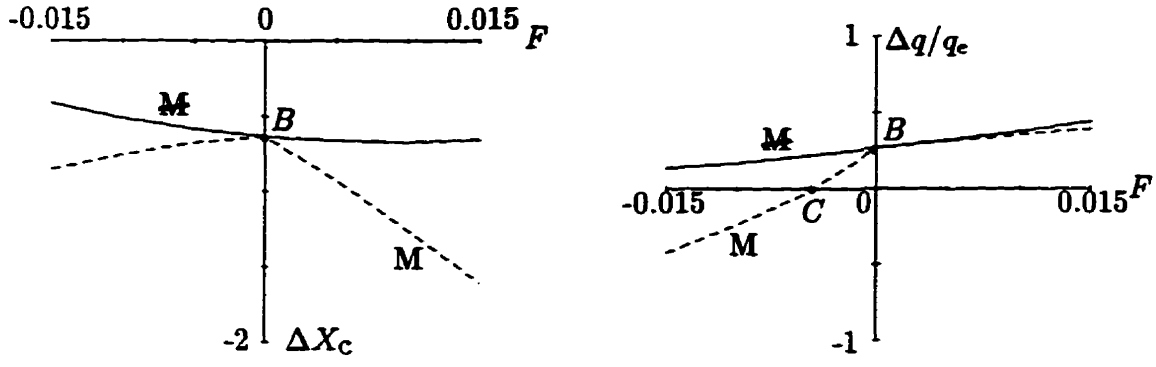

Fig. 7.5: (a)Variation of H–Ti chemisorption energy with field strength. Solid (broken) curve represents ~~M~~ (M) solution. (b) Adatom charge transfer versus field strength for H–Ti. Solid (broken) line depicts ~~M~~ (M) case.

but M solutions appear immediately with the application of F. The field brings two major effects into play. First, it raises the Fermi level which, on its own, lowers ΔX_c. Second, it alters the adatom occupancy.

For the ~~M~~ case, the field increases both $\langle \mathbb{N}_{a\sigma} \rangle$ and $\langle \mathbb{N}_{a-\sigma} \rangle$ along the diagonal, the latter raising the effective adatom state via (7.1) which, in turn, raises ΔX_c. Under these competing effects, ΔX_c remains essentially constant, as shown in Fig. 7.5a. More particularly, X_f is slightly more affected for $F < 0.010$, while the z_σ effect takes over for $F > 0.010$.

We note that both plots show a smooth transition through the $F = 0$ point for the ~~M~~ solutions, whereas a cusp appears there in the M curves, due to the asymmetry of the occupied levels in the presence of the field. States shifted above the band are above the FL and have only an indirect effect on the energies of the occupied states. States shifted below the band are, however, filled states and the field effect is more pronounced when they exist.

In both cases, the field stabilizes the system. Our findings indicate that che-

misorption reactions can be induced by the presence of a field on a system, which would otherwise remain inert.

7.4 H–Cr

We next apply field-enhanced chemisorption theory to the system composed of hydrogen chemisorbing onto a 100-atom chromium substrate, which will admit fields of up to $|F| = 0.015$. The conversion of experimental data to reduced notation is presented in Table 7.3.

As with the H–Ti case, we use $\langle \mathbb{N}_{a,-\sigma} \rangle$ as an independent variable at specified F strengths to solve for $\langle \mathbb{N}_{a\sigma} \rangle$ and then locate the intersection with its own inverse (Fig. 7.6). These results are tabulated in Table 7.4 for both M and ~~M~~ solutions.

	4β	ε_a	U	ϕ	β_a
Expt.	6.10 eV	-13.60 eV	12.9 eV	4.56 eV	3.75 eV
	β	z_a	$\hat{U}$	α	η
Reduced	1.525 eV	-2.96	4.23	4.56 eV	2.46

Table 7.3: Experimental data [94] for chemisorbed H on Cr and corresponding reduced parameters.

F	-.015	-.010	-.005	.000	.005	.010	.015
~~M~~	0.574	0.588	0.602	0.616	0.631	0.645	0.656
M	N/A	N/A	N/A	N/A	N/A	0.803	0.962
	N/A	N/A	N/A	N/A	N/A	0.476	0.335

Table 7.4: ~~M~~ and M solutions $\langle \mathbb{N}_{a\sigma} \rangle$ and $\langle \mathbb{N}_{a-\sigma} \rangle$ of the H–Cr system.

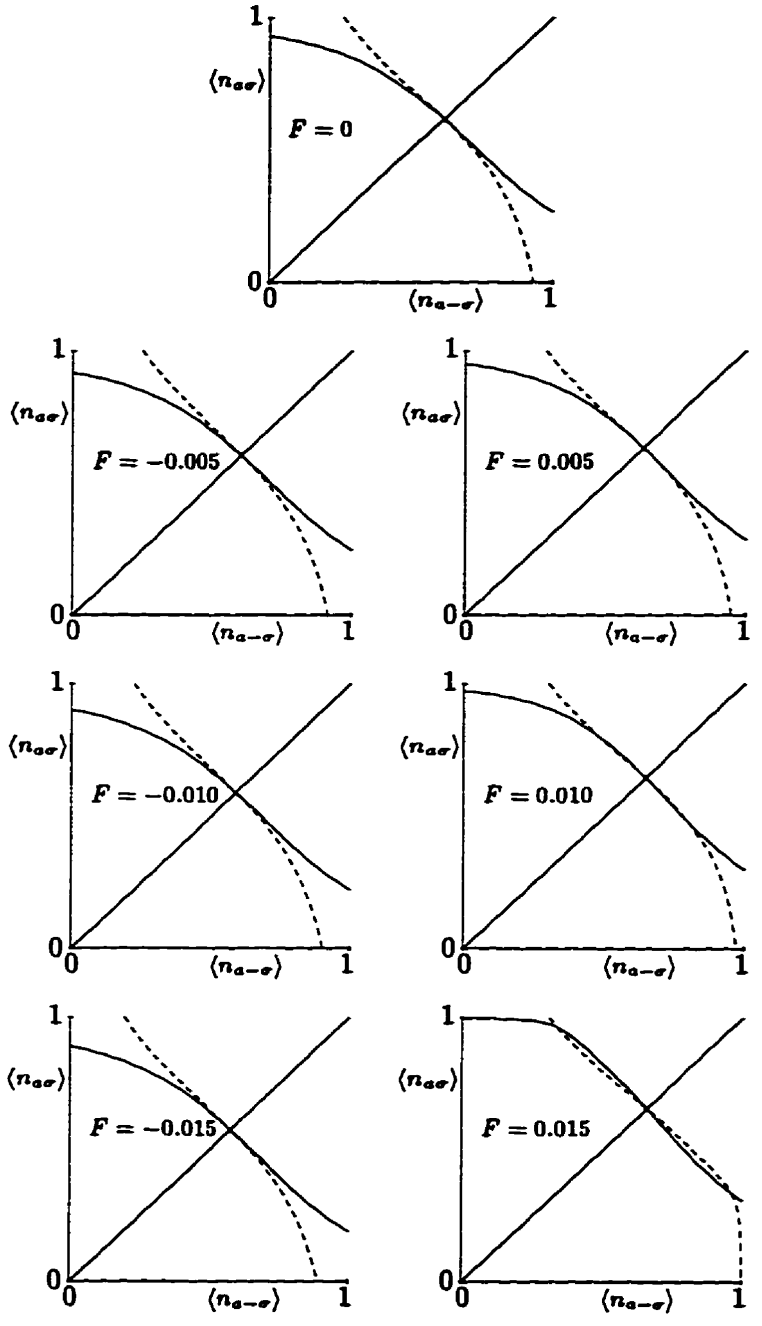

Fig. 7.6: Self-consistency (adatom occupation number) plots are shown for H–Cr system with parameter values $\eta = 2.46$, $z_a = -2.96$, and $\hat{U} = 4.23$.

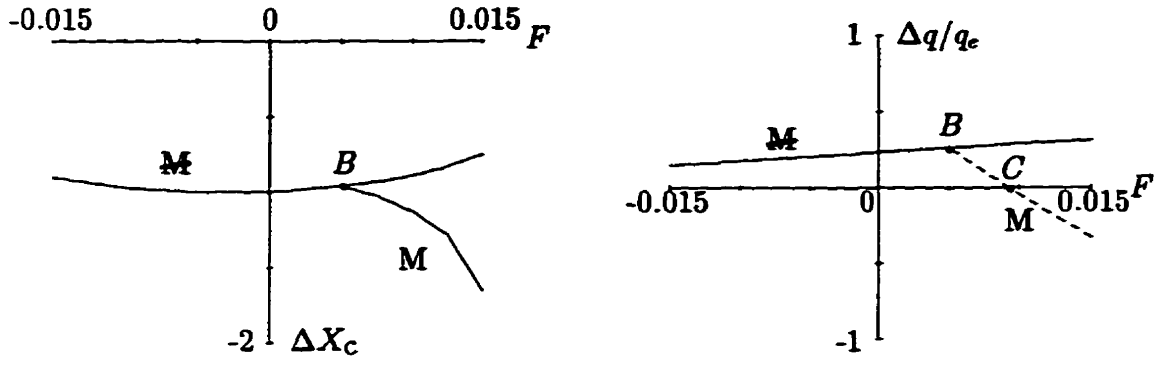

Fig. 7.7: Variation of (a) H–Cr chemisorption energy and (b) charge transfer with field strength. Solid (broken) curve depicts ~~M~~ (M) solution. Point B locates the bifurcation threshold for M solutions.

Unlike the H–Ti case, H–Cr does not develop M solutions until $F > 0.005$, where a *bifurcation* occurs, and none for negative fields. In particular, since the ~~M~~ curve for ΔX_c is concave up (Fig. 7.7a), low fields will actually cause the chemisorption process to be slightly less favourable than at zero-field. Once the M solutions appear, increasing F will again result in enhanced chemisorption.

In Fig. 7.7b, we see that while the ~~M~~ charge transfer behaves identically to that of H–Ti under changing field strength, the M curve does not. Indeed, while the charge transfer increases with F in the H–Ti case, the M result for H–Cr has a *negative* slope.

In both systems, when Δq *changes sign*, the *direction* of charge transfer is *reversed.* For $\Delta q > 0$ ($\Delta q < 0$), charge flows to (from) the adatom from (to) the substrate.

Chapter 8

Molecular Electronics

8.1 Zero-Field Model

Several mechanisms for providing a *molecular switch* have been previously investigated [100]. Aviram *et al.* [100, 101] studied the use of a hemiquinone molecule, which has two forms that can be controlled by application of a potential field, perpendicular to the direction of current, allowing the molecule to be switched from an acceptor to a donor state.

Potember and his colleagues [100, 102] have prepared crystals of *tetracyanoquinodimethane* (TCNQ) derivatives complexed with metal ions which, under the influence of high voltage, are converted to TCNQ and metallic atoms, switching from high to low resistivity.

Much interest has been aroused in *photoswitches.* Following biological examples, Shipman considered the molecules used in photosynthesis [103], while Keszthelyi *et al.* examined Bacteriorhodopsin [104]. Carter proposed using an organic chromophore [100, 105]. In the presence of light, the charges and double bonds in the

molecule are altered.

Whichever method of switching is used, we may model them all via the change in the electronic configuration of a single impurity embedded in a conducting polymer.

Using a TB Hamiltonian, and considering only NN effects, the one-dimensional system $\ldots AAABAAA\ldots$ corresponds to an impurity B inserted into a periodic host chain of A atoms. The elements of the conducting polymers, represented by A, have in reality many orbitals, but for a qualitative view of the impurity effects, a single-orbital approach is taken. A more detailed analysis of the system will be required to determine the optimal *chemical* description of the impurity. In this model, there are two methods of altering the electronic configuration of an impurity in the chain. One is to alter the site energy, the other is to change one of the bonds connecting the impurity to the chain.

Such a system has been examined with equal bonds between the atoms of the homogeneous chain by Sautet and Joachim [1], and with alternating semiconductor bonds by English and Davison [3], both using the scattering-matrix technique to determine the transmission coefficient through the impurity and the change in density of states. Mišković *et al.* [106, 107] considered the system with two impurities and the single-impurity system via the many-neighbour approximation, using the *Lippmann-Schwinger* (LS) scattering equation in both cases. It is in the context of this latter theory that we shall proceed.

We take the infinite chain Hamiltonian

$$\mathbb{H}^0 = \sum_{n=-\infty}^{\infty} \left[\alpha \left|n\right\rangle \left\langle n\right| + \beta(\left|n\right\rangle \left\langle n+1\right| + \left|n+1\right\rangle \left\langle n\right|)\right], \tag{8.1}$$

which has the well-known GF (cf. § 4.4)

$$G^0_\infty(n,m) = \frac{i}{2\beta}\frac{e^{i|n-m|\theta}}{\sin\theta}. \tag{8.2}$$

If we decompose the eigenfunctions of (8.1) with respect to the AO basis functions, i.e.,

$$|\phi\rangle = \sum_n c_n^0 |n\rangle , \tag{8.3}$$

the coefficients are plane-wave solutions, $c_n^0 = e^{in\theta}$, where we have chosen the sign of θ to correspond to waves moving to the right.

We modify (8.1) by introducing a localized perturbation, V, well away from the ends ($n \to \pm\infty$) of the chain, whence, the perturbed Hamiltonian is

$$\mathbb{H} = \mathbb{H}^0 + \mathbf{V} \tag{8.4}$$

with eigenfunctions,

$$|\psi\rangle = \sum_n c_n |n\rangle . \tag{8.5}$$

From these results, we call upon the LS equation (see Appendix F),

$$|\psi\rangle = |\phi\rangle + \mathbb{G}^0 \mathbf{V} |\psi\rangle , \tag{8.6}$$

which is equivalent to the Dyson equation, except it applies to the wavefunctions of the system (cf. (3.8)). Expanding the wavefunctions in (8.6) and multiplying on the left by $\langle n|$, we obtain

$$\begin{aligned} c_n &= c_n^0 + \sum_m \langle n| \mathbb{G}^0 \mathbf{V} |m\rangle c_m \\ &= c_n^0 + \sum_{l,m} G^0(n,l) \langle l| \mathbf{V} |m\rangle c_m, \end{aligned} \tag{8.7}$$

which is the LS relation for the wavefunction coefficients.

In a general scattering situation, incoming waves are transmitted or reflected according to the characteristics of the system. Consider two independent plane

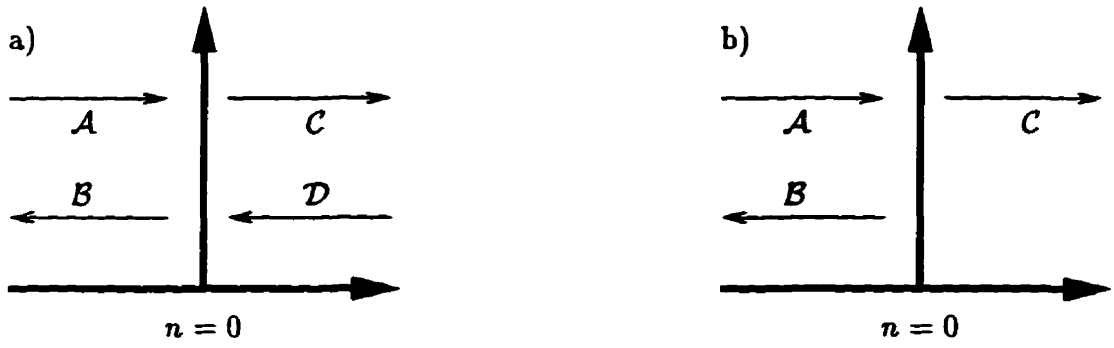

Fig. 8.1: Scattering amplitudes of incoming and outgoing waves. a) General scattering relationships. b) Scattering due to incoming wave from left only.

waves $\mathcal{A}e^{ikx}$ from the left and $\mathcal{D}e^{-ikx}$ from the right, incident upon some perturbation region. The incident waves are scattered into outgoing waves $\mathcal{B}e^{-kx}$ and $\mathcal{C}e^{ikx}$, respectively (Fig. 8.1a), which are related to the incident waves via

$$\begin{aligned} \mathcal{C} &= \tau\mathcal{A} + r'\mathcal{D} \\ \mathcal{B} &= r\mathcal{A} + \tau'\mathcal{D}, \end{aligned} \tag{8.8}$$

where τ is the transmission coefficient, r is the reflection coefficient from the left, and r' is the reflection coefficient from the right. In matrix notation, (8.8) becomes

$$\begin{bmatrix} \mathcal{C} \\ \mathcal{B} \end{bmatrix} = \mathbb{S}(E) \begin{bmatrix} \mathcal{A} \\ \mathcal{D} \end{bmatrix} = \begin{bmatrix} \tau & r' \\ r & \tau' \end{bmatrix} \begin{bmatrix} \mathcal{A} \\ \mathcal{D} \end{bmatrix}, \tag{8.9}$$

which defines the *scattering matrix*, $\mathbb{S}(E)$.

If we now consider a single incident wave from the left, i.e., $\mathcal{D} = 0$, (8.8) tells us $\mathcal{C} = \tau\mathcal{A}$ and $\mathcal{B} = r\mathcal{A}$. Identifying these amplitudes (Fig. 8.1b) with the AO wavefunction coefficients in (8.3), we obtain

$$c_n = \begin{cases} e^{in\theta} + re^{-in\theta}, & n \to -\infty \\ \tau e^{in\theta}, & n \to \infty, \end{cases} \tag{8.10}$$

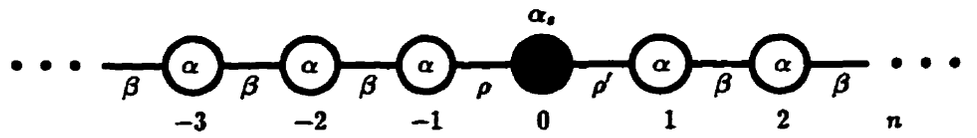

Fig. 8.2: Model of molecular switch embedded in a linear monatomic chain.

where we have normalized the incident wave by setting $\mathcal{A} = 1$, and replaced the plane waves with crystal Bloch waves by setting $\theta = ka$ and $x = na$.

Restricting the scattering potential to a region near the origin, i.e., $\langle l|\,\mathbf{V}\,|m\rangle = 0$ when either $|l| > N$ or $|m| > N$ for some finite N, we apply (8.2) to (8.7) as $n \to -\infty$, whereby

$$c_n \to e^{in\theta} + \sum_{l,m} \frac{i}{2\beta \sin\theta} e^{i(l-n)\theta} \langle l|\,\mathbf{V}\,|m\rangle\, c_m. \tag{8.11}$$

Comparing (8.11) to (8.10), we find the reflection coefficient to be

$$r = \frac{i}{2\beta \sin\theta} \sum_{l,m} e^{il\theta} \langle l|\,\mathbf{V}\,|m\rangle\, c_m. \tag{8.12}$$

Similarly, taking $n \to \infty$ in (8.7) yields

$$c_n \to e^{in\theta} + \sum_{l,m} \frac{i}{2\beta \sin\theta} e^{i(n-l)\theta} \langle l|\,\mathbf{V}\,|m\rangle\, c_m, \tag{8.13}$$

which, via (8.10), leads to the transmission coefficient,

$$\tau = 1 + \frac{i}{2\beta \sin\theta} \sum_{l,m} e^{-il\theta} \langle l|\,\mathbf{V}\,|m\rangle\, c_m. \tag{8.14}$$

We model a *molecular switch* by parameterizing the bond and site energies of the atom at the origin [1, 3] using the perturbation potential (Fig. 8.2)

$$\begin{aligned} \mathbf{V} &= (\alpha_s - \alpha)\,|0\rangle\langle 0| + (\rho - \beta)\left[|-1\rangle\langle 0| + |0\rangle\langle -1|\right] + (\rho' - \beta)\left[|0\rangle\langle 1| + |1\rangle\langle 0|\right] \\ &= \beta\left\{2z_s\,|0\rangle\langle 0| + (\sigma - 1)\left[|-1\rangle\langle 0| + |0\rangle\langle -1|\right] + (\sigma y - 1)\left[|0\rangle\langle 1| + |1\rangle\langle 0|\right]\right\}, \end{aligned} \tag{8.15}$$

where $\sigma = \rho/\beta$, $y = \rho'/\rho$ and

$$z_s = \frac{\alpha_s - \alpha}{2\beta}. \tag{8.16}$$

Applying (8.15) to (8.14) yields

$$\begin{aligned}\tau &= 1 + \frac{i}{2\sin\theta}\left\{c_{-1}(\sigma-1) + c_0\left[e^{-i\theta}(\sigma y - 1) + 2z_s + e^{i\theta}(\sigma - 1)\right] + c_1(\sigma y - 1)\right\} \\ &= 1 + c_{-1}A + c_0\left[e^{i\theta}A + B + e^{-i\theta}C\right] + c_1 C,\end{aligned} \tag{8.17}$$

where

$$A = \frac{i(\sigma-1)}{2\sin\theta}, \qquad B = \frac{iz_s}{\sin\theta}, \qquad C = \frac{i(\sigma y - 1)}{2\sin\theta}. \tag{8.18}$$

To solve (8.17), we need the three coefficients c_{-1}, c_0 and c_1, which we obtain by returning to (8.7) with (8.15) and (8.2). Setting $n = -1$, we find

$$c_{-1} = e^{-i\theta} + c_{-1}e^{i\theta}A + c_0\left[A + e^{i\theta}B + e^{i2\theta}C\right] + c_1 e^{i\theta}C. \tag{8.19}$$

For $n = 0$, we obtain

$$c_0 = 1 + c_{-1}A + c_0\left[e^{i\theta}A + B + e^{i\theta}C\right] + c_1 C, \tag{8.20}$$

while $n = 1$ yields

$$c_1 = e^{i\theta} + c_{-1}e^{i\theta}A + c_0\left[e^{i2\theta}A + e^{i\theta}B + C\right] + c_1 e^{i\theta}C. \tag{8.21}$$

Combining (8.19), (8.20) and (8.21) into a matrix equation, we have

$$\begin{bmatrix} e^{i\theta}A - 1 & A + e^{i\theta}B + e^{i2\theta}C & e^{i\theta}C \\ A & e^{i\theta}A + B + e^{i\theta}C - 1 & C \\ e^{i\theta}A & e^{i2\theta}A + e^{i\theta}B + C & e^{i\theta}C - 1 \end{bmatrix} \begin{bmatrix} c_{-1} \\ c_0 \\ c_1 \end{bmatrix} = -\begin{bmatrix} e^{-i\theta} \\ 1 \\ e^{i\theta} \end{bmatrix}, \tag{8.22}$$

which yields solutions

$$c_{-1} = -\frac{\left(-2e^{i2\theta} + 1 + e^{i4\theta}\right)C^2 + \left(-2e^{i3\theta} + 2e^{i\theta}\right)C + \left(1 - e^{i2\theta}\right)B - 1}{e^{i\theta}\left[\left(e^{i2\theta} - 1\right)C^2 - 2e^{i\theta}C + \left(e^{i2\theta} - 1\right)A^2 - 2e^{i\theta}A + 1 - B\right]}, \tag{8.23}$$

$$c_0 = -\frac{\left(e^{i2\theta}-1\right)A - e^{i\theta}}{e^{i\theta}\left[\left(e^{i2\theta}-1\right)C^2 - 2e^{i\theta}C + \left(e^{i2\theta}-1\right)A^2 - 2e^{i\theta}A + 1 - B\right]}, \tag{8.24}$$

$$c_1 = \frac{\left[\left(e^{i2\theta}-1\right)C - e^{i\theta}\right]\left[\left(e^{i2\theta}-1\right)A - e^{i\theta}\right]}{e^{i\theta}\left[\left(e^{i2\theta}-1\right)C^2 - 2e^{i\theta}C + \left(e^{i2\theta}-1\right)A^2 - 2e^{i\theta}A + 1 - B\right]} \tag{8.25}$$

which we insert back into (8.17) to obtain

$$\begin{aligned}
\tau &= \frac{\left[\left(-2+e^{-2i\theta}+e^{2i\theta}\right)A + e^{-i\theta} - e^{i\theta}\right]C + \left(-e^{i\theta}+e^{-i\theta}\right)A + 1}{\left(e^{2i\theta}-1\right)C^2 - 2e^{i\theta}C + \left(e^{2i\theta}-1\right)A^2 - 2e^{i\theta}A + 1 - B} \\
&= \frac{1 - 4AC\sin^2\theta - 2i(A+C)\sin\theta}{e^{i\theta}\left[2i(A^2+C^2)\sin\theta - 2(A+C)\right] + 1 - B} \\
&= \frac{(\sigma)(\sigma y)}{1 + \dfrac{\left\{2z_s + (\cos\theta + i\sin\theta)\left[(\sigma-1)^2 + (\sigma y - 1)^2 + 2(\sigma-1) + 2(\sigma y - 1)\right]\right\}}{2i\sin\theta}} \\
&= \frac{(\sigma)(\sigma y)}{1 + \dfrac{1}{2i\sin\theta}\left\{2z_s + 2\cos\theta\left[\dfrac{1}{2}\sigma^2(y^2+1) - 1\right]\right\} + \dfrac{1}{2}\sigma^2(y^2+1) - 1} \\
&= \frac{(\sigma)(\sigma y)}{w^2 - i\dfrac{z_s + X(w^2-1)}{\sqrt{1-X^2}}} \qquad .
\end{aligned} \tag{8.26}$$

where we have defined $w = \sigma\sqrt{(1+y^2)/2}$.

The *transmission probability* is extracted via

$$\mathcal{T}(X) = |\tau|^2 = \frac{4}{\left(y + \dfrac{1}{y}\right)^2}\frac{1}{1 + \dfrac{\left[z_s + X(w^2-1)\right]^2}{w^4(1-X^2)}}, \tag{8.27}$$

which is the same result obtained via the transfer-matrix method [1, 3]. Implementing Azbel's energy-independent technique [108, 109], we integrate (8.27) over the energy band, but weighted by the energy-derivative of the *Fermi-Dirac distribution*, viz.,

$$f(E, E_f, T) = \frac{1}{e^{(E-E_f)/(k_bT)} + 1}, \tag{8.28}$$

where T is the absolute temperature and k_b is *Boltzmann's constant*. Introducing the *dimensionless reduced temperature*, $\zeta = k_b T/\beta$, the derivative of (8.28) is

$$-\frac{\partial f}{\partial E} = \frac{1}{4k_b T \cosh^2\left[\dfrac{(E-E_f)}{2k_b T}\right]} = \frac{1}{4\beta\zeta \cosh^2\left[\dfrac{(X-X_f)}{2\zeta}\right]}. \tag{8.29}$$

Thus, the *effective-transmission probability* is given by

$$t_{\text{eff}} = \int_{\text{bands}} \mathcal{T}(E)\left(-\frac{\partial}{\partial E} f(E, E_f, T)\right) dE = \int_{\text{band}} \frac{\mathcal{T}(X)}{4\zeta \cosh^2\left[\dfrac{(X-X_f)}{2\zeta}\right]} dX. \tag{8.30}$$

We shall consider the temperature independent limit $\zeta \to 0$, where (8.29) becomes a Dirac δ-function centered at the Fermi energy. Hence, (8.30) becomes

$$t_{\text{eff}} = \mathcal{T}(X_f). \tag{8.31}$$

8.2 Embedding Field-Enhanced Regions

Instead of limiting the perturbation region to a single atom, we now consider replacing it with a *finite chain* from $n = 0$ to $n = N$, with site (bond) energies α' (β'), which is attached to the crystal with bond energies δ. The application of an applied field of gradient Γ, restricted to this portion of the chain, introduces a *potential difference*, $\phi = N\Gamma$, between the site energies of the *crystal leads* on either side of the field region.

As in the chemisorption case, we must ensure that the field strength is such as to avoid ionization of the crystal. Again, we require the restraint $|N\Gamma/(2\beta')| < 2$, which allows at least one state to remain delocalized across the field region. In fact, for ideal transmission to be possible through the crystal, a state must remain

delocalized across the entire system. In particular, we must have an overlap between the allowed energy bands in the crystal leads, whence, $|\phi| < 4|\beta|$.

We define the energy in the right lead by

$$X' = \frac{E - \alpha - \phi}{2\beta} = X - U, \tag{8.32}$$

where $U = \phi/(2\beta)$, and effective wavenumber ω via

$$X' = \cos\omega. \tag{8.33}$$

The overlap between bands is, therefore, $U - 1 < X < 1$.

Since we set the *reduced-field strength* relative to β, the argument of the BFs now becomes

$$\chi = -\eta/F = -\eta N/U, \tag{8.34}$$

where $\eta = \beta'/\beta$.

To use the LS equation, we consider the unperturbed system to consist of three isolated pieces, the left semi-infinite crystal lead, the finite field-modified region, and the right semi-infinite lead. A right-moving Bloch wave is introduced at $n = -\infty$. Since the energy references in the two crystal leads are different, we must be careful with the normalization of the Bloch waves. The required condition is that the *local probability current* must be constant throughout the chain.

Following Caroli *et al.* [110], we define the *probability-current operator* to be proportional to the *projected difference* between adjacent sites, namely,

$$\mathbb{J}_n = J\left[|n+1\rangle\langle n| - |n\rangle\langle n+1|\right], \tag{8.35}$$

which has the expectation value

$$\langle\psi|\,\mathbb{J}_n\,|\psi\rangle = J\left(c_{n+1}^{*}c_n - c_n^{*}c_{n+1}\right). \tag{8.36}$$

An incoming Bloch wave, $c_n = ae^{in\theta}$, in the left lead will have a probability current

$$J_{n\to-\infty} = Ja^2\left(e^{-i\theta} - e^{i\theta}\right) = -2iJa^2\sin\theta, \tag{8.37}$$

while for an outgoing wave, $c_n = be^{i\omega}$, in the right lead

$$J_{n\to\infty} = Jb^2\left(e^{-i\omega} - e^{i\omega}\right) = -2iJb^2\sin\omega. \tag{8.38}$$

Requiring (8.37) and (8.38) to be equal leads to the *energy-independent solution* in which

$$a = \frac{1}{\sqrt{\sin\theta}}, \qquad b = \frac{1}{\sqrt{\sin\omega}}. \tag{8.39}$$

Thus, (8.10) can be rewritten as

$$c_n = \begin{cases} \dfrac{e^{in\theta}}{\sqrt{\sin\theta}} + r\dfrac{e^{-in\theta}}{\sqrt{\sin\theta}}, & n\to-\infty, \\ t\dfrac{e^{in\theta}}{\sqrt{\sin\omega}}, & n\to\infty. \end{cases} \tag{8.40}$$

We now turn to the LS equation to obtain c_n^0 for the semi-infinite chains from the infinite system by breaking the bond between $n = -1$ and $n = 0$, i.e., we introduce

$$\mathbf{V} = -\beta\left[|-1\rangle\langle 0| + |0\rangle\langle -1|\right], \tag{8.41}$$

which gives

$$c_n^0 = \frac{e^{in\theta}}{\sqrt{\sin\theta}} - \beta G_\infty(n,-1)c_0^0 - \beta G_\infty(n,0)c_{-1}^0. \tag{8.42}$$

Therefore, we find

$$\begin{aligned} c_0^0 &= \frac{1}{\sqrt{\sin\theta}} + \frac{e^{i\theta}}{2i\sin\theta}c_0^0 + \frac{1}{2i\sin\theta}c_{-1}^0, \\ c_{-1}^0 &= \frac{e^{-i\theta}}{\sqrt{\sin\theta}} + \frac{1}{2i\sin\theta}c_0^0 + \frac{e^{i\theta}}{2i\sin\theta}c_{-1}^0. \end{aligned} \tag{8.43}$$

Rewriting these as

$$\begin{aligned} e^{-i\theta}c_0^0 \quad + c_{-1}^0 \quad &= -2i\sqrt{\sin\theta}, \\ c_0^0 + e^{-i\theta}c_{-1}^0 &= -2i\sqrt{\sin\theta}e^{-i\theta}, \end{aligned} \tag{8.44}$$

we find solutions

$$c_0^0 = 0, \qquad c_{-1}^0 = -2i\sqrt{\sin\theta}, \tag{8.45}$$

whereby, (8.42) yields,

$$c_n^0 = \frac{e^{in\theta} - e^{i|n|\theta}}{\sqrt{\sin\theta}} = \begin{cases} \dfrac{2i\sin n\theta}{\sqrt{\sin\theta}}, & n \leq -1, \\ 0, & n \geq 0. \end{cases} \tag{8.46}$$

The GFs for the crystal leads are determined by cleaving the infinite chain with the potential

$$\mathbf{V} = -\beta\left[|-1\rangle\langle 0| + |0\rangle\langle -1| + |N\rangle\langle N+1| + |N+1\rangle\langle N|\right]. \tag{8.47}$$

With the aid of (3.8), the GFs for the semi-infinite chains are given by

$$\begin{aligned} G^0(n,m) \;=\; & G_\infty(n,m) - \beta G_\infty(n,-1)G^0(0,m) - \beta G_\infty(n,0)G^0(-1,m) \\ & - \beta G_\infty(n,N)G^0(N+1,m) - \beta G_\infty(n,N+1)G^0(N,m). \end{aligned} \tag{8.48}$$

In the left lead, where the energy is $X = \cos\theta$, we consider $n, m \leq -1$ and note that G^0 is zero whenever one of the indices is outside the lead. Hence, we have

$$G^0(n^-,m^-) = -\frac{e^{|n-m|\theta}}{2i\beta\sin\theta} + \frac{e^{i|n|\theta}}{2i\sin\theta}G^0(-1,m), \tag{8.49}$$

which we use to obtain

$$G^0(-1,m) = -\frac{e^{|m+1|\theta}}{2i\beta\sin\theta} + \frac{e^{i\theta}}{2i\sin\theta}G^0(-1,m). \tag{8.50}$$

Solving (8.50) gives

$$G^0(-1,m) = \beta^{-1}e^{i|m+1|\theta}e^{i\theta}, \tag{8.51}$$

which in (8.49) results in

$$G^0(n^-,m^-) = \frac{e^{i|n|\theta}e^{i|m+1|\theta}e^{i\theta} - e^{i|n-m|\theta}}{2i\beta\sin\theta}. \tag{8.52}$$

In particular, on setting $m = -1$, we have

$$G^0(n^-, -1) = \frac{e^{-in\theta}e^{i\theta} - e^{-i(n+1)\theta}}{2i\beta \sin\theta} = \beta^{-1}e^{-in\theta}. \tag{8.53}$$

Likewise, the right-crystal lead will have $X' = \cos\omega$, so, for $n, m \geq N+1$, we see that

$$G^0(n^+, m^+) = -\frac{e^{|n-m|\omega}}{2i\beta \sin\omega} + \frac{e^{i|n-N|\omega}}{2i \sin\omega} G^0(N+1, m), \tag{8.54}$$

where again any element of G^0 with an index outside the lead is zero. Setting $n = N+1$, (8.54) becomes

$$G^0(N+1, m) = -\frac{e^{|m-N-1|\omega}}{2i\beta \sin\omega} + \frac{e^{i\omega}}{2i \sin\omega} G^0(N+1, m), \tag{8.55}$$

which leads to

$$G^0(N+1, m) = \beta^{-1}e^{i|m-N-1|\omega}e^{i\omega}. \tag{8.56}$$

On inserting (8.56) in (8.54), we arrive at

$$G^0(n^+, m^+) = \frac{e^{i|n-N|\omega}e^{i|m-N-1|\omega}e^{i\omega} - e^{i|n-m|\omega}}{2i\beta \sin\omega}, \tag{8.57}$$

which for $m = N+1$ becomes

$$G^0(n^+, N+1) = \frac{e^{i(n-N)\omega}e^{i\omega} - e^{i(n-N-1)\omega}}{2i\beta \sin\omega} = \beta^{-1}e^{i(n-N)\omega}. \tag{8.58}$$

Having the required components for the crystal leads, we attach them to the finite region, which we describe through its Greenian G_{0N}, by using the potential

$$\mathbf{V} = \delta\left[|-1\rangle\langle 0| + |0\rangle\langle -1|\right], \tag{8.59}$$

and the unperturbed GFs,

$$G^0(n, m) = \begin{cases} G_{-1^-}(n, m), & n, m \leq -1, \\ G_{0N}(n, m), & 0 \leq n, m \leq N, \\ G_{(N+1)^+}(n, m), & n, m \geq N+1, \\ 0, & \text{otherwise.} \end{cases} \tag{8.60}$$

The LS equation in the left lead, $n \leq -1$, is therefore

$$\begin{aligned} c_{n-} &= c_n^0 + \delta G^0(n,-1)c_0 \\ &= \frac{2i\sin n\theta}{\sqrt{\sin\theta}} + \lambda e^{-in\theta}c_0, \end{aligned} \tag{8.61}$$

where $\lambda = \delta/\beta$ which, in particular, provides

$$c_{-1} = -2i\sqrt{\sin\theta} + \lambda e^{i\theta}c_0. \tag{8.62}$$

In the field-modified region, the LS equation (8.7) gives

$$c_0 = \delta G_{0N}(0,0)c_{-1} + \delta G_{0N}(0,N)c_{N+1}, \tag{8.63}$$

and

$$c_N = \delta G_{0N}(N,0)c_{-1} + \delta G_{0N}(N,N)c_{N+1}. \tag{8.64}$$

In the right lead, $m \geq N+1$, we have

$$c_m = \delta G^0(m,N+1)c_N = \lambda e^{i(m-N)\omega}c_N, \tag{8.65}$$

which at $m = N+1$ produces

$$c_{N+1} = \lambda e^{i\omega}c_N. \tag{8.66}$$

The transmission coefficient is obtained from (8.65) by equating it to (8.40), which leads to

$$\tau = \lambda\sqrt{\sin\omega}e^{-iN\omega}c_N. \tag{8.67}$$

Inserting (8.63) in (8.62), we obtain the implicit equation

$$c_{-1} = -2i\sqrt{\sin\theta} + \lambda^2 e^{i\theta}\beta G_{0N}(0,0)c_{-1} + \lambda^2 e^{i\theta}\beta G_{0N}(0,N)c_{N+1}, \tag{8.68}$$

which yields the solution

$$c_{-1} = \frac{-2i\sqrt{\sin\theta} + \lambda^2 e^{i\theta}\beta G_{0N}(0,N)c_{N+1}}{1 - \lambda^2 e^{i\theta}\beta G_{0N}(0,0)}. \tag{8.69}$$

Using (8.69) and (8.66) in (8.64) leads to

$$c_N = \frac{-2i\sqrt{\sin\theta}\lambda\beta G_{0N}(N,0)}{1-\lambda^2 e^{i\theta}\beta G_{0N}(0,0)} + \left[\frac{\lambda^3 e^{i\theta}\beta G_{0N}(0,N)\beta G_{0N}(N,0)}{1-\lambda^2 e^{i\theta}\beta G_{0N}(0,0)} + \lambda\beta G_{0N}(N,N)\right]\lambda e^{i\omega}c_N, \quad (8.70)$$

which is again implicitly defined, so that we may write

$$c_N = \frac{-2i\sqrt{\sin\theta}\lambda\beta G_{0N}(N,0)}{D(\theta,\omega)}, \quad (8.71)$$

where

$$D(\theta,\omega) = \left[1-\lambda^2\beta G_{0N}(0,0)e^{i\theta}\right]\left[1-\lambda^2\beta G_{0N}(N,N)e^{i\omega}\right] - \lambda^4 e^{i(\theta+\omega)}\beta G_{0N}(0,N)\beta G_{0N}(N,0). \quad (8.72)$$

Thus, the transmission coefficient (8.67) becomes,

$$\tau = \frac{-2i\sqrt{\sin\theta\sin\omega}\lambda^2\beta G_{0N}(N,0)e^{-iN\omega}}{D(\theta,\omega)}, \quad (8.73)$$

whence, the transmission probability is

$$\mathcal{T} = |\tau|^2 = \frac{4\sin\theta\sin\omega\lambda^4|\beta G_{0N}(N,0)|^2}{|D(\theta,\omega)|^2}. \quad (8.74)$$

In terms of the reduced energy, (6.5), (8.32) and (8.33)show that

$$\mathcal{T} = |\tau|^2 = \frac{4\lambda^4\sqrt{(1-X^2)(1-(X+U)^2)}|\beta G_{0N}(N,0)|^2}{|D(X)|^2}, \quad (8.75)$$

where

$$D(X) = \left[1-\lambda^2\beta G_{0N}(0,0)(X+i\sqrt{1-X^2})\right] \times \left[1-\lambda^2\beta G_{0N}(N,N)(X+U+i\sqrt{1-(X+U)^2})\right] - \lambda^4(X+i\sqrt{1-X^2})(X+U+i\sqrt{1-(X+U)^2})\beta G_{0N}(0,N)\beta G_{0N}(N,0). \quad (8.76)$$

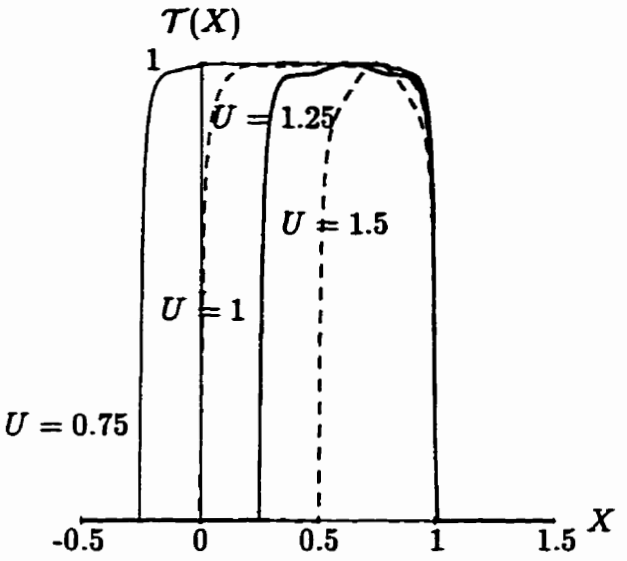

Fig. 8.3: Band overlap regions for indicated potential differences.

It now remains only to determine the GF elements of the field-modified region.

Since we have altered the bond and site energies in the finite region, we must renormalize our parameters according to $\beta \to \beta' = \beta\eta$. In particular,

$$X \to \frac{X - z}{\eta} \tag{8.77}$$

is now the effective energy parameter inside the field region. Along with $x \to \chi$ as defined in (8.34), equation (8.77) requires $\nu \to \mu$, where

$$\mu = \chi\frac{X - z}{\eta} = -\frac{N(X - z)}{U}. \tag{8.78}$$

With these conversions in mind, we modify the results of § 5.2 to obtain the required GF elements of the finite chain.

Next, we consider the parameter effects on the transmission probability (8.75). If the field-modified region material is the same as the leads, ramping the potential difference, U, narrows the band-overlap region (Fig. 8.3). If we choose $U = 1$,

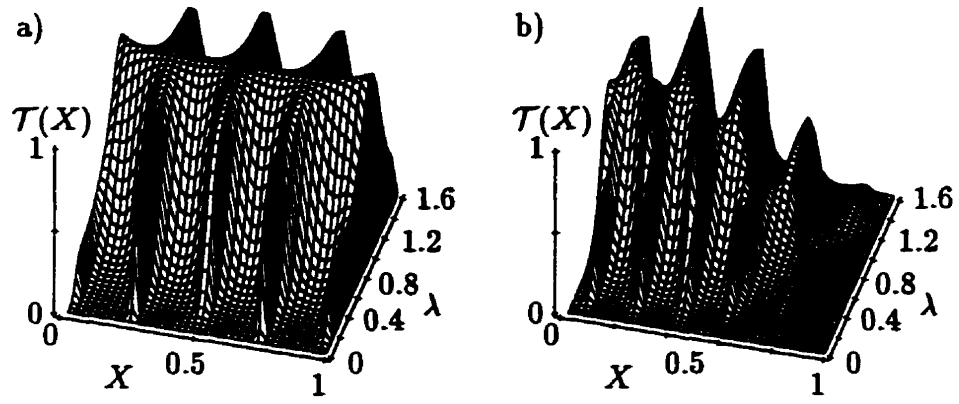

Fig. 8.4: Transmission probability of embedded field-states in (X, λ) space with $U = 1$ for a) identical material, $z = 0$, $\eta = 1$, b) different material, $z = -0.25$, $\eta = 0.75$.

the overlap region's width is half that of the conduction bands, so that $N/2$ of the discrete states are embedded in the overlap region. Varying the interface bond strength, λ, we see that as it increases, the separation between the states spreads, while the states themselves broaden and increase in intensity until full transmission occurs at $\lambda = 1$, after which they become narrower and drop in intensity, while continuing to separate (Fig. 8.4a).

Moving on, we consider altering the material in the field-modified region. Adjusting z will rigidly shift the embedded field-states behind the overlap window. Changing η modifies the band-width of the field region. For $\eta = 0.75$ and $z = -0.25$ (Fig. 8.4b), we see that the states are shifted downward, leaving little transmission at the higher energies. The separation between field-states is narrowed and the states themselves are reduced for low interface bond energies, but sharpened for $\lambda > 1$.

8.3 Field Effect on Molecular Switching

In this section, we wish to investigate the possibility of securing control of the transmission probability by means of a single-site impurity inside the field-modified region. Since (8.75) and (8.76) require only the GFs involving the end sites for the region, here we only need to construct a finite chain with an embedded impurity in a linear potential. To do this, we attach finite chains to either side of the impurity located at site M. Thus, the unperturbed GF is in three parts, i.e.,

$$G^0(n,m) = \begin{cases} G_{0,M-1}(n,m), & 0 \le n,m \le M-1, \\ G_{M,M}(M,M), & n = m = M, \\ G_{M+1,N}(n,m), & M+1 \le n,m \le N, \\ 0, & \text{otherwise}, \end{cases} \tag{8.79}$$

which we attach via the potential

$$\mathbb{V} = \rho\left(|M-1\rangle\langle M| + |M\rangle\langle M-1|\right) + \rho'\left(|M\rangle\langle M+1| + |M+1\rangle\langle M|\right). \tag{8.80}$$

Using the Dyson equation (3.8), we have

$$G_{0N}(0,0) = G^0(0,0) + \rho G^0(0,M-1)G_{0N}(M,0), \tag{8.81}$$

which requires us to find

$$G_{0N}(M,0) = G_{0N}(0,M) = \rho G^0(0,M-1)G_{0N}(M,M). \tag{8.82}$$

The on-site GF at the impurity is given by

$$G_{0N}(M,M) = G^0(M,M)\left[1 + \rho G_{0N}(M-1,M) + \rho' G_{0N}(M+1,M)\right], \tag{8.83}$$

which uses

$$G_{0N}(M-1,M) = \rho G^0(M-1,M-1)G_{0N}(M,M), \tag{8.84}$$

and

$$G_{0N}(M+1,M) = \rho' G^0(M+1,M+1) G_{0N}(M,M). \tag{8.85}$$

Inserting (8.84) and (8.85) into (8.83) generates the implicit equation

$$\begin{aligned} G_{0N}(M,M) &= G^0(M,M) \\ &\quad + \left[\rho^2 G^0(M-1,M-1) + (\rho')^2 G^0(M+1,M+1)\right] G_{0N}(M,M), \end{aligned} \tag{8.86}$$

which, on rearranging, gives

$$\begin{aligned} G_{0N}(M,M) &= \frac{G^0(M,M)}{1 - \left[\rho^2 G^0(M-1,M-1) + (\rho')^2 G^0(M+1,M+1)\right]} \\ &= \frac{1}{G^0(M,M)^{-1} - \left[\rho^2 G^0(M-1,M-1) + (\rho')^2 G^0(M+1,M+1)\right]}. \end{aligned} \tag{8.87}$$

Returning to (8.81) and using (8.87), we obtain

$$\begin{aligned} G_{0N}(0,0) &= G^0(0,0) \\ &\quad + \frac{\rho^2 G^0(0,M-1)^2}{G^0(M,M)^{-1} - \left[\rho^2 G^0(M-1,M-1) + (\rho')^2 G^0(M+1,M+1)\right]}. \end{aligned} \tag{8.88}$$

Similarly, we have

$$G_{0N}(N,N) = G^0(N,N) + \rho' G^0(N,M+1) G_{0N}(M,N), \tag{8.89}$$

and

$$G_{0N}(M,N) = G_{0N}(N,M) = \rho' G^0(N,M+1) G_{0N}(M,M), \tag{8.90}$$

which, by (8.87), yields

$$\begin{aligned} G_{0N}(N,N) &= G^0(N,N) \\ &\quad + \frac{(\rho')^2 G^0(N,M+1)^2}{G^0(M,M)^{-1} - \left[\rho^2 G^0(M-1,M-1) + (\rho')^2 G^0(M+1,M+1)\right]}. \end{aligned} \tag{8.91}$$

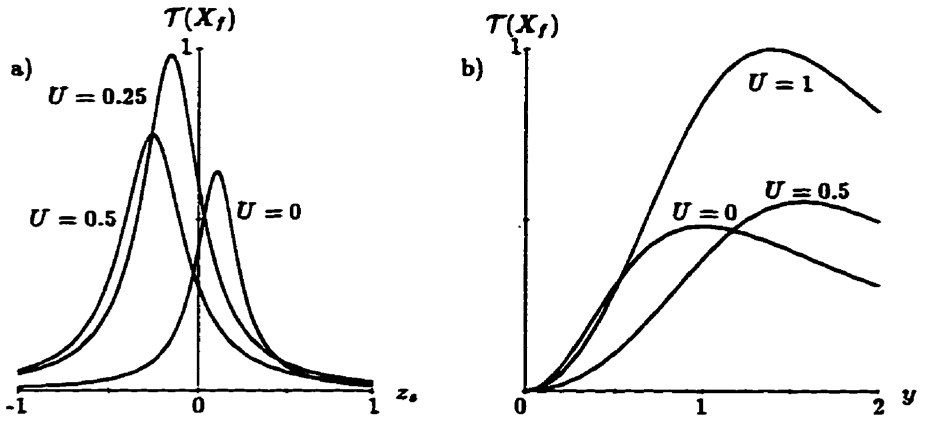

Fig. 8.5: Field effects on switching parameters for indicated values of the potential difference, a) $y = 0.5$ and z_s variable, b) $z_s = 0.25$ and y variable.

The cross-terms involving the end sites are generated by

$$\begin{aligned} G_{0N}(0,N) &= G_{0N}(N,0) = \rho G^0(0,M-1)G_{0N}(M,N) \\ &= \frac{\rho\rho' G^0(0,M-1)G^0(N,M+1)}{G^0(M,M)^{-1} - \left[\rho^2 G^0(M-1,M-1) + (\rho')^2 G^0(M+1,M+1)\right]}. \end{aligned} \tag{8.92}$$

Finally, we use the parameters of the impurity (8.15) at site M to show that

$$G^0(M,M)^{-1} = 2\beta(X - z_s - MF). \tag{8.93}$$

Along with the modified results of § 5.2, (8.93) allows us to obtain the GF elements to insert into (8.75).

Employing (8.31), we choose z_s and y as the candidate parameters for describing the space over which we wish to control the impurity [1, 3]. We take the system shown in Fig. 8.4b with $\lambda = 0.75$. Taking $X_f = 0.25$ and $\sigma = 0.8$, we first set $y = 0.5$ and consider the effect of ramping the field on the z_s curve (Fig. 8.5a). As

U is increased, the transmission peak increases in height to a resonance at $U = 0.25$ before decreasing again.

Turning to the case of $z_s = X_f = 0.25$, we treat y as the switching parameter (Fig. 8.5b). Here, the peak transmission probability is increased both in height and y location, as U is increased, doubling from $U = 0$ to $U = 1$.

Chapter 9

Conclusion

9.1 Results and Discussion

There has been considerable debate over the modeling of electrified solids. While numerical computation has gone far in resolving these controversies, we have been able to provide a greater understanding of the phenomenon by developing a rigorous *analytical* GF method to describe the application of a constant field to 1-D crystal TB models, resulting in exact solutions involving combinations of BFs.

Access to the finite, semi-infinite and infinite chains has generated insight into the mechanisms by which characteristic energy-spectra properties appear as we traverse from one type to another. We have also seen how the zero-field properties arise from those of a *large* field by passing through intermediate results.

The breadth of application for this method has only been touched upon by the investigations chosen here. The discretization of the energy band has major implications in the definition and location of *surface states*, due to the absence of traditional existence conditions, but, at the same time, introduces *surface resonance*

phenomenon.

In looking at field-enhanced *chemisorption*, we have found that electrifying the substrate may enhance the *chemisorption process* through the creation of magnetic solutions, or weaken it, depending on the properties of the material.

In ME, we have been able to embed a field-enhanced region into a conducting material and model the transmission properties through the system using a LS approach. The transmission probability can be manipulated through the control of the single impurity-site parameters, thereby producing a *molecular switch.*

In all three areas, the ability to include field-modified regions will expand the types of problems accessible to researchers.

9.2 Future Directions

The application of this method is restricted only by meeting the hypotheses of Pincherle's theorem, which allows us to consider more general systems than the simple models we have used here. The introduction of alternating bonds gives rise to a model for semiconductors, allowing the field to perturb the bond energies gives rise to hypergeometric function solutions instead of BFs [45].

In the surface states and chemisorption treatments, screening effects have been neglected. The reaction of the electron gas to the applied field will alter the electronic configuration.

The next step in developing a working ME circuit is to design atomic-level analogs to other macroscopic electronic devices, e.g., resistors, capacitors, inductors.

The electronic properties of *molecular capacitors* can be investigated by embedding a short chain of dielectric material in an polymeric molecular wire. The static

electronic structure can be obtained from the application of our GF approach. To properly analyze capacitance, however, we must consider the charge build-up and relaxation time dependence of the material.

By considering molecules based on a stacked benzene-ring structure embedded in a polymeric chain, a conceptual model for inductors can be developed. When current flows though this system, energy should be stored through the creation of an applied field. To obtain the static electronic structure of such a chain under the influence of an applied field will require the present Green function approach to be implemented beyond one-dimension. The extension to two dimensions of Pendry's causal-surface GF method [91] suggests the direction that such a generalization should take.

Once the conceptual models for these ME devices have been analyzed, the electronic structure of candidate designs can be investigated via scanning tunneling microscopy. Results from such experiments will provide valuable information on improvements to the theoretical models.

Appendix A

Rydberg Atomic Units

The one-dimensional time-independent Schrödinger equation is given by

$$-\frac{\hbar^2}{2m}\frac{\partial^2\Psi(\mathsf{x})}{\partial\mathsf{x}^2} + q\mathsf{V}(\mathsf{x})\Psi(\mathsf{x}) = \mathsf{E}\Psi(\mathsf{x}) \tag{A.1}$$

where $\Psi(\mathsf{x})$ is the wavefunction for a particle of mass m, charge q and energy E affected by a potential $\mathsf{V}(\mathsf{x})$.

Often, as in the case of this thesis, the particle we are describing is an electron, which has a rest mass $m = m_e \approx 9.10956 \times 10^{-28}\mathrm{g}$ and a charge $q = -e \approx -4.80325 \times 10^{-10}\mathrm{esu}$. In CGS units, where the permittivity of free space of is *not* required to determine the electrostatic field equations, we combine these characteristic electron values with Planck's constant, $\hbar = h/(2\pi) \approx 1.05459 \times 10^{-27}\mathrm{erg\,s}$, to obtain a relative length scale based on the Bohr radius $r_0 = \hbar^2/(me^2) \approx 5.29177 \times 10^{-9}\mathrm{cm}$, and a relative energy scale based on the Rydberg constant $R_\infty = m_e e^4/2\hbar^2 \approx 2.17991 \times 10^{-11}\mathrm{erg}$.

If we convert our length scale to multiples of the Bohr radius,

$$\mathsf{x} = xa_0 = \frac{\hbar^2}{m_e e^2}x \tag{A.2}$$

then, switching to the dimensionless length variable via $\psi(x) \equiv \sqrt{a_0}\Psi(a_0 x) = \sqrt{a_0}\Psi(\mathsf{x})$, we have

$$-\frac{\hbar^2}{2m_e}\frac{\partial^2\Psi(\mathsf{x})}{\partial \mathsf{x}^2} = -\frac{\hbar^2}{2m_e}\frac{\partial^2\Psi(\mathsf{x})}{\partial x^2}\left(\frac{dx}{d\mathsf{x}}\right)^2 = -\frac{\hbar^2}{2m_e\sqrt{a_0}}\frac{\partial^2\psi(x)}{\partial x^2}\frac{m_e^2e^4}{\hbar^4}$$
$$= -\frac{m_e e^4}{2\hbar^2\sqrt{a_0}}\frac{\partial^2\psi(x)}{\partial x^2}. \tag{A.3}$$

Converting our energy terms to multiples of Rydbergs,

$$\mathsf{E} = ER_\infty = \frac{m_e e^4}{2\hbar^2}E \tag{A.4}$$

and

$$\mathsf{V}(\mathsf{x}) = \mathsf{V}(a_0 x) = -\frac{1}{e}V(x)R_\infty = -\frac{m_e e^3}{2\hbar^2}V(x), \tag{A.5}$$

(A.1) becomes

$$-\frac{m_e e^4}{2\hbar^2\sqrt{a_0}}\frac{\partial^2\psi(x)}{\partial x^2} + \frac{m_e e^4}{2\hbar^2\sqrt{a_0}}V(x)\psi(x) = \frac{m_e e^4}{2\hbar^2\sqrt{a_0}}E\psi(x) \tag{A.6}$$

or, rewriting,

$$\frac{\partial^2\psi(x)}{\partial x^2} + [E - V(x)]\psi(x) = 0, \tag{A.7}$$

where all the variables are now dimensionless, lengths normalized to the Bohr radius, and energies normalized to Rydbergs.

Turning to the application of a constant applied field, ε, the electric potential is given by

$$\Phi(\mathsf{x}) = -\varepsilon\mathsf{x}. \tag{A.8}$$

To obtain the potential in Rydberg atomic units, the application of (A.5) to (A.8) yields

$$-\varepsilon\mathsf{x} = -\varepsilon x a_0 = -\frac{1}{e}\phi(x)R_\infty, \tag{A.9}$$

so that

$$\phi(x) = -\frac{q_e\varepsilon a_0}{R_\infty}x \equiv \gamma x, \tag{A.10}$$

which defines the field *gradient*, γ.

Appendix B

Creation and Annihilation Operators

In a collection of *Fermi* particles, each state, n, can either be empty or occupied, i.e.. $N_n \in \{0, 1\}$ is the number of particles in the state n. If we order the states, the total wavefunction can be labeled by the state occupancy [98],

$$|N_1, N_2, \ldots, N_n, \ldots\rangle . \tag{B.1}$$

We wish to introduce creation operators, $\mathbb{C}_n^\dagger$, with the properties that, if $N_n = 0$, operation will yield the wavefunction with $N_n = 1$ and, if $N_n = 1$, operation gives zero, since we cannot create a particle in an occupied state. Hence,

$$\mathbb{C}_n^\dagger \, |N_1, N_2, \ldots, N_n, \ldots\rangle = (-1)^{\nu_n}(1 - N_n) \, |N_1, N_2, \ldots, 1 - N_n, \ldots\rangle , \tag{B.2}$$

where the sign is determined by the number of occupied states below n, viz.,

$$\nu_n = \sum_{m=1}^{n-1} N_m, \tag{B.3}$$

due to the necessity of requiring Fermi wavefunctions to be antisymmetric.

The conjugate operator, $\mathbb{C}_n$, is the annihilation operator, producing a wavefunction missing a particle in the n^{th} state, if there was one, or zero, if not.

$$\mathbb{C}_n \left|N_1, N_2, \ldots, N_n, \ldots\right\rangle = (-1)^{\nu_n} N_n \left|N_1, N_2, \ldots, 1 - N_n, \ldots\right\rangle, \tag{B.4}$$

From (B.2) and (B.4), we can construct the number operator for the n^{th} state,

$$\mathbb{N}_n = \mathbb{C}_n^\dagger \mathbb{C}_n, \tag{B.5}$$

which returns the eigenvalue at state n,

$$\mathbb{N}_n \left|N_1, N_2, \ldots, N_n, \ldots\right\rangle = N_n^2 \left|N_1, N_2, \ldots, N_n, \ldots\right\rangle = N_n \left|N_1, N_2, \ldots, N_n, \ldots\right\rangle, \tag{B.6}$$

since N_n is either 0 or 1. Note that (B.6) is an eigenvalue equation. Since the $\mathbb{N}_n$ operator has only two possible eigenvalues, we can represent it as a 2×2 matrix,

$$\mathbb{N}_n = \begin{bmatrix} 0 & 0 \\ 0 & 1 \end{bmatrix}, \tag{B.7}$$

with the eigenvectors

$$\left|0\right\rangle_n = \left|N_1, N_2, \ldots, 0, \ldots\right\rangle = \begin{bmatrix} 1 \\ 0 \end{bmatrix}, \qquad \left|1\right\rangle_n = \left|N_1, N_2, \ldots, 1, \ldots\right\rangle = \begin{bmatrix} 0 \\ 1 \end{bmatrix}. \tag{B.8}$$

Hence, (B.2) becomes

$$\mathbb{C}_n^\dagger \left|0\right\rangle_n = (-1)^{\nu_n} \left|1\right\rangle_n, \qquad \mathbb{C}_n^\dagger \left|1\right\rangle_n = 0, \tag{B.9}$$

so that

$$\mathbb{C}_n^\dagger = (-1)^{\nu_n} \begin{bmatrix} 0 & 0 \\ 1 & 0 \end{bmatrix}. \tag{B.10}$$

Thus, we must have

$$\mathbb{C}_n = (-1)^{\nu_n} \begin{bmatrix} 0 & 1 \\ 0 & 0 \end{bmatrix}, \tag{B.11}$$

which does indeed have the required properties,

$$\mathbb{C}_n \left|0\right\rangle_n = 0, \qquad \mathbb{C}_n \left|1\right\rangle_n = (-1)^{\nu_n} \left|0\right\rangle_n . \tag{B.12}$$

We now have enough information to derive the anticommutation rules for the creation and annihilation operators.

First, we consider operation on a single state. The four relevant equations are

$$\begin{aligned}
\mathbb{C}_n \mathbb{C}_n^\dagger \left|\ldots, N_n, \ldots\right\rangle &= (1 - N_n) \left|\ldots, N_n, \ldots\right\rangle , \\
\mathbb{C}_n^\dagger \mathbb{C}_n \left|\ldots, N_n, \ldots\right\rangle &= N_n \left|\ldots, N_n, \ldots\right\rangle , \\
\mathbb{C}_n \mathbb{C}_n \left|\ldots, N_n, \ldots\right\rangle &= N_n(1 - N_n) \left|\ldots, N_n, \ldots\right\rangle = 0, \\
\mathbb{C}_n^\dagger \mathbb{C}_n^\dagger \left|\ldots, N_n, \ldots\right\rangle &= 0.
\end{aligned} \tag{B.13}$$

From which we assemble the anticommutators,

$$\{\mathbb{C}_n, \mathbb{C}_n\} = \{\mathbb{C}_n^\dagger, \mathbb{C}_n^\dagger\} = 0, \qquad \{\mathbb{C}_n^\dagger, \mathbb{C}_n\} = 1. \tag{B.14}$$

Next, we consider two states, $m < n$. We have,

$$\begin{aligned}
\mathbb{C}_m \mathbb{C}_n \left|\ldots, N_m, \ldots, N_n, \ldots\right\rangle &= (-1)^{\nu_n} N_n \mathbb{C}_m \left|\ldots, N_m, \ldots, 1 - N_n, \ldots\right\rangle \\
&= (-1)^{\nu_n + \nu_m} N_n N_m \left|\ldots, 1 - N_m, \ldots, 1 - N_n, \ldots\right\rangle , \\
\mathbb{C}_n \mathbb{C}_m \left|\ldots, N_m, \ldots, N_n, \ldots\right\rangle &= (-1)^{\nu_m} N_m \mathbb{C}_n \left|\ldots, 1 - N_m, \ldots, N_n, \ldots\right\rangle \\
&= (-1)^{\nu_m + \nu_n - 1} N_m N_n \left|\ldots, 1 - N_m, \ldots, 1 - N_n, \ldots\right\rangle ,
\end{aligned} \tag{B.15}$$

since the operation of $\mathbb{C}_m$ first reduces ν_n by 1, but $\mathbb{C}_n$ leaves ν_m unchanged, hence,

$$\{\mathbb{C}_m, \mathbb{C}_n\} = 0. \tag{B.16}$$

Similarly,

$$\begin{aligned}
\mathbb{C}_m^\dagger \mathbb{C}_n^\dagger \,|\ldots, N_m, \ldots, N_n, \ldots\rangle &= (-1)^{\nu_n}(1-N_n)\mathbb{C}_m^\dagger \,|\ldots, N_m, \ldots, 1-N_n, \ldots\rangle \\
&= (-1)^{\nu_n+\nu_m}(1-N_n)(1-N_m)\,|\ldots, 1-N_m, \ldots, 1-N_n, \ldots\rangle\,, \\
\mathbb{C}_n^\dagger \mathbb{C}_m^\dagger \,|\ldots, N_m, \ldots, N_n, \ldots\rangle &= (-1)^{\nu_m}(1-N_m)\mathbb{C}_n^\dagger \,|\ldots, 1-N_m, \ldots, N_n, \ldots\rangle \\
&= (-1)^{\nu_m+\nu_n-1}(1-N_m)(1-N_n)\,|\ldots, 1-N_m, \ldots, 1-N_n, \ldots\rangle\,,
\end{aligned} \tag{B.17}$$

whence,

$$\{\mathbb{C}_m^\dagger, \mathbb{C}_n^\dagger\} = 0, \qquad m < n. \tag{B.18}$$

Finally,

$$\begin{aligned}
\mathbb{C}_m^\dagger \mathbb{C}_n \,|\ldots, N_m, \ldots, N_n, \ldots\rangle &= (-1)^{\nu_n} N_n \mathbb{C}_m^\dagger \,|\ldots, N_m, \ldots, 1-N_n, \ldots\rangle \\
&= (-1)^{\nu_n+\nu_m} N_n(1-N_m)\,|\ldots, 1-N_m, \ldots, 1-N_n, \ldots\rangle\,, \\
\mathbb{C}_n \mathbb{C}_m^\dagger \,|\ldots, N_m, \ldots, N_n, \ldots\rangle &= (-1)^{\nu_m}(1-N_m)\mathbb{C}_n^\dagger \,|\ldots, 1-N_m, \ldots, N_n, \ldots\rangle \\
&= (-1)^{\nu_m+\nu_n-1}(1-N_m)N_n\,|\ldots, 1-N_m, \ldots, 1-N_n, \ldots\rangle\,,
\end{aligned} \tag{B.19}$$

leads to

$$\{\mathbb{C}_m^\dagger, \mathbb{C}_n\} = 0, \qquad m < n. \tag{B.20}$$

Choosing $m > n$ in (B.15) through (B.20) yields the same results. Thus, we have

$$\{\mathbb{C}_m, \mathbb{C}_n\} = \{\mathbb{C}_m^\dagger, \mathbb{C}_n^\dagger\} = 0, \qquad \{\mathbb{C}_m^\dagger, \mathbb{C}_n\} = \delta_{mn}, \tag{B.21}$$

for any m, n.

Appendix C

Summing Series of Matrices

The series form for the elements of the Greenian G_{N+1} given in (3.34) can be written as

$$G_{N+1}(i,j) = G_N(i,j) + \sum_{a\in\{l,m\}} \sum_{b\in\{l,m\}} G_N(i,a)\left\{h_{ab} + [hgh]_{ab} + [hghgh]_{ab} + \cdots\right\} G_N(b,j), \quad \text{(C.1)}$$

where the bond between mesh sites l and m have been added at the $(N+1)^{st}$ iteration.

We wish to consider the summation of the ab elements of products of the h and g matrices given by (3.33). Since matrix addition is linear, the sum of ab elements is the ab element of the sum of the matrices, i.e.,

$$h_{ab} + [hgh]_{ab} + [hghgh]_{ab} + \cdots = [h + hgh + hghgh + \cdots]_{ab}, \quad \text{(C.2)}$$

which reduces the problem to considering the matrix series.

Let us define the N^{th} partial sum to be the matrix S_N, and then multiply on

the right by gh,

$$\begin{aligned} S_N &= h + hgh + hghgh + \cdots + h\prod_{i=1}^{N} gh, \\ S_N gh &= \quad hgh + hghgh + \cdots + h\prod_{i=1}^{N} gh + h\prod_{i=1}^{N+1} gh. \end{aligned} \tag{C.3}$$

The difference between these two equation is simply

$$S_N(1 - gh) = h - h\prod_{i=1}^{N+1} gh. \tag{C.4}$$

To proceed, we must address the final term in (C.4). We require $|\det(gh)| < 1$ in order for the right-hand side to remain finite as $N \to \infty$. When this condition is satisfied, the product converges to 0 so, by multiplying on the right by $(1 - gh)^{-1}$, we find that, in the limit $N \to \infty$, the series converges to

$$S_\infty = h(1 - gh)^{-1} = \left[(1 - gh)h^{-1}\right]^{-1} = \left[h^{-1} - g\right]^{-1}. \tag{C.5}$$

Hence, the ab element of this result is exactly what appears in (3.34),

$$\left[h^{-1} - g\right]^{-1}_{ab} = [S_\infty]_{ab} = [h + hgh + hghgh + \cdots]_{ab}. \tag{C.6}$$

Returning to the condition for convergence, we use (3.33) to expand the determinant into the CF and Hamiltonian elements,

$$\begin{aligned} 1 > |\det(gh)| &= \left|\det\left(\begin{bmatrix} G_N(l,l) & G_N(l,m) \\ G_N(m,l) & G_N(m,m) \end{bmatrix}\begin{bmatrix} 0 & H_{lm} \\ H_{ml} & 0 \end{bmatrix}\right)\right| \\ &= \left|\det\begin{bmatrix} G_N(m,l)H_{lm} & G_N(l,l)H_{ml} \\ G_N(m,m)H_{lm} & G_N(l,m)H_{lm} \end{bmatrix}\right| \\ &= |G_N(m,l)H_{lm}G_N(l,m)H_{lm} - G_N(l,l)H_{ml}G_N(m,m)H_{lm}|. \end{aligned} \tag{C.7}$$

Since there will be cases where one of the mesh-sites being linked is *not* already part of the cluster, i.e., $G_N(m,l) = G_N(l,m) = 0$, the condition in (C.7) includes the limitation that

$$|G_N(l,l)H_{ml}G_N(m,m)H_{lm}| < 1 \tag{C.8}$$

for convergence of the geometric series.

Appendix D

Matrix-Determinant Approach

The following derivation, based on communications with Dr. A.T. Amos, provides an alternant derivation of the IF (3.50) for the surface GF element.

Using the LCAO wavefunctions as a basis, the subspace containing the *connected* sites between M and n allow us to write the the Schrödinger equation, i.e., the inverse of the Greenian $\mathbb{G}_{M,n}$, as an $n+1-M, n+1-M$ *tri-diagonal matrix*, namely,

$$\begin{aligned}\mathbb{M}_{M,n} &= \mathbb{G}_{M,n}^{-1} = E\mathbb{I} - \mathbb{H}_{M,n} \\ &= \begin{bmatrix} E-\alpha_M & \beta & 0 & \cdots & & \\ \beta & E-\alpha_{M+1} & \beta & & & \\ 0 & \beta & \ddots & & & \\ & & & \ddots & \beta & 0 \\ & & & \beta & E-\alpha_{n-1} & \beta \\ & & & 0 & \beta & E-\alpha_n \end{bmatrix}. \end{aligned} \tag{D.1}$$

Thus, we need to invert $\mathbb{M}$ in order to obtain the Greenian, and so the GF elements

are

$$G_{M,n}(i,j) = \left[\mathbf{M}_{M,n}^{-1}\right]_{i,j} = \frac{(-1)^{i+j}\mathrm{det}\mathbf{M}_{M,n}(i|j)}{\mathrm{det}\mathbf{M}_{M,n}}, \tag{D.2}$$

where the numerator is the i,j *cofactor* of $\mathbf{M}_{M,n}$. In particular, for $i = j = n$ being the last row and column, (D.2) becomes,

$$G_{M,n}(n,n) = \frac{\mathrm{det}\mathbf{M}_{M,n}(n|n)}{\mathrm{det}\mathbf{M}_{M,n}} = \frac{\mathrm{det}\mathbf{M}_{M,n-1}}{\mathrm{det}\mathbf{M}_{M,n}}. \tag{D.3}$$

By artificially defining $\mathrm{det}\mathbf{M}_{M,M-1} = 1$ and $\mathrm{det}\mathbf{M}_{M,M-2} = 0$, the determinants can be expanded along the n^{th} row to be

$$\mathrm{det}\mathbf{M}_{M,n} = (E - \alpha_n)\mathrm{det}\mathbf{M}_{M,n-1} - \beta^2\mathrm{det}\mathbf{M}_{M,n-2}, \tag{D.4}$$

since the matrix is tri-diagonal.

Inserting (D.4) into (D.3), we obtain

$$\begin{aligned} G_{M,n}(n,n) &= \frac{\mathrm{det}\mathbf{M}_{M,n-1}}{(E - \alpha_n)\mathrm{det}\mathbf{M}_{M,n-1} - \beta^2\mathrm{det}\mathbf{M}_{M,n-2}} = \frac{1}{(E - \alpha_n) - \dfrac{\beta^2\mathrm{det}\mathbf{M}_{M,n-2}}{\mathrm{det}\mathbf{M}_{M,n-1}}} \\ &= \frac{1}{(E - \alpha_n) - \beta^2 G_{M,n-1}(n-1,n-1)}, \end{aligned} \tag{D.5}$$

which reproduces the result in (3.50).

Appendix E

Crystal Orbital Surface States

The properties of an N-atom crystal can be extracted from those of the infinite, periodic crystal which satisfies the Born-von-Karman boundary conditions (2.10). Consider a *cyclic* crystal of N identical sites (Fig. E.1). We start with (6.2) and note that the AO states are spatial translations of one another, i.e.,

$$|n\rangle = \int |x\rangle\, \phi(x - na)\, dx, \tag{E.1}$$

where $\phi(x)$ is the wavefunction of an isolated atom centered at $x = 0$.

Because (6.5) is independent of the sign of θ, and since the periodicity of the crystal makes the θ-interval arbitrary, we need only consider the positive solution at this time. Thus, the coefficients (6.3) become

$$c_m = Ae^{im\theta}. \tag{E.2}$$

Recalling the Bloch-Floquet condition (2.4),

$$\langle x + a \mid \psi \rangle = e^{ika} \langle x \mid \psi \rangle, \tag{E.3}$$

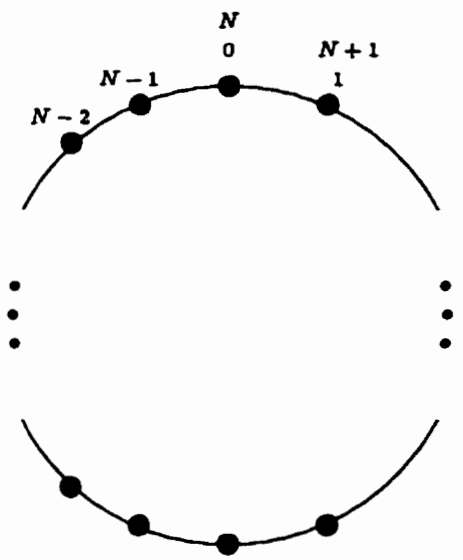

Fig. E.1: Cyclic representation of 1-dimensional infinite chain satisfying Born-von-Karman periodic boundary conditions. Breaking single bonds results in N-atom finite chains with surfaces.

and utilizing (6.2), (E.1) and (E.2) to expand both sides of (E.3), we have

$$\begin{aligned}
\sum_n c_n \langle x+a \mid n\rangle &= \sum_m e^{ika} c_m \langle x \mid m\rangle \\
\sum_n A e^{in\theta} \int \langle x+a \mid x'\rangle \, \phi(x'-na)\, dx' &= \sum_m A e^{ika} e^{im\theta} \int \langle x \mid x'\rangle \, \phi(x'-ma)\, dx' \\
\sum_n e^{in\theta} \int \delta(x+a-x')\phi(x'-na)\, dx' &= \sum_m e^{i(ka+m\theta)} \int \delta(x-x')\phi(x'-ma)\, dx' \\
\sum_n e^{in\theta} \phi(x-(n-1)a) &= \sum_m e^{i(ka+m\theta)} \phi(x-ma). \qquad \text{(E.4)}
\end{aligned}$$

Putting $m = n-1$, and reordering the second sum, we find

$$1 = e^{i(ka-\theta)}, \qquad \text{(E.5)}$$

so that

$$\theta = ka, \qquad \text{(E.6)}$$

indicating that θ is the effective *wavenumber* of the crystal wavefunction.

Applying the normalization condition to the wavefunction gives

$$1 = \langle \psi \mid \psi \rangle = \sum_{n,m} A^* e^{-im\theta} \langle m| \, A e^{in\theta} \, |n\rangle = \sum_{n,m} A^2 e^{i(n-m)\theta} \delta_{nm}, \qquad \text{(E.7)}$$

where we have used the orthonormality of the AO basis wavefunctions. This leads to

$$\sum_{n=0}^{N-1} A^2 = 1, \qquad \text{(E.8)}$$

and so

$$A = N^{-1/2}. \qquad \text{(E.9)}$$

Thus, the wavefunction coefficients (E.2) for the cyclic crystal are

$$c_n = N^{-1/2} e^{in\theta}. \qquad \text{(E.10)}$$

Returning to the structure of the cyclic crystal, we eliminate the bond between the N and $N+1$ atoms (Fig. E.1), which produces a finite chain starting at site $n = 1$ and ending at $n = N$. The recursion relation for the internal sites remains as above,

$$(E - \alpha)c_n = \beta(c_{n+1} + c_{n-1}), \qquad n = 2, 3, \ldots, N-1, \tag{E.11}$$

while the surface sites provide the boundary conditions

$$(E - \alpha')c_1 = \beta c_2, \qquad (E - \alpha)c_N = \beta c_{N-1}, \tag{E.12}$$

which breaks the previous cyclic periodicity. The site energies at the surfaces may be modified, since the surface atoms are bonded to only a single neighbour atom instead of two. To consider the effects of a single surface at $n = 1$, where we set $\alpha_1 = \alpha'$, we terminate the chain at $n = N$ without modifying the site energy there, which is equivalent to setting $c_{N+1} = 0$.

Without periodicity, we need to consider both solutions to (6.4). Taking a linear combination of the two, the general solution is given by

$$c_n = ae^{in\theta} + be^{-in\theta} = A\cos n\theta + B\sin n\theta. \tag{E.13}$$

At $n = N + 1$, the second boundary shows that

$$B = -A\frac{\cos(N+1)\theta}{\sin(N+1)\theta}, \tag{E.14}$$

so (E.13) becomes

$$c_n = A\frac{\sin(N+1-n)\theta}{\sin(N+1)\theta}. \tag{E.15}$$

In reduced notation, (E.12) takes the form

$$(2X - z)c_1 = c_2. \tag{E.16}$$

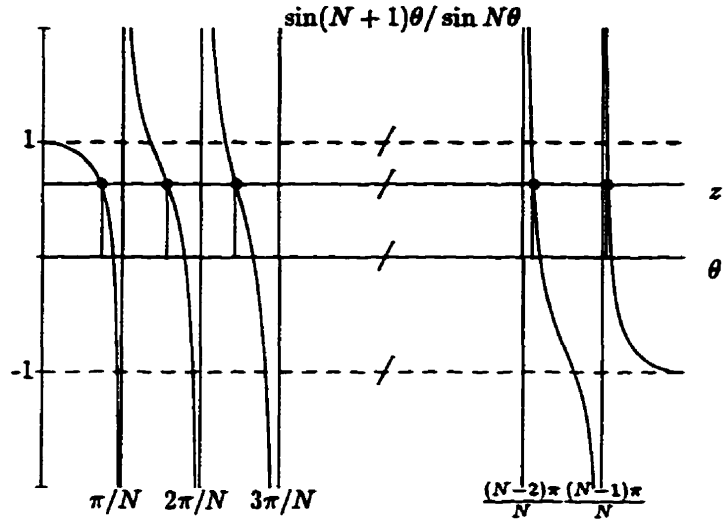

Fig. E.2: Solutions to $z = \sin(N+1)\theta/\sin N\theta$, showing N intercepts for $|z| < N/(N+1)$ and $N-1$ intercepts otherwise.

With the aid of (6.5) and (E.15), equation (E.16) leads to the *eigenvalue equation*

$$z = \frac{\sin(N+1)\theta}{\sin N\theta}, \tag{E.17}$$

which defines the energy spectrum of the *finite* crystal.

Graphically, solutions to (E.17) are shown in Fig. E.2. A single solution for any z occurs between consecutive roots of $\sin N\theta$, except perhaps in the first and last intervals, where both numerator and denominator become zero simultaneously at $\theta = 0$ and $\theta = \pi$. We use L'hôpital's rule to evaluate (E.17) at these points,

$$\left.\frac{\sin(N+1)\theta}{\sin N\theta}\right|_{\theta=0,\pi} = \left.\frac{(N+1)\cos(N+1)\theta}{N\cos N\theta}\right|_{\theta=0,\pi} = \begin{cases} 1+1/N, & \theta = 0, \\ -1-1/N, & \theta = \pi. \end{cases} \tag{E.18}$$

Hence, solutions fail to exist in the first interval when $z > 1 + 1/N$ and in the last interval when $z < -1 - 1/N$. The disappearance of a single solution when

$|z| > 1+1/N$ is related to the restriction placed on θ in (6.5). The missing solution defines a *surface state*, which lies *outside* the energy band of the unperturbed crystal. Again, to access energies outside the band, we must allow θ to become complex. Inserting (6.18) into (6.5), we obtain

$$X = \cos\zeta \cosh\mu - i \sin\zeta \sinh\mu, \tag{E.19}$$

which must be real, so $\mu \neq 0$ requires

$$\zeta = m\pi, \qquad m = 0, 1, \ldots, \tag{E.20}$$

or, without loss of generality, places θ at either endpoint shown in Fig. E.2, i.e.,

$$\theta = i\mu, \qquad \theta = \pi + i\mu. \tag{E.21}$$

Taking the first of these choices, we find that (6.5) becomes

$$X = \cosh\mu, \tag{E.22}$$

which is strictly *above* the energy band, and so defines a positive *P-state*. Since we are only considering the surface at $n = 1$, we let $N \to \infty$ in (E.18), whence,

$$z = \lim_{N\to\infty} \left(1 + \frac{1}{N}\right) \frac{e^{-(2N+1)\mu} + e^{\mu}}{e^{-2N\mu} + 1} = e^{\mu}, \tag{E.23}$$

which gives us the *existence condition* for a P-state, viz.,

$$z > 1. \tag{E.24}$$

Applying our choice of θ to (E.15), we find that in the limit $N \to \infty$,

$$c_n = \lim_{N\to\infty} A \frac{e^{-(N+1-n)\mu} - e^{(N+1-n)\mu}}{e^{-(N+1)\mu} - e^{(N+1)\mu}} = \lim_{N\to\infty} A \frac{e^{-(2N+2-n)\mu} - e^{-n\mu}}{e^{-2(N+1)\mu} - 1} = Ae^{-n\mu}, \tag{E.25}$$

which exhibits exponential decay away from the surface, i.e., the wavefunction is *localized* on the surface site, which we take as a defining property of a *surface state.*

Conversely, if we choose $\theta = \pi + i\mu$, (6.5) yields

$$X = -\cosh\mu, \tag{E.26}$$

which is always *below* the band and indicates a negative N-*state.* The surface perturbation parameter is again obtained from (E.18), namely,

$$\begin{aligned} z &= \lim_{N\to\infty} \frac{(N+1)\cos(N+1)\pi \cosh(N+1)\mu}{N\cos N\pi \cosh N\mu} \\ &= \lim_{N\to\infty} \left(1+\frac{1}{N}\right)(-1)\frac{(e^{(N+1)\mu}+e^{-(N+1)\mu})}{e^{N\mu}+e^{-N\mu}} \\ &= -e^{\mu}, \end{aligned} \tag{E.27}$$

which leads to the *existence condition* for an N-state,

$$z < -1. \tag{E.28}$$

Likewise, the coefficients of the N-state are obtained from (E.15) in the limit $N \to \infty$, with the result that

$$c_n = A(-1)^n e^{-n\mu}, \tag{E.29}$$

which again shows an exponential decay away from the surface, but has an oscillatory feature not present in the P-state case.

These last results have been obtained in the limit as $N \to \infty$, which transforms the finite chain into the semi-infinite one, described in § 4.3. In particular, the energy spectrum becomes the continuous band $-1 \leq X \leq 1$, and it is with respect to this continuum that the existence conditions (E.24) and (E.28) indicate the presence of a *discrete* surface state.

Appendix F

Lippmann-Schwinger Equation

We derive the Lippmann-Schwinger (LS) equation following the procedure given by Liboff [111]. First, we introduce the *Heisenberg picture* of Quantum Mechanics, which is equivalent to the usual *Schrödinger picture*, the difference being that Heisenberg placed the time evolution with the *operators* of the system instead of the *wavefunctions*.

Subject to a *time-independent* Hamiltonian, $\mathbb{H}^0$, the Schrödinger wavefunction, $|\psi(t)\rangle$, develops via

$$|\psi(t)\rangle = e^{-i(t-t_0)\mathbb{H}^0/\hbar}\,|\psi(t_0)\rangle\,, \tag{F.1}$$

so that on differentiating with respect to time, and multiplying by $i\hbar$, (F.1) becomes the Schrödinger equation

$$i\hbar\frac{\partial}{\partial t}\,|\psi(t)\rangle = (i\hbar)\left(-\frac{i}{\hbar}\mathbb{H}^0\right)e^{-i(t-t_0)\mathbb{H}^0/\hbar}\,|\psi(t_0)\rangle = \mathbb{H}^0\,|\psi(t)\rangle\,. \tag{F.2}$$

The Heisenberg picture makes use of the unitary operator applied in (F.1),

$$U = e^{-i(t-t_0)\mathbb{H}^0/\hbar}, \tag{F.3}$$

to transform the Schrödinger wavefunctions and operators. Even if the Hamiltonian is time-dependent, i.e., (F.1) no longer holds, the Heisenberg wavefunction can be obtained from the time-independent part of the Hamiltonian via

$$|\Psi\rangle = U^{-1}\,|\psi(t)\rangle = e^{i(t-t_0)\mathbb{H}^0/\hbar}\,|\psi(t)\rangle\,. \tag{F.4}$$

Since the results of quantum mechanics must remain unaltered by the choice of formalism, we use the operator expectation value

$$\langle \mathbb{A}\rangle_S = \langle\psi(t)|\,\mathbf{A}\,|\psi(t)\rangle = \langle\psi(t_0)|\,U^{-1}\mathbf{A}U\,|\psi(t_0)\rangle = \langle\psi(t_0)|\,\mathbf{A}\,|\psi(t_0)\rangle = \langle\mathbf{A}\rangle_H, \tag{F.5}$$

to obtain a Heisenberg operator

$$\mathbf{A} = U^{-1}\mathbf{A}U, \tag{F.6}$$

from the equivalent Schrödinger operator.

We now introduce the *interaction picture* perturbation technique. To $\mathbb{H}^0$, we add a time-dependent perturbation, $\mathbf{V}(t)$, with perturbation parameter λ, i.e.,

$$\mathbb{H} = \mathbb{H}^0 + \lambda\mathbf{V}(t). \tag{F.7}$$

Since the Hamiltonian is now time-dependent, so also are the Heisenberg wavefunctions. Differentiating (F.4), we find

$$\begin{aligned}
i\hbar\frac{\partial}{\partial t}\,|\Psi(t)\rangle &= -\mathbb{H}^0 e^{i(t-t_0)\mathbb{H}^0/\hbar}\,|\psi(t)\rangle + e^{i(t-t_0)\mathbb{H}^0/\hbar} i\hbar\frac{\partial}{\partial t}\,|\psi(t)\rangle \\
&= -\mathbb{H}^0 e^{i(t-t_0)\mathbb{H}^0/\hbar}\,|\psi(t)\rangle + e^{i(t-t_0)\mathbb{H}^0/\hbar}\mathbb{H}\,|\psi(t)\rangle \\
&= -\mathbb{H}^0 e^{i(t-t_0)\mathbb{H}^0/\hbar}\,|\psi(t)\rangle + e^{i(t-t_0)\mathbb{H}^0/\hbar}\left(\mathbb{H}^0 + \lambda\mathbf{V}(t)\right)|\psi(t)\rangle \\
&= \lambda e^{i(t-t_0)\mathbb{H}^0/\hbar}\mathbf{V}(t)e^{-i(t-t_0)\mathbb{H}^0/\hbar}e^{i(t-t_0)\mathbb{H}^0/\hbar}\,|\psi(t)\rangle \\
&= \lambda\mathbf{V}(t)\,|\Psi(t)\rangle\,.
\end{aligned} \tag{F.8}$$

Integrating (F.8) from t_0 to t and rearranging, we find

$$|\Psi(t)\rangle = |\Psi(t_0)\rangle + \frac{\lambda}{i\hbar}\int_{t_0}^{t} \mathbf{V}(\tau)\,|\Psi(\tau)\rangle\,d\tau, \tag{F.9}$$

which can be iterated to give a *λ-perturbation series* solution

$$\begin{aligned}|\Psi(t)\rangle \;=\; |\Psi(t_0)\rangle &+ \frac{\lambda}{i\hbar}\,|\Psi(t_0)\rangle \int_{t_0}^{t} \mathbf{V}(\tau)\,d\tau \\ &+ \left(\frac{\lambda}{i\hbar}\right)^2 |\Psi(t_0)\rangle \int_{t_0}^{t}\int_{t_0}^{t} \mathbf{V}(\tau_1)\mathbf{V}(\tau_2)\,d\tau_2\,d\tau_1 + \cdots .\end{aligned} \tag{F.10}$$

For the LS derivation, we begin with the unperturbed Hamiltonian, $\mathbb{H}^0$, and its corresponding wavefunctions

$$\mathbb{H}^0\,|\phi\rangle = E_0\,|\phi\rangle\,. \tag{F.11}$$

A scattering perturbation, V, is introduced via

$$\mathbb{H}(t) = \mathbb{H}^0 + \mathbf{V}e^{-\epsilon|t|/\hbar}, \tag{F.12}$$

where $\epsilon \to 0^+$, thus giving the desired perturbed Hamiltonian at $t = 0$, and the unperturbed Hamiltonian for $t \to \pm\infty$. Since we shall be using (F.9), which gives an exact λ-solution, instead of approximating with the series expansion, we set $\lambda = 1$.

The scattering wavefunctions, which we wish to obtain, viz.,

$$|\psi\rangle = |\psi(0)\rangle\,. \tag{F.13}$$

are extracted from the time-dependent wavefunctions of (F.12), namely,

$$|\psi(t)\rangle = e^{-it\mathbb{H}/\hbar}\,|\psi(0)\rangle\,. \tag{F.14}$$

In the limit $\epsilon \to 0^+$, the $t = 0$ solutions can be considered eigenstates of the total Hamiltonian, i.e.,

$$\mathbb{H}\,|\psi\rangle = E\,|\psi\rangle\,. \tag{F.15}$$

Transforming into the Heisenberg picture via (F.4) and (F.6), we consider $t_0 \to \pm\infty$, where the Hamiltonian approaches the unperturbed one. Thus, at $t = t_0 = \pm\infty$, we make the connection

$$|\Psi(\pm\infty)\rangle = |\phi\rangle\,. \tag{F.16}$$

This choice of t_0 also allows us to set

$$|\Psi(t)\rangle = e^{it\mathbf{H}^0/\hbar}\,|\psi(t)\rangle\,, \tag{F.17}$$

whence,

$$|\Psi(0)\rangle = |\psi(0)\rangle = |\psi\rangle\,. \tag{F.18}$$

Inserting (F.16) and (F.18) into (F.9), we obtain

$$|\psi\rangle = |\phi\rangle + \frac{1}{i\hbar}\int_{\pm\infty}^{0} \mathbf{V}(\tau)\,|\Psi(\tau)\rangle\,d\tau, \tag{F.19}$$

for our choices of λ and t_0. Using (F.6), (F.17), (F.14), (F.13) and (F.15), equation (F.19) becomes the desired LS result, i.e.,

$$\begin{aligned}
|\psi\rangle &= |\phi\rangle + \frac{1}{i\hbar}\int_{\pm\infty}^{0} \left(e^{i\tau\mathbf{H}^0/\hbar}\mathbf{V}e^{-\epsilon|\tau|/\hbar}e^{-i\tau\mathbf{H}^0/\hbar}\right) e^{i\tau\mathbf{H}^0/\hbar}\,|\psi(\tau)\rangle\,d\tau \\
&= |\phi\rangle + \frac{1}{i\hbar}\int_{\pm\infty}^{0} e^{i\tau\mathbf{H}^0/\hbar}\mathbf{V}e^{-\epsilon|\tau|/\hbar}e^{-i\tau\mathbf{H}/\hbar}\,|\psi(0)\rangle\,d\tau \\
&= |\phi\rangle + \frac{1}{i\hbar}\int_{\pm\infty}^{0} e^{i\tau\mathbf{H}^0/\hbar}\mathbf{V}e^{-\epsilon|\tau|/\hbar}e^{-i\tau E/\hbar}\,|\psi\rangle\,d\tau \\
&= |\phi\rangle + \frac{1}{i\hbar}\int_{\pm\infty}^{0} e^{i\tau(\mathbf{H}^0 - E\mp i\epsilon)/\hbar}\,d\tau\mathbf{V}\,|\psi\rangle \\
&= |\phi\rangle + \frac{1}{E - \mathbf{H}^0 \pm i\epsilon}\mathbf{V}\,|\psi\rangle \\
&= |\phi\rangle + \mathbb{G}^0\mathbf{V}\,|\psi\rangle\,,
\end{aligned} \tag{F.20}$$

where $\mathbb{G}^0$ is the Greenian for the *unperturbed* Hamiltonian.

Appendix G

Maple Source Code

All plots were generated using the MAPLE V release 3 [112] symbolic computation software.

G.1 Surface States

```
> F:=0.02;
> P:=[];
> M:=1;
> !mdata si+2.in
> read 'si+2.in';
> Digits:=100:
> gc(0):
> J:=(n,x)->BesselJ(n,x);
> djd:=proc(n,x)
>   k:=0;
>   g:=0;
>   h:=0;
>   while g > -55 do
>     f:=(-x^2/4)^k*Psi(n+k+1)/(k!*GAMMA(n+k+1));
```

```
>     k:=k+1;
>     h:=h+f;
>     g:= evalf(log10(abs(f/h)));
>   od;
>   j:=J(n,x)*ln(x/2)-(x/2)^n*h;
>   RETURN(j);
> end:
> dj:=(n,X,F)->djd(X/F-n-1,1/F);
> dos:=(n,X,F)->evalf(2*F*J(X/F-n,1/F)/dj(n,X,F));
> den:=(n,X,F)->J(X/F-n-1,1/F);
> zero:=proc(site,a,b,field) global P,Start,M,H;
>   c:=b-a:
>   Start:=M:
>   H:=P:
>   bins:=ceil(c/abs(field)):
>   for n from Start to bins do
>     A:=a+(n-1)*abs(field):
>     B:=a+n*abs(field):
>     da:=den(site,A,field):
>     db:=den(site,B,field):
>     if da*db <= 0 then
>       d:=(A+B)/2:
>       dd:=den(site,d,field):
>       while B-A>10^(-50) do
>         if da*dd <= 0 then
>           B:=d:
>         else
>           A:=d:
>           da:=dd:
>         fi:
>         d:=(A+B)/2:
>         dd:=den(site,d,field):
>       od:
>       H:=[op(H),[[d,0],[d,dos(site,d,field)]]]:
>       P:=H:
```

```
>     fi:
>     M:=n+1:
>     save M,P,'si+2.in';
>     print(n,bins);
>   od:
> end:
> zero(0,-2,2,F):
> save H,'si+2';
> !mdata si+2
> quit;
```

G.2 Chemisorption

```
> N:=100;
> F:=0.0125;
> Z:=-2.96;
> U:=4.23;
> Eta:=2.46;
> Left:=Z*(1+abs(F));
> Right:=2.0;
> FL:=61;
> Fa:=0:
> P:=[]:M:=1:T:=0:V:=[]:
> !mdata f+35.in
> !mdata f+35.in2
> read 'f+35.in':
> read 'f+35.in2':
> Digits:=100:
> build:=proc(first,last,field) local a,n;\
>   global G,Num,Den,DiffCrys,DiffAd;
>   a[-2]:=0:a[-1]:=1:
>   for n from 0 to last-first do
>     a[n]:=collect(2*(x-(last-n)*field)*a[n-1]-a[n-2],x):
>   od:
```

```
>   Num:=a[last-first-1]:
>   Den:=a[last-first]:
>   G:=Num/Den:
>   DiffCrys:=diff(a[last-first-2]/a[last-first-1],x):
>   DiffAd:=diff(a[last-first-1]/a[last-first],x):
> end:
> build(1,N,F):
> den:=(eta,site,X)->subs(x=X,Den):
> dos:=(eta,X)->subs(x=X,1/(1-eta^2*DiffCrys/2)):
> zero:=proc(eta,site,a,b,field) global H,M,P,Fa,Start;
>   c:=b-a:
>   Start:=M:
>   H:=P:
>   Factor:=Fa:
>   bins:=ceil(2^Factor*c/abs(field)):
>   print(Start,bins);
>   for n from Start to bins do
>     A:=a+(n-1)*abs(field)/2^Factor:
>     B:=a+n*abs(field)/2^Factor:
>     da:=den(eta,site,A,field):
>     db:=den(eta,site,B,field):
>     if da*db <= 0 then
>       d:=(A+B)/2:
>       dd:=den(eta,site,d,field):
>       while B-A>10^(-50) do
>         if da*dd <= 0 then
>           B:=d:
>         else
>           A:=d:
>           da:=dd:
>         fi:
>         d:=(A+B)/2:
>         dd:=den(eta,site,d,field):
>       od:
>       H:=[op(H),[[d,0],[d,dos(eta,d)]]]:
```

```
>       P:=H:
>     fi:
>     M:=n+1:
>     save M,P,'f+35.in';
>     print(n);
>   od:
> end:
> if T = 0 then
>   zero(1,0,Left,Right,F):
>   C:=H:
>   T:=1:V:=[]:
>   save T,C,V,'f+35.in2';
>   M:=1:P:=[]:
>   save M,P,'f+35.in';
> fi;
> Ek:=sum(C[k][2][1],k=1..FL);
> den:=(eta,site,X)->subs(x=X,2*(X-site)*Den-eta^2*Num):
> dos:=(eta,X)->subs(x=X,1/(1-eta^2*DiffAd/2)):
> occ:=proc(eta,site,coreng,a,b,field,fermi)\
>   global K,L,T,V,Start2,M,P,C;
>   Start2:=T:
>   K:=V:
>   for n from Start2 to 26 do
>     zero(eta,site+coreng*((n-1)/25),a,b,field):
>     K:=[op(K),[(n-1)/25,sum(H[k][2][2],k=1..fermi)]]:
>     V:=K:
>     T:=n+1:
>     save T,C,V,'f+35.in2';
>     M:=1:P:=[]:
>     save M,P,'f+35.in';
>     print(point=n);
>   od:
>   L:=[]:
>   for n from 1 to 26 do
>     L:=[op(L),[K[27-n][2],K[27-n][1]]]:
```

```
>   od:
> end:
> occ(Eta,Z,U,Left,Right,F,FL):
> cor:=proc() global kx,ky,Self;
>   kx:=[seq(K[i][1],i=1..26)]:
>   ky:=[seq(K[i][2],i=1..26)]:
>   nk:=x->subs(n=x,interp(kx,ky,n)):
>   Self:=fsolve(nk(x)-x=0,x=0..1):
> end:
> cor(1);
> zero(Eta,Z+U*Self,Left,Right,F):
> En:=sum(H[n][2][1],n=1..FL);
> Delta:=2*(En-Ek) + H[FL+1][2][1] - Z - U*Self^2;
> Q:=2*Self-1;
> save C,H,K,L,Self,Ek,En,Delta,Q,'f+35';
> !mdata f+35
> quit;
```

G.3 Molecular Electronics

```
> M:=5:
> N:=10:
> Y:=1.2:
> U:=0.3:
> Z:=-0.25:
> w:=0.75:
> s:=0.8:
> #y:=0.5:
> zs:=0.25:
> Digits:=100:
> build:=proc(first,last,field,bond,site)\
>   local a,b,n,Numa,Numb,Dena,Denb; global GOO,GNN
> ,GON,GNO;
>   a[-2]:=0:a[-1]:=1:b[-2]:=0:b[-1]:=1:
```

```
>   for n from 0 to last-first do
>     a[n]:=collect(2*((X-site)/bond-(last-n)*field)*a[n-1]-
> a[n-2],X):
>     b[n]:=collect(2*((X-site)/bond-(first+n)*field)*b[n-1]-
> b[n-2],X):
>   od:
>   Numa:=a[last-first-1]:
>   Numb:=b[last-first-1]:
>   Dena:=a[last-first]:
>   Denb:=b[last-first]:
>   G00:=Numa/Dena:
>   GNN:=Numb/Denb:
>   G0N:=1/b[last-first]:
>   GN0:=1/a[last-first]:
> end:
> build(M+1,N,U/(N*w),w,Z):
> Gnn:=GNN:Gmn:=G0N:Gmm:=G00:Gnm:=GN0:
> build(0,M-1,U/(N*w),w,Z):
> g00:=G00:g0m:=G0N:gmm:=GNN:gm0:=GN0:
> G00:=g00+s^2*g0m*gm0/(2*(X-zs-M*U/N)-(s^2*gmm+
> s^2*y^2*Gmm)):
> GNN:=Gnn+s^2*y^2*Gnm*Gmn/(2*(X-zs-M*U/N)-(s^2
> *gmm+s^2*y^2*Gmm)):
> G0N:=s^2*y*gm0*Gmn/(2*(X-zs-M*U/N)-(s^2*gmm+s
> ^2*y^2*Gmm)):
> GN0:=s^2*y*gm0*Gmn/(2*(X-zs-M*U/N)-(s^2*gmm+s
> ^2*y^2*Gmm)):
> f:=X+I*sqrt(1-X^2):
> f1:=subs(X=X-U,f):
> zet:=sqrt(1-X^2):
> zet1:=subs(X=X-U,zet):
> DD:=(1-Y^2/w*f*G00)*(1-Y^2/w*f1*GNN)-Y^4/w^2*f*f1
> *G0N*GN0:
> T:=2*sqrt(zet*zet1)*Y^2/w*G0N/DD:
> TT:=collect((abs(T))^2,X)*(Heaviside(X-U+1)*Heavisid
```

```
> e(1-X)):
> save TT,'y30';
> quit;
```

Bibliography

[1] P. Sautet and C. Joachim, *Phys. Rev. B*, **38** (1988), 12 238.

[2] R. A. English, Master's thesis, University of Waterloo, Waterloo, Ontario, Canada, 1993.

[3] R. A. English and S. G. Davison, *Phys. Rev. B*, **49** (1994), 8718.

[4] A. Aviram, in *Proceeding of the Annual International Conference of the IEEE Engineering in Medicine and Biology Society*, **11** (1989), 1385. Eds. F. A. Spelman and Y. Kim, Washington, DC.

[5] M. Pomerantz, in *Proceeding of the Annual International Conference of the IEEE Engineering in Medicine and Biology Society*, **12** (1990), 1687. Eds. P. C. Pedersen and B. Onaral, Washington, DC.

[6] F. T. Hong, to appear in *Particle Technology Review*, Volume 1 (unpublished).

[7] C. Nicolini, M. Adami, F. Antolini, F. Beltram, M. Sartore, and S. Vakula, *Physics World*, **5** (1992), 30.

[8] A. G. MacDiarmid and A. J. Epstein, in *Proceeding of the Annual International Conference of the IEEE Engineering in Medicine and Biology Society*, **11** (1989), 1299. Eds. F. A. Spelman and Y. Kim, Washington, DC.

[9] G.H. Wannier, *Phys. Rev.*, **117** (1960), 432.

[10] C. Zener, *Proc. Roy. Soc. (Lond.)*, **145** (1934), 523.

[11] W.V. Houston, *Phys. Rev.*, **57** (1940), 184.

[12] J.C. Slater, *Phys. Rev.*, **76** (1949), 1592.

[13] H.M. James, *Phys. Rev.*, **76** (1949), 1611.

[14] S. Katsura, T. Hatta and A. Morita, *Sci. Rep. Tôhoku Imp. Univ.*, **35** (1950), 19.

[15] K. Hacker and G. Obermair, *Z. Phys.*, **234** (1970), 1.

[16] P. Feuer, *Phys. Rev.*, **88** (1952), 92.

[17] E.N. Adams, *J. Chem. Phys.*, **21** (1953), 2013.

[18] E.N. Adams, *Phys. Rev.*, **89** (1953), 633.

[19] G.H. Wannier, *Phys. Rev.*, **100** (1955), 1227.

[20] G.H. Wannier, *Phys. Rev.*, **101** (1956), 1835.

[21] E.N. Adams and P.N. Argyres, *Phys. Rev.*, **102** (1956), 605.

[22] E.N. Adams, *Phys. Rev.*, **107** (1957), 698.

[23] E.O. Kane, *J. Phys. Chem. Solids*, **12** (1959), 181.

[24] G.H. Wannier, *Rev. Mod. Phys.*, **34** (1962), 645.

[25] H.D. Rees, *J. Phys. Chem. Solids*, **28** (1967), 353.

[26] R. Enderlein, R. Keiper and W. Tausendfreund, *Phys. Stat. Sol.*, **33** (1969), 69.

[27] K. Henneberger and J. Rõseler, *Phys. Stat. Sol. B*, **58** (1973), 575.

[28] J. Fiddicke and R. Enderlein, *Phys. Stat. Sol. B*, **71** (1975), 497.

[29] J. Callaway, *Phys. Rev.*, **130** (1963), 549.

[30] J. Callaway, *Phys. Rev.*, **134** (1964), A998.

[31] G.H. Wannier and D.R. Fredkin, *Phys. Rev.*, **125** (1962), 1810.

[32] A. Rauh and H.H. Wannier, *Solid St. Commun.*, **15** (1974), 1239.

[33] A.G. Chynoweth, G.H. Wannier, R.H. Logan, and D.E. Thomas, *Phys. Rev. Lett.*, **5** (1960), 57.

[34] B.B. Snavely, *Solid St. Commun.*, **4** (1966), 561.

[35] V.S. Vavilov, V.B. Stopabchinskii and V.Sh. Chanbarisov, *Sov. Phys. Sol. St.*, **8** (1967), 2126.

[36] J. Zak, *Phys. Rev. Lett.*, **19** (1967), 1385.

[37] J. Zak, *Phys. Rev.*, **168** (1968), 686.

[38] J. Zak, *Phys. Rev. Lett.*, **20** (1968), 1477.

[39] J. Zak, *Phys. Rev.*, **181** (1969), 1366.

[40] A. Rabinovitch, *Phys. Lett.*, **33A** (1970), 403.

[41] A. Rabinovitch, *Phys. Rev. B*, **4** (1971), 1017.

[42] A. Rabinovitch and J. Zak, *Phys. Rev. B*, **4** (1971), 2358.

[43] A. Rabinovitch and J. Zak, *Phys. Lett.*, **40A** (1972), 189.

[44] S.G. Davison and K.P. Tan, *Z. Phys.*, **251** (1972), 6.

[45] M.J. Richardson and S.G. Davison, *Can. J. Phys.*, **52** (1974), 2395.

[46] W. Shockley, *Phys. Rev. Lett.*, **28** (1972), 349.

[47] J. Heinrichs and R.O. Jones, *J. Phys. C: Solid St. Phys.*, **5** (1972), 2149.

[48] G.C. Stey and G. Gusman, *J. Phys. C: Solid St. Phys.*, **6** (1973), 650.

[49] M. Saitoh, *J. Phys. C: Solid St. Phys.*, **6** (1973), 3255.

[50] H. Fukuyama, R.A. Bari and H.C. Fogedby, *Phys. Rev. B*, **8** (1973), 5579.

[51] A. Rabinovitch, *Phys. Lett.*, **48A** (1974), 149.

[52] J. Avron, L. Gunther and J. Zak, *Solid St. Commun.*, **16** (1975), 189.

[53] J.E. Avron, J. Zak, A. Grossmann and L. Gunther, *J. Math. Phys.*, **18** (1977), 918.

[54] T. Lukes and K.T.S. Somaratna, *Phys. Lett.*, **29A** (1969), 69.

[55] T. Lukes and K.T.S. Somaratna, *J. Phys. C: Solid St. Phys.*, **2** (1969), 586.

[56] T. Lukes and D.J. Morgan, *Phys. Stat. Sol. B*, **57** (1973), K47.

[57] R.P. Feynman and A.R. Hibbs, *Quantum Mechanics and Path Integrals* (McGraw-Hill, New York, 1965).

[58] C.A. Moyer, *Phys. Rev. B*, **7** (1973), 5025.

[59] C.A. Moyer, *J. Phys. C: Solid St. Phys.*, **6** (1973), 1461.

[60] T. Lukes and G. Ringwood, *Phys. Lett.*, **44A** (1973), 477.

[61] S. Maekawa, *Phys. Rev. Lett.*, **24** (1970), 1175.

[62] R.W. Koss and L.M. Lambert, *Phys. Rev. B*, **5** (1972), 1479.

[63] D. May and A. Vecht, *J. Phys. C: Solid St. Phys.*, **8** (1975), L505.

[64] A. Rabinovitch, *Phys. Lett.*, **59A** (1977), 475.

[65] J.E. Avron, *Phys. Rev. B*, **16** (1977), 711.

[66] J. Zak, *Phys. Lett.*, **76A** (1980), 287.

[67] V. Sessa and J. Sitte, *J. Phys. C: Solid St. Phys.*, **11** (1978), 1599.

[68] D. Emin and C.F. Hart, *Phys. Rev. B*, **36** (1987), 7353.

[69] C.F. Hart and D. Emin, *Phys. Rev. B*, **37** (1988), 6100.

[70] J. Leo and A. MacKinnon, *J. Phys.: Cond. Mat.*, **1** (1989), 1449.

[71] E.E. Mendez, F. Agulló-Rueda and J.M. Hong, *Phys. Rev. Lett.*, **60** (1988), 2426.

[72] P. Voisin, J. Bleuse, C. Bouche, S. Gaillard, C. Alibert and A. Regreny, *Phys. Rev. Lett.*, **61** (1988), 1639.

[73] R.P. Leavitt, J.L. Bradshaw and F.J. Towner, *Phys. Rev. B*, **44** (1991), 11266.

[74] R.P. Leavitt, *Phys. Rev. B*, **44** (1991), 11270.

[75] M. Ritze, N.J.M. Horing and R. Enderlein, *Phys. Rev. B*, **47** (1993), 10437.

[76] X.-G. Zhao, *J. Phys.: Cond. Mat.*, **3** (1991), 6021.

[77] X.-G. Zhao, *Phys. Lett. A*, **154** (1991), 275.

[78] X.-G. Zhao, *Phys. Lett. A*, **167** (1992), 391.

[79] D. Ahn, *Phys. Rev. B*, **48** (1993), 7981.

[80] A.F.M. Anwar and M.M Jahan, *Phys. Rev. B*, **50** (1994), 10864.

[81] M.M. Vrubel and V.M. Borzdov, *Physica B*, **215** (1995), 201.

[82] H. Sari, H. Metin, I. Sökmen, S. Elagöz and Y. Ergün, *Superlat. Microst.*, **17** (1995), 457.

[83] G. Cohen, I. Bar-Joseph and H. Shtrikman, *Phys. Rev. B*, **50** (1994), 17316.

[84] J. Kavalianskas, G. Kivaité, A. Galickas, I. Šimkiené, U. Olin and M. Ottosson, *Phys. Stat. Sol. B*, **191** (1995), 155.

[85] V. Dolcher, G. Grosso, L. Martinelli and G.P. Parravicini, *Phys. Rev. B*, **53** (1996), 10 813.

[86] V.M. Gvozdikov, *Phys. Rev. B*, **53** (1996), 10133.

[87] N. Zekri, M. Schreiber, R. Ouasti, R. Bouamrane and A. Brezini, *Z. Phys. B*, **99** (1996), 386.

[88] S. G. Davison and M. Stęślicka, *Basic Theory of Surface States* (Clarendon Press, Oxford, 1992).

[89] *Handbook of Mathematical Functions*, edited by M. Abramowitz and I.A. Stegun (U.S. Department of Commerce, Washington, D.C., 1972).

[90] H. C. Ohanian, *Principles of Quantum Mechanics* (Prentice-Hall, Englewood Cliffs, New Jersey, 1990).

[91] J.B. Pendry, A. Prêtre, P.J. Rous and L. Martín-Moreno, *Surf. Sci.*, **244** (1991), 160.

[92] L. Lorentzen and H. Waadeland, *Continued Fractions with Applications* (North-Holland, Amsterdam, 1992).

[93] C. Brezinski, *History of Continued Fractions and Padé Approximants* (Springer-Verlag, New York, 1980).

[94] D.M. Newns, *Phys. Rev.*, **178** (1969), 1123.

[95] H.A. Priestley, *Introduction to Complex Analysis* (Oxford, New York, 1985).

[96] W. Magus and F. Oberhettinger, *Formeln und Sätze für die speziellen Funktionen der mathematischen Physik*, 2nd ed. (Springer-Verlag, Berlin, 1948).

[97] R.A. English, S.G. Davison, Z.L. Mišković, F.O. Goodman, A.T. Amos and B.L. Burrows, *Prog. Surf. Sci.*, **53** (1996), 323.

[98] A.S. Davydov, *Quantum Mechanics*, 2nd ed. (Pergamon, Oxford, 1991).

[99] R.A. English, S.G. Davison, Z.L. Mišković, F.O. Goodman, A.T. Amos and B.L. Burrows, *Prog. Surf. Sci.*, **54** (1997), (in press).

[100] M. T. Jarvis, *Molecular Electronics: Beyond the Silicon Chip*, 2nd ed. (Technical Insights, Fort Lee, New Jersey, 1985).

[101] A. Aviram, P. E. Seiden, and M. A. Ratner, in *Molecular Electronic Devices*, edited by F. L. Carter (Marcel Dekker, New York, 1982), p. 5.

[102] R. S. Potember, T. O. Poehler, D. O. Cowan, F. L. Carter, and P. Brant, in *Molecular Electronic Devices*, edited by F. L. Carter (Marcel Dekker, New York, 1982), p. 73.

[103] L. L. Shipman, in *Molecular Electronic Devices*, edited by F. L. Carter (Marcel Dekker, New York, 1982), p. 73.

[104] L. Keszthelyi, P. Ormos, G. Varó, and G. Groma, in *Proceeding of the Annual International Conference of the IEEE Engineering in Medicine and Biology Society*, **12** (1990), 1712. Eds. P. C. Pedersen and B. Onaral, Washington, DC.

[105] F. L. Carter, in *Molecular Electronic Devices*, edited by F. L. Carter (Marcel Dekker, New York, 1982), p. 51.

[106] Z.L. Mišković, R.A. English, S.G. Davison and F.O. Goodman, *Phys. Rev. B*, **54** (1996), 225.

[107] Z.L. Mišković, R.A. English, S.G. Davison and F.O. Goodman, *Chem. Phys. Lett.*, **260** (1996), 647.

[108] M.Ya. Azbel, *Phys. Lett.*, **78A** (1980), 410.

[109] M.Ya. Azbel, *Solid State Commun.*, **45** (1983), 527.

[110] C. Caroli, R. Combescot, P. Nozieres and D. Saint-James, *J. Phys. C: Solid St. Phys.*, **4** (1971), 916.

[111] R. Liboff, *Introductory Quantum Mechanics*, 2nd ed. (Addison-Wesley, Reading, Mass., 1991).

[112] B. W. Char, K. O. Geddes, G. H. Gonnet, B. L. Leong, M. B. Monagan, and S. M. Watt, *Maple V Library Reference Manual* (Waterloo Maple Publishing, Waterloo, Ontario, 1991).